

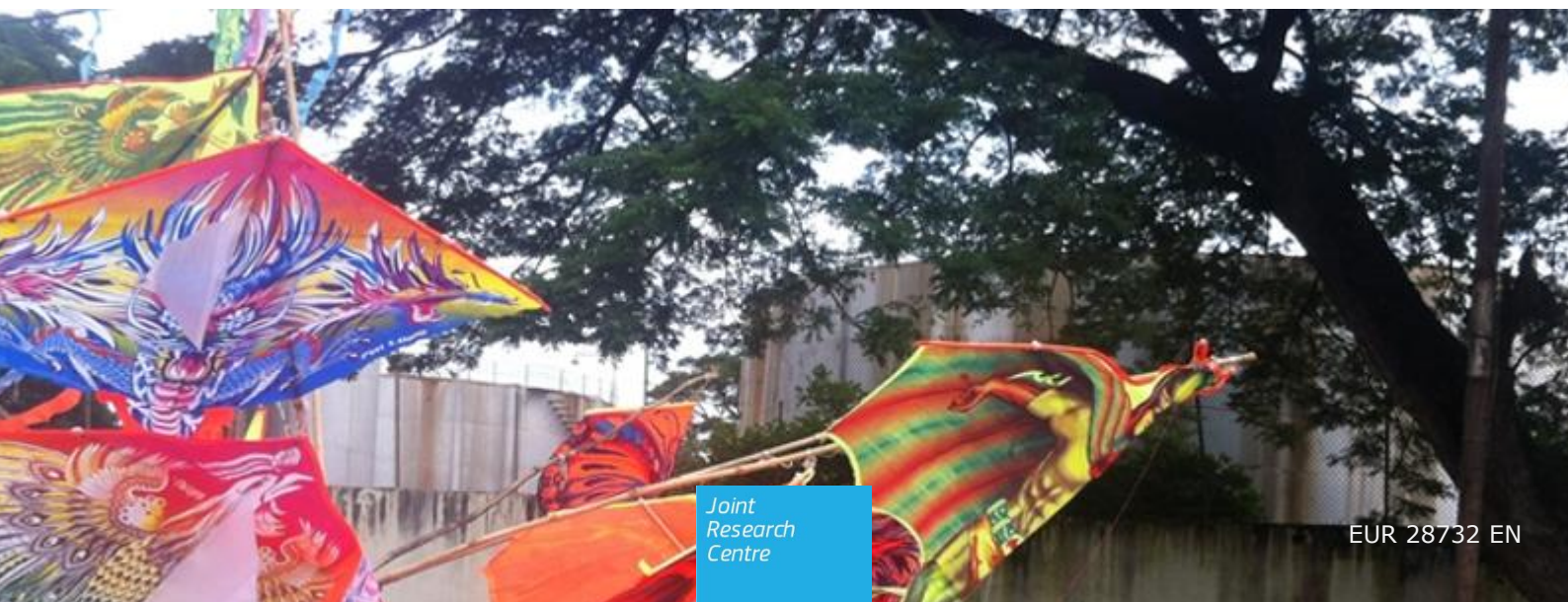
JRC TECHNICAL REPORTS

Accident Damage Analysis Module (ADAM) – Technical Guidance

*Software tool for
Consequence Analysis
calculations*

Fabbri, L Binda, M Bruinen de Bruin, Y

2017



This publication is a Technical report by the Joint Research Centre (JRC), the European Commission's science and knowledge service. It aims to provide evidence-based scientific support to the European policymaking process. The scientific output expressed does not imply a policy position of the European Commission. Neither the European Commission nor any person acting on behalf of the Commission is responsible for the use that might be made of this publication.

Contact information

Name: Luciano FABBRI
Address: EC JRC, Ispra
Email: luciano.fabbri@ec.europa.eu
Tel.: +39.0332.785801

JRC Science Hub

<https://ec.europa.eu/jrc>

JRC107633

EUR 28732 EN

PDF	ISBN 978-92-79-71879-3	ISSN 1831-9424	doi:10.2760/719457
Print	ISBN 978-92-79-71880-9	ISSN 1018-5593	doi:10.2760/523638

Luxembourg: Publications Office of the European Union, 2017, Ispra: European Commission, 2017

© European Union, 2017

Reuse is authorised provided the source is acknowledged. The reuse policy of European Commission documents is regulated by Decision 2011/833/EU (OJ L 330, 14.12.2011, p. 39).

For any use or reproduction of photos or other material that is not under the EU copyright, permission must be sought directly from the copyright holders.

How to cite this report: Fabbri, L Binda, M Bruinen de Bruin, Y; *Accident Damage Analysis Module (ADAM) – Technical Guidance*, EUR 28732 EN, 2017, ISBN 978-92-79-71879-3, doi:10.2760/719457

All images © European Union 2017

CONTENTS

Abstract.....	5
Introduction.....	7
SOURCE TERMS CALCULATION (Module 1)	9
Source Term.....	11
Outflow of compressed vapours and vessel response	13
Flow rate of an outflow from a leak or hole in a vessel.....	14
Flow rate of an outflow from pipe failure	16
Outflow of non-boiling liquids and vessel response.....	18
Outflow of pressurised liquefied gases and vessel response	20
Hole-up procedure ($H_{\text{hole}} \geq H_L$)	20
Hole-down procedure ($H_{\text{hole}} < H_L$).....	26
Vessel Dynamic during outflow.....	27
Jet flashing, droplet formation and rainout.....	29
Post-expansion parameters	29
Aerosol droplets' formation and rainout.....	33
Rainout.....	37
Discharge Coefficient	42
Catastrophic Releases.....	43
Pool spreading and vaporisation.....	47
Spreading model.....	47
Mass conservation	49
Evaporation model	50
Energy Balance.....	52
PHYSICAL EFFECTS CALCULATION (Module 2).....	55
General.....	57
Fire accidents due to the combustion of liquid and gases	59
Pool Fires	62
Pool diameter D	63
Burning rate, m	64
Flame length L	64
Tilt angle, θ	65
Drag diameter	66
Surface Emitting Power, SEP (kW m^{-2})	67
View Factor.....	68
Jet Fires.....	69
Vertical and inclined Flames.....	72
Horizontal Flames	74
Fireballs.....	77
Sphere geometry.....	77

Surface Emitting Power, SEP (kW m ⁻²)	78
Flash Fires	79
Vapour Cloud Explosions (VCE).....	81
TNT-equivalent mass method.....	84
TNO Multi-Energy method	86
Obstructed regions and sub-explosions	86
Effects parameters calculation.....	87
Backer-Strehlow-Tang (BST)	90
Effects parameters calculation.....	92
Atmospheric Dispersion of Toxic or Flammable Clouds	95
General.....	95
The SLAB dispersion model.....	96
Instantaneous releases (Transient Puff mode)	97
Continuous releases (steady state plume mode).....	99
ADAM-SLAB model	102
General	102
Alternative calculus of the <i>average concentration</i>	104
Calculus for time-varying releases.....	105
Inclusion of the contribution from Pool Evaporation in case of Rainout.....	107
Modification of the SLAB routine for the calculus of plume velocity	109
Dispersion and explosion of Flammable Clouds	110
Flash Fire contours	110
Explosive mass.....	110
VULNERABILITY (Module 3).....	113
Introduction.....	115
What is vulnerability.....	115
Vulnerable populations.....	115
Built Environment.....	116
Natural Environment.....	116
Vulnerability models.....	117
Vulnerability to Fires.....	118
Vulnerability to Vapour Cloud Explosions.....	120
Vulnerability to inhalation of toxics	122
Substances' Probit functions	123
References	125

Abstract

This report provides a technical description of the modelling and assumptions of the Accident Damage Analysis Module (ADAM) software application, which has been recently developed by the Joint Research Centre (JRC) of the European Commission (EC) to assess physical effects of an industrial accident resulting from an unintended release of a dangerous substance.

This software is specifically intended to assist the EU Competent Authorities, who are responsible for the implementation of the Seveso Directive in their countries, in assessing the potential consequences of an industrial accident in a structured and comprehensive manner. More specifically, ADAM is designed to implement the calculation of the physical effects of an industrial accident in terms of thermal radiation, overpressure or toxic concentration that may result from the loss of containment of a flammable or toxic substance. For this purpose, suitable models have been used and combined to simulate the possible evolution of an accident, from the time of release to the final damage. In addition, ADAM will be incorporated as a calculus module within the next version of the GIS Area Risk Assessment tool, developed by the JRC, which is intended to aggregate the contribution to risk of different risk sources resulting from the single installations of different establishments located in a certain area, by including the transport of dangerous substances.

All implemented models, were tested during the research phase, and as such might provide great support to several operators involved in the industrial safety sector, such as the risk analysts, site inspectors and reviewers of safety reports. The outcome of ADAM calculations is of fundamental importance for any risk estimate, but it is also essential for decision support related activities such as, for instance, identification of cost effective protection measures, organization of internal and external emergency plans, provision of the correct information to the public, and definition of land use around an industrial facility. In addition, the analysis of the exposure to the effects of an accident involving a certain dangerous substance can also be used to assess the inherent potential of the substance to produce harm.

ADAM was funded by the Institutional programme of the EC Joint Research Centre and the EC Directorate General on EU Humanitarian Aid and Civil Protection (DG ECHO) via Administrative Arrangements on Seveso Capacity Building in EU Neighbour Countries¹.

¹ There are three Administrative Arrangements: N° ECHO/SER/2014/691549 JRC Contract No. 33545, N° ECHO/SER/2015/709788 JRC Contract No. 33957 and ECHO/SER/2016/732857 JRC Contract No. 34057 between DG ECHO and DG Joint Research Centre (DG JRC).

Introduction

ADAM is specifically designed to calculate the exposure to physical effects of an industrial accident in terms of thermal radiation, overpressure or toxic concentration resulting from an unintended release of a dangerous substance. The focus is on human health related impacts associated with thermal radiation from chemical fires, blast effects of vapour cloud explosions, and inhalation of toxic chemical vapours. Environmental consequences, which involve other vulnerable receptors, are beyond the scope of the current version of ADAM and are therefore not reported in this technical guidance.

Since ADAM is expected to address the overall consequence assessment cycle, ranging from unintended release of a dangerous substance (i.e., *loss of containment*) to the final physical effect (i.e., *top event*), and impact on humans (i.e., *vulnerability*), the overall structure of this tool consists of three interconnected calculus moduli:

- *Source Term* (Module 1)
- *Physical Effects* (Module 2)
- *Vulnerability* (Module 3)

The first module refers to the implementation of models for source term calculation i.e. estimate of the amount of substance released as a consequence of the assumed loss of containment. This estimate requires the knowledge of the type and amount of substance involved in the accident, the physical and storage conditions, the type and mode of rupture, and the release time. Each substance is characterised by specific thermodynamic, fluid mechanic and transport properties, which may influence significantly the release behaviour. These properties were gathered and stored in the ADAM database and are available for the consequence analysis calculations. The thermodynamic conditions of the storage (typically pressure and temperature) highly influence the release outcome. In particular, a substance may be stored as a compressed gas, a non-boiling liquid or a pressurised liquid.

The second module uses the outcome of module 1 to estimate the physical effects resulting from the accidental development following the loss of containment in terms of thermal radiation of the chemical fire, explosion of the flammable cloud, or dispersion of a toxic vapour into the atmosphere. This calculation is normally influenced by the atmospheric conditions (i.e., air temperature, air stability, wind speed) and by other parameters such as for instance average time for vapour dispersions or ignition time or ignition location for flash fires and vapour explosions.

The third module is designed to transform the exposure to physical effects calculated in module 2 into the resulting effects on humans using lethality or damage levels by using probit functions or reference threshold levels such as Protective Action Criteria (PAC) for inhalation toxicity or other empirical average criteria for fires and explosions.

The overall structure of ADAM is depicted in Figure 1.

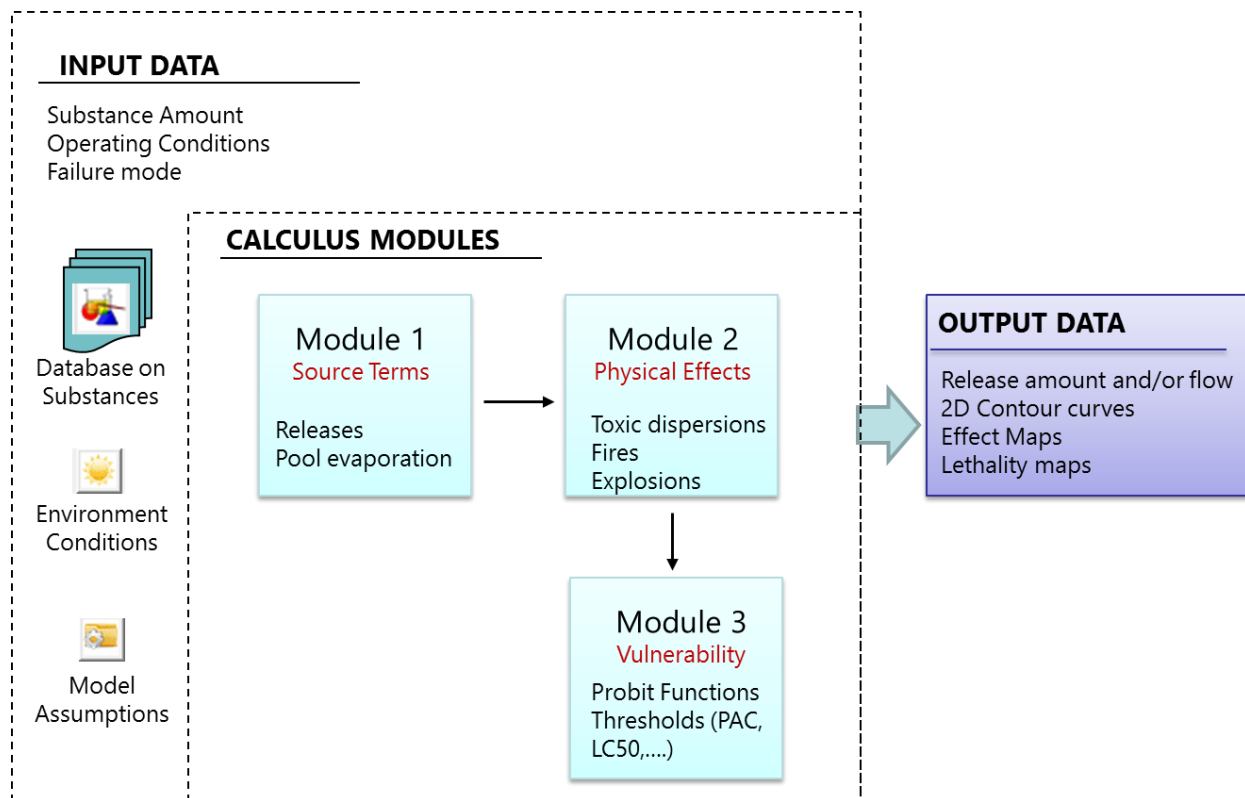


Figure 1: ADAM structure

In addition to the three calculus moduli, there is a series of *auxiliary modules* that are necessary to run the models. In particular:

- *Input Data* module: for the scenario description and associated data (i.e. substance type and amount, operating conditions and failure mode);
- *Database on Substances*, containing the physical properties of the dangerous substances and the Probit parameters of the vulnerability models;
- *Environmental Conditions*: to set air, weather and territorial conditions;
- *Model assumptions* to select some model criteria and assumptions amongst the available alternatives;
- *Output Data module*: to provide the results of the calculations. This will consist of graphs depicting the relevant parameters of the accident releases and iso-effect contours and maps to depict the consequences and lethality curves. These can also be obtained in kml or gpx formats. Output data can also be obtained in tabular forms such as Excel sheets.

SOURCE TERMS CALCULATION

(Module 1)

Source Term

The first module refers to the calculation of source term, i.e. the estimate of the amount of substance released as a consequence of the loss of containment. This estimate requires the knowledge of type and amount of substance involved in the release, physical and storage conditions, type and mode of rupture, and release time.

ADAM addresses a variety of different accident scenarios. These depend upon several factors:

	DESCRIPTION
STORED SUBSTANCE	Outflow scenario depends on the properties of stored material
THERMODYNAMIC STATE OF STORED SUBSTANCE	Compressed vapour, non-boiling liquid (i.e. pure liquid), and pressurised liquefied gas (i.e. vapour and liquid at saturation condition)
STORAGE GEOMETRY	Horizontal or vertical cylinder vessel, sphere
RUPTURE TYPE	Catastrophic rupture, release from an orifice, release from a leak or a rupture from a pipe

Table 1: Key factors on accident scenarios

Each substance is characterised by specific thermodynamic, fluid mechanic and transport properties, which may influence significantly the release behaviour. Depending on model used, failure mechanism, and level of detail required, the substance information that is necessary to execute the source term calculation may vary even quite significantly. All the required information is collected in the ADAM database.

The storage thermodynamic conditions (typically pressure and temperature) are very influential on the release dynamic and outcome. In particular, the substances may be stored as:

- *Compressed vapour*; when superheated with respect to the saturated state at the storage pressure (i.e. the storage temperature is higher than the saturation temperature at the storage pressure). In this case, the release is vapour only.
- *Non-boiling liquid (i.e. pure liquid)*; when subcooled with respect to the saturated state at the storage pressure (i.e. the storage temperature is lower than the saturation temperature at the storage pressure). Typically, this is the case of substances stored as liquids at ambient temperature and pressure such as many petrochemical products (e.g., gasoline, kerosene, diesel oil), but also includes refrigerated liquefied gases. In this case, the release could be either liquid or two-phase depending on initial superheat.
- *Pressurised liquid*; when the storage temperature and pressure are in a saturation condition, or the storage pressure is above saturation level. In this case, both liquid and vapour are present in the vessel and the release is two-phase either due to substance flash after release or because of two-phase mixing within the vessel.

With the exception of materials stored as compressed vapours, storage geometry also influences the release dynamic. ADAM covers the following vessel types: vertical, horizontal, and sphere. Geometrical location of the rupture also plays an important effect on release behaviour. *For non-boiling liquids at ambient pressure*, the vessel hole or pipe have to be located under the liquid level, otherwise there is no substance outflow (except from the pad gas layer above it or the evaporated vapours from the refrigerated liquefied gases). *For pressurised liquids* (saturated or above saturation) the situation is more complex. A release is expected also when the hole/pipe is above the liquid level, because of substance flash occurring within the vessel due to depressurisation.

Finally, ADAM addresses the possible catastrophic releases from vessel of compressed vapours, non-boiling liquids, and pressurised liquids.

Depending on the first input parameters selected by the operator (i.e. substance, storage condition and type of rupture), ADAM automatically sets the category of model to be used. Particular attention should be paid to those cases in which the substance is initially in a supercritical state (i.e. storage pressure and temperature higher than the critical pressure P_{cr} and the critical temperature T_{cr}). In such a case, the assumptions made and the models used might not function properly, and the programme gives a warning.

The main output of Module 1 (Source Term) consists of the following information:

- release flow rate at the rupture exit or overall amount of the substance released in case of a catastrophic rupture;
- other relevant parameters, such as for instance, substance pressure, temperature, vapour quality and discharge velocity at rupture exit;
- vessel response during outflow (i.e. how internal parameters vary with time);
- flow behaviour and thermodynamic state in the near region after rupture exit caused by depressurisation (i.e. flashing), if present;
- droplets formation and rainout calculation to estimate the amount of release that remains airborne and the part of liquid forming a pool;
- Evaporation rate and other relevant parameters when a release of non-boiling liquid or a release with pool formation are involved.

Outflow of compressed vapours and vessel response

The present section describes the dynamic behaviour of a compressed gas in a vessel during outflow from a leak (e.g. corrosion), a hole (e.g., flange rupture, safety valve malfunctioning), or a pipe connected to it. The gas expansion due to outflow will result in a decrease of gas temperature (cooling) and pressure (decompression).

Gas outflow is considered *isentropic* (absence of friction), and gas transformation within the vessel is assumed *adiabatic* by default. As an alternative, this transformation can also be considered as *isothermal*, to simulate those cases in which an exothermal reaction occurs, and for which the cooling due to gas expansion is compensated by the energy produced by the reaction. This option can be set in the ADAM Option menu.

Knowledge of gas density as a function of pressure and temperature is of key importance in the outflow prediction. ADAM allows the use of different equation of states, which can be selected in the Option menu, particularly:

1. Ideal gases
2. Soave modification of Redlich–Kwong (Redlich, 1949)
3. Peng–Robinson (Peng, 1976)

Soave Redlich–Kwong is used by default. The operator can modify this in the Option menu, however the use of the Ideal gas approximation is never recommended. This was included only for comparison purposes with other tools that make use of this approximation. In future, we intend to incorporate the GERG-2008 equation of state (Kunz and Wagner, 2012) to deal with the supercritical cases (very high pressures) typical of pipelines.

The overall iterative procedure in which the gas outflow is described in minor steps used within ADAM is as follows:

1. Setting of initial conditions, i.e., storage temperature T_0 (K), gauge pressure P_0 (barg) and calculus of the initial gas density ρ_0 (kg/m^3) by using the selected equation of state. Calculus of the initial flow rate q_0 (using the equations 4 or 7, described in the following pages).
2. Selection of the first time step Δt_1 (s), which is set on the basis of the ratio between the initial amount of substance released and the total mass of the substance contained in the vessel (<0.2%). From this step on, an iterative procedure starts.
3. Calculus of the reduced gas mass m_1 (kg) within the vessel, as a consequence of the gas outflow. The gas density ρ_1 (kg/m^3) is simply calculated by assuming constant volume.
4. Calculus of reduced gas pressure P_1 (bar) and temperature T_1 (K) caused by gas expansion, assuming an adiabatic isentropic transformation (T is not recalculated if the isothermal assumption is made).
5. Calculus of flow rate q_1 by using the same equation in step 1 but using the newly calculated parameters derived in step 4, along with an updated time step.

Steps 3 to 5 are repeated iteratively until the pressure within the vessel approaches ambient pressure P_a (the lowest limit of flow rate considered in ADAM is 0.002 Kg/s).

To account for adiabatic isentropic transformation, the reduced pressure and temperature within the vessel at i -th iteration step are calculated by using the following expressions²:

$$P_i = P_{i-1} \frac{z_i}{z_{i-1}} \left(\frac{\rho_i}{\rho_{i-1}} \right)^\zeta \quad (1)$$

$$T_i = T_{i-1} \left(\frac{z_{i-1}}{z_i} \right)^{\frac{\zeta-1}{\zeta}} \left(\frac{P_i}{P_{i-1}} \right)^{\frac{\zeta-1}{\zeta}} \quad (2)$$

with the Poisson ratio $\zeta(-)$ given by:

$$\zeta = 1 + z \frac{R}{c_V M_W} \quad (3)$$

and

- z gas compressibility factor (-),
- R gas constant (i.e. 8,314472 JK⁻¹mol⁻¹)
- c_V specific heat at constant volume (J kg⁻¹K⁻¹)
- M_W molecular weight (kg mol⁻¹).

The above equations are also based on the assumption that the vessel is not deformable i.e., with constant volume. ADAM also takes into account the case of isothermal outflow, to simulate those cases associated with exothermal reaction within the vessel.

Some care should be taken in all those situations in which cooling, due to depressurisation, would lead to a stagnation temperature that approaches the melting temperature. In such a case, condensation will affect the flow significantly.

Flow rate of an outflow from a leak or hole in a vessel

By assuming isentropic outflow at the vessel release exit (i.e. orifice), the following relation gives the expression of the gas flow rate, q (kg/s):

$$q^{hole} = C_d A_h \sqrt{2 c_p \frac{M_W}{R} \frac{\rho P}{z} r \left(\frac{z}{\zeta} \right) (1-r) \left(\frac{\zeta-1}{\zeta} \right)} \quad (4)$$

² From the adiabatic isentropic assumption: $C_v dT + P dV = 0$, where C_v (J K⁻¹) is the heat capacity, and considering the gas equation of state: $P = z \rho RT/M_W$, resulting in: $dT/T = -z R/(c_v M_W) dV/V$, where c_v is the specific heat at constant volume. By integrating this equation, the above expressions are obtained.

in which:

r	critical pressure ratio, i.e. $r = (P_{exit}/P) / (z_{exit}/z)$ (-)
C_d	discharge coefficient (-)
A_h	orifice area (m ²)
P	stagnation pressure within the vessel (Pa)
P_{exit}	pressure at the orifice (Pa)
ρ	gas density within the vessel (K)
M_w	substance molecular weight (kg mol ⁻¹)
z	gas compressibility factor within the vessel (-)
z_{exit}	gas compressibility factor at the orifice (-)
R	gas constant (i.e. 8,314472 JK ⁻¹ mol ⁻¹).

The gas properties at the orifice (indicated with the suffix *exit*) depends mainly on the ratio between ambient pressure P_a and stagnation pressure P (i.e. the pressure within the vessel). When this ratio is above a critical value, i.e.:

$$\frac{P}{P_a} \geq \left(\frac{\zeta + 1}{2} \right)^{\frac{\zeta}{\zeta - 1}} \quad (5)$$

the flow presents a “*choked*” behaviour (sonic) i.e., the gas will move across the hole at its maximum possible speed that is the local speed of sound in the gas (i.e. the Mach number $M = 1$). In this case, the gas pressure at the orifice is critical and given by the following relationships:

$$P_{exit} = P \left(\frac{2}{\zeta + 1} \right)^{\frac{\zeta}{\zeta - 1}} \quad (6)$$

Otherwise, the flow is said “*unchoked*” (subsonic), the gas exit speed is smaller than the local speed of sound in the gas (i.e. the Mach number $M < 1$), and the gas exit pressure at the orifice is equal to the atmospheric pressure P_a .

The discharge coefficient C_d (-) accounts for the phenomenon of *vena contracta* consisting of a reduction in the cross-sectional area flow at the exit, when compared to the actual orifice surface. This coefficient depends on the type of orifice and on the P/P_a ratio. For sharp edged orifices, C_d is approximately about 0.6 in the incompressible flow regime (i.e. unchoked flows with lower pressure drops) and slightly below 0.9 in the compressible regime (choked flows with high pressure drops). Since in most of the practical releases, compressed gases are under choked conditions, the recommended value in ADAM is equal to 0.88, which is a conservative choice.

Flow rate of an outflow from pipe failure

When a horizontal pipe (connected to a vessel) with constant diameter, fails (i.e., leak of bore-rupture), the flow rate can be expressed as follows:

$$q^{pipe} = A_h \sqrt{\frac{2 \int_{P_e}^P \rho(P') dP'}{f_D \left(\frac{L_p}{D_p}\right) + \sum_i K_i}} \quad (7)$$

in which:

- A_h orifice area (m²)
- P stagnation pressure within the vessel (Pa)
- P_e pressure at the downstream point of the pipe (Pa)
- ρ gas density within the pipe (Kg/m³)
- L_p Distance from pipe inlet to rupture (m)
- D_p inner pipe diameter (mm)
- f_D Darcy friction factor (-)
- K_i i-th loss term (pipe inlet, pipe exit, fittings) (-)

The Darcy friction factor f_D , accounts for the flow loss due to friction with the walls of the pipe and can be determined by using the following relation (Papaevangelou, 2010; Brkić, 2011):

$$f_D = \frac{0.2479 - 0.0000947 (7 - \log_{10}(Re))^4}{\log_{10}^2 \left(\frac{\epsilon}{3.615 D_p} + \frac{7.366}{Re^{0.9142}} \right)} \quad (8)$$

with the Reynolds number (-):

$$Re = 4 q / (\pi D_p k_g) \quad (9)$$

- ϵ roughness of the inner surface of the pipe (mm)
- k_g kinematic viscosity of the gas (Pa s)

The term $\sum_i K_i$ represents all other sources of frictional losses in the pipe, such as pipe inlet, pipe exit and all fittings i.e., elbows, tees, valves and reducers, representing a significant pressure loss in most pipe systems. ADAM takes this term into account by using the 2K method (Hooper, 1981, Darby 2001). This method allows characterising pressure loss through fittings in a pipe, and in turn the term K_i , for each frictional loss source, by using two K coefficients:

$$K_i = \frac{K_{1i}}{Re} + K_{\infty i} \left(1 + \frac{25.4}{D_p(\text{mm})} \right) \quad (10)$$

The terms K_{1i} and $K_{\infty i}$ for each frictional loss term, were empirically obtained and are labelled for quite a large number of different fittings (Hooper, 1981). These values are included in the ADAM database.

A special case is the frictional loss term for *pipe inlet* and *pipe exit*, for which the size correction term (i.e., $25.4/D_p$) does not apply and equation (10) is simplified as follows:

$$K = \frac{K_1}{Re} + K_\infty \quad (11)$$

Specific K_1 and K_∞ values are available for pipe entrance and pipe exit, depending on their geometry. These are also included in the ADAM database.

Since K_i and f_D depend on the Reynold number, and in turn, on the flow rate q , the above equations are solved in ADAM, iteratively, by using the following procedure:

1. Estimation of pressure at the downstream point of the pipe P_e within the range: P_a (atmospheric pressure) and P_h (vessel stagnation pressure). The downstream point is the inner pipe point that corresponds to the position where the pipe opening is located (either the hole or the full-bore rupture).
2. Calculus of the gas flow rate by using the equation valid for the release from a hole from vessel $q^{hole}(P = P_e)$ (eq. 4) by assuming a stagnation pressure equal to P_e .
3. Calculus of the Reynold number (eq. 9).
4. Calculus of the Darcy friction factor f_D from eq. 8 by using the Reynold number as calculated in step 3, and calculus of the gas flow rate by using the equation of release from pipe (eq. 7).
5. Comparison of the two values of the gas flow rate from step 2 and 4, and if they are not equal within a tolerable value, repeat the procedure from step 1 by changing the pressure guess at the downstream point of the pipe (P_e).

The above procedure is implemented in ADAM by using two separate functions based on Brent's method (Numerical Recipes, 1992).

Outflow of non-boiling liquids and vessel response

The liquid substance contained in the vessel is in a subcooled state, i.e., its storage temperature T is below its boiling temperature T_b at ambient pressure P_a . Thus, there is no flash during release and the release type is a pure *liquid*. Clearly, the vessel hole or pipe rupture have to be located under the liquid level, otherwise there is no substance outflow (except for the pad gas layer above it).

In case of a leak or hole from vessel, the release flow rate can be calculated by using Bernoulli's equation, i.e.:

$$q^{hole} = C_d A_h \sqrt{2(P_h - P_a)\rho} \quad (12)$$

where ρ is the liquid density, P_h is the sum of the storage pressure (normally the ambient pressure P_a) and the hydrostatic term $\rho g \Delta h$, with Δh the difference between liquid level h_L and the distance of the hole centre from the vessel bottom h_{out} , ρ is the liquid density (kg/m^3), and g is the acceleration due to gravity (m/s^2).

For releases from pipes, the following equation is considered, with the parameters having the same meaning of the case presented in the previous section:

$$q^{pipe} = A_h \sqrt{\frac{2(P_h - P_e)\rho}{f_D \left(\frac{L_p}{D_p}\right) + \sum_i K_i}} \quad (13)$$

where P_h is the stagnation pressure (i.e. pressure of the gas pad above the liquid plus the hydrostatic head), and P_e is the downstream pressure in the pipe in correspondence to the pipe rupture. Darcy friction factor f_D , and the losses coefficients are as in the case for compressed gases (equations 8 and 10). Note that the dependency of f_D and K_i on q via the Reynold number requires the resolution of eq. (13) via the iterative procedure described in the previous section, which was addressed to estimate the pressure at the downstream point P_e . Clearly, in this case it is necessary to use the appropriate equation for the release of a liquid from a hole (i.e. eq. 12) instead of eq. 4).

Again, the overall approach to assess the process dynamic and the vessel response is similar to the previous case:

1. Set of the initial conditions and calculus of liquid density. Calculus of the initial flow rate q_0 (using equations 12) or 13).
2. Selection of the first time step Δt_1 (s), which is set on the basis of the ratio between the initial mass outflow and the total mass contained in the vessel (<0.2%). From this step on, the iterative procedure starts.
3. Calculus of the reduced mass m_1 (kg) within the vessel, the associated volume V_1 , and in turn the reduced liquid level ($h_{L,1}$), as a consequence of the liquid outflow. The liquid level is obtained from the liquid volume in the vessel by inverting the expressions reported on the table below.
4. If the vessel is atmospheric and not sealed, storage pressure and temperature are considered constant during the liquid outflow. By contrast, if the vessel is sealed,

whilst the liquid drops internal pressure is reduced, due to a partial formation of vacuum in the upper part of the vessel and it is estimated by assuming that the gas above the liquid undergoes to an adiabatic transformation. When the sum of this pressure and the hydrostatic term is below the atmospheric pressure, the storage pressure is set again to the atmospheric pressure, since it is assumed that air will enter from the hole, resulting in the outflow gushes.

5. Calculus of the flow rate q_1 by using the same equation as in step 1 using the newly calculated parameters, and update of the time step.

Steps 3 to 5 are repeated iteratively until the pressure within the vessel approaches the ambient pressure P_a (the lowest limit of flow rate considered in ADAM is 0.002 Kg/s).

VESSEL GEOMETRY

VERTICAL CYLINDER	$V = \pi \frac{D^2}{4} h_L$
HORIZONTAL CYLINDER	$V = h_L \left(\frac{D^2}{4} \arccos \left(1 - \frac{2h_L}{D} \right) - \left(\frac{D}{2} - h_L \right) \sqrt{\left((D - h_L) h_L \right)} \right)$
SPHERE	$V = \frac{\pi}{3} h_L^2 \left(\frac{3}{2} D - h_L \right)$

Table 2: Liquid volume within the vessel vs liquid level

Outflow of pressurised liquefied gases and vessel response

The discharge from a leak or a hole from a vessel or from a pipe connected to a vessel containing a pressurised liquid is much more complex if compared with the previous two cases. The substance contained in the vessel is stored under saturated conditions or with a pressure above the saturation level. Both liquid and vapour phases are present and in an initial thermodynamic equilibrium within the vessel. During the outflow that follows a rupture, the metastable liquid undergoes to a rapid depressurisation (flash). Its temperature is initially kept constant by thermal inertia and the liquid is submitted to rapid evaporation to reach its equilibrium state, which occurs through bubble growth. Since a maximum surface exchange is key for evaporation, the jet will break into small droplets. Equilibrium will be established when partial vapour pressure at the vapour-liquid interface equals to that far away from the droplets. The presence of vapour and droplets makes the discharge a two-phase release.

The main factor influencing the type of scenario is the relative position of the rupture and the vapour-liquid interface. If the rupture is above the liquid level, a sudden depressurisation will take place (i.e. flash) and a two-phase release at the exit might occur depending on how close is the rupture from the liquid interface, the orifice size, and the ability of vapour bubbles to move across the liquid phase. If the rupture is near the liquid-vapour interface, the liquid swells due to its volume increase after depressurisation, which may lead to a two-phase release. Finally, when the rupture is below the liquid-vapour interface, then the release will be liquid and it will remain as such until the liquid level remains above the hole. ADAM addresses all these situations by using the two main procedures described in the following sub-sections.

Hole-up procedure ($H_{hole} \geq H_L$)

This refers to the case in which the rupture is above the liquid level (i.e. $H_{hole} > H_L$). The immediate opening of a hole in a vessel or a pipe containing superheated liquid leads to a sudden depressurisation and, in turn, the formation of bubbles within the liquid phase via nucleation. Due to bubble formation, the liquid volume will expand by producing a liquid swell. The depressurisation level depends on the operation conditions, the rupture size and the substance properties. High storage pressures and great rupture sizes will lead to stronger depressurisation and larger liquid expansion. At the same time, the substance viscosity and foaming tendency play a relevant role in the amount of liquid swell. When the expanded liquid will reach the rupture exit, a two-phase release will occur. Since the two-phase mixture created within the vessel will be more or less skewed with a general tendency to form higher void concentration at the top, the resulting vapour quality (i.e. fraction mass of vapour in the mixture) at the rupture exit will depend upon the drift-flux model used.

Depending on the specific operating conditions, the rupture size and location, and the substance properties (i.e. viscosity and tendency to foaming) different situations may occur. When, after depressurisation, the vapour-liquid (VL) interface remains still below the rupture level, single vapour release will occur. This situation is referred to as *complete VL disengagement* and the outflow consists of vapour only. By contrast, when the entrainment of liquid droplets appear at the orifice, a two-phase release will occur. This situation is referred to as *partial VL disengagement*, which contains a variety of intermediate situations associated with different flow regimes (e.g. bubbly and churn). In

all these cases, the void distribution is skewed, with a tendency to have a higher concentration at the top. Finally, when the liquid swell is such that the void concentration tends to equal the average void concentration before rupture (i.e. the vessel will be filled with a homogeneous two-phase mixture after depressurisation), a homogeneous two-phase release will take place. This is the case of substances that have a high foamy tendency or/and when the venting time is very short due to a large rupture that can drive the VL interface up to the vessel top. This is referred to as *no VL disengagement*. All the different flow regimes addressed by ADAM are summarised in the table below:

	X_E	FLOW REGIME	DESCRIPTION
COMPLETE VL DISENGAGEMENT	1	Vapour	Liquid level is below the hole even after swell.
PARTIAL (STRONG) VL DISENGAGEMENT	<1	Two-Phase: Churn	Low viscosity fluids (liquid dynamic Viscosity < 0.1 Pa s) with no foaming tendency. This is the case of uniformly distributed vapour bubbles, characterised by irregular shape due to coalescence and dispersed in a continuous fluid. In this case, a high degree of VL disengagement is present. (Fisher, 1992; D. Alessandro, 2004).
PARTIAL (LIMITED) VL DISENGAGEMENT	<1	Two-Phase: Bubbly	High viscosity fluids (Liquid dynamic Viscosity > 0.1 Pa s) with no foaming tendency. This is the case of isolated uniformly distributed vapour bubbles, with shape (no coalescence) and dispersed in a continuous fluid. In this case, a low degree of VL disengagement is present (Fisher, 1992; D. Alessandro, 2004).
NO VL DISENGAGEMENT	x	Two-phase (homogeneous)	The depressurisation drives the VL interface up to the vessel top. Typical of foamy fluids and/or the venting time very short), which is achieved when the bubble rise velocity is negligible if compared to the superficial vapour velocity at the liquid surface. The vapour quality of the release at the exit is identical to that of the swelled liquid (Fisher Plant/Opns Prog, Fauske DIERS; Leung, 1989).

Table 3: Different flow regimes for releases with the rupture above the liquid level

In order to establish which is the main regime controlling the vessel dynamic and the release flow rate, the average liquid swell $\bar{\alpha}$ of the boiling liquid due to depressurisation have to be estimated. This depends on the ability of vapour bubbles to move across the liquid phase and finally to escape from the VL interface, which is strictly related to the physical behaviour of the liquid and the distribution of bubbles in the liquid. There are different drift-flux models to estimate the average void fraction that is formed in the liquid under steady state conditions (Viecenz, 1980). ADAM uses the results of the Design Institute for Emergency Relief System (DIERS report, 1983, Fisher, 1992), but using new closed-form analytical expressions for the two-phase release requirements developed by D'Alessandro (D'Alessandro, 2004).

According to the above results, during depressurisation, the superficial vapour velocity at the top of the liquid surface j_g and the average void fraction within the swelled liquid $\bar{\alpha}$ is given by the following relationship:

$$\frac{j_g}{U_\infty} = \frac{\alpha_T (1 - \alpha_T)^n}{(1 - p \alpha_T^m)(1 - C_0 \alpha_T)} \quad (14)$$

in which:

U_∞	characteristic bubble rise velocity (m/s)
j_g	superficial vapour velocity (m/s)
C_0	the disengagement parameter (-)
$n, p,$ and m :	correlation parameters (-)
α_T	void fraction at the top of the liquid surface (-)

This is the dimensionless form of DIERS coupling expressions, where the dimensionless superficial vapour velocity $\psi_T = j_g/U_\infty$ is given as a function of the void fraction at the top of the liquid surface, α_T .

The superficial vapour velocity j_g can be easily expressed in terms of the vapour flow rate from the hole q_v :

$$j_g = \frac{q_v}{A_L \rho_V} \quad (15)$$

A_L	vessel cross-sectional area (m ²)
ρ_V	substance vapour density (kg/m ³)

The bubble rise velocity U_∞ in Eq. 14 can be expressed in terms of the substance properties:

$$U_\infty = k \left(\sigma g \frac{\rho^L - \rho^V}{\rho^{L^2}} \right)^{0.25} \quad (16)$$

in which:

σ	liquid surface tension (N/m)
g	the acceleration due to gravity (m/s ²)
ρ^L	substance liquid density (kg/m ³)
ρ^V	substance vapour density (kg/m ³)
k	dimensionless constant (1.53 and 1.18, for churn and bubbly flow behaviour, respectively)

The values for the correlation parameters n , p , and m determine the different flow regimes (i.e. $n=p=m=0$ for churn and $n=2, p=1, m=3$, for churn and bubbly, respectively).

The liquid swell is determined by the value of the average void fraction $\bar{\alpha}$ through an inversion of Eq. 14. Unfortunately, this equation does not contain $\bar{\alpha}$ explicitly, but the value at the top, α_T . These two variables are related by a rather complex functional dependency (transcendental), which for the sake of simplicity is not described here. Equations (11) and (12) of the previously mentioned paper (D'Alessandro, 2004) report

this functional dependency, which are used by ADAM to relate the average vapour void fraction to the dimensionless superficial vapour velocity $\psi_T = j_g/U_\infty$. The results of this numerical calculation are provided in Figure 2, which were conducted for the two flow regimes: Churn and Bubbly.

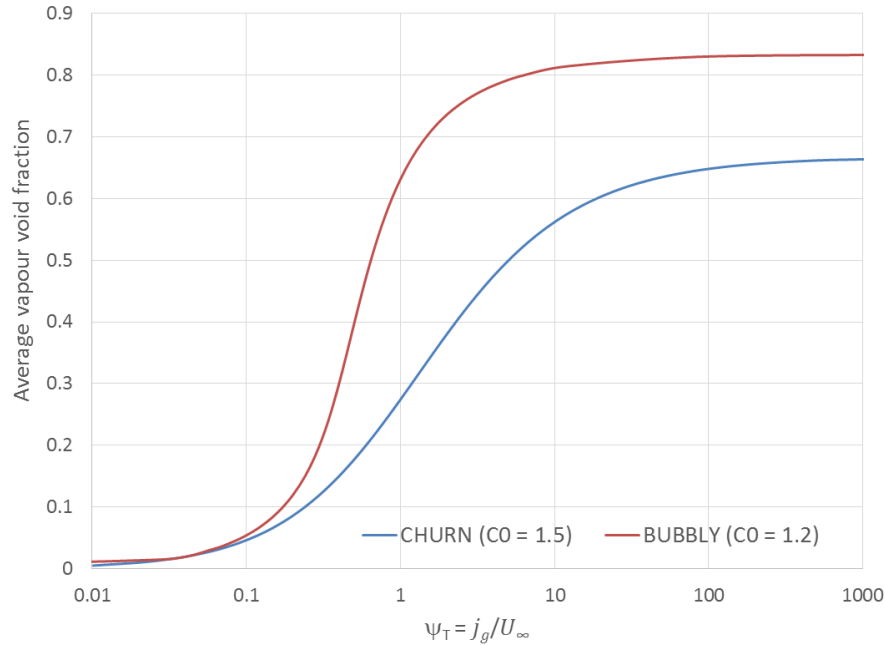


Figure 2: Average vapour void fraction $\bar{\alpha}$ vs the dimensionless superficial vapour velocity $\psi_T = j_g/U_\infty$ for Churn and Bubbly flow regimes (from equations (11) and (12) by D'Alessandro, 2004).

ADAM uses these curves to estimate the liquid swell by calculating first the dimensionless superficial vapour velocity, ψ_T . Whence the $\bar{\alpha}$ value is established, the expanded volume of the liquid within the vessel is determined:

$$V^{swell} = \frac{V_0}{(1 - \bar{\alpha})} \quad (17)$$

and, by inversion (see Table 2), it is possible to establish the swelled liquid level H_L^{swell} . This value is then compared to the rupture height H_{hole} to distinguish amongst the following situations:

$H_L^{swell} < H_{hole}$ (Complete VL Disengagement)

Since the hole is above the liquid level, the vapour quality $x_e = 1$ (vapour release only) and the vapour flow rate are simply calculated by using the standard formulas for vapour release from vessel or pipe (i.e. Equations 4 and 7).

$H_L^{swell} \geq H_{hole}$ (Partial VL Disengagement)

When the level swell reaches the exit hole, a two-phase release will occur. The resulting flow rate q (kg/s) of the two-phase mixture is given by the following expression:

$$q(x_e) = C_d A_h \sqrt{2(P_h - P_a) \rho_{2phase}(x_e)} \quad (18)$$

where the density of the two-phase mixture is given by:

$$\frac{1}{\rho_{2phase}(x_e)} = \frac{x_e}{\rho^V} + \frac{(1-x_e)}{\rho^L} \quad (19)$$

From equation 18, the dependence of q on the release vapour quality at the exit x_e can clearly be observed.

Case Top Venting

When the venting occurs at the top of the vessel, the vapour quality, x_e can be calculated by using the following expression (D' Alessandro, 2004):

$$x_e = \frac{(K_1 K_2 \Psi_T + C_0 K_4)}{(K_1 + C_0 K_4)} \quad (20)$$

$$K_1 = \frac{(1 - C_0 \alpha_T)}{\alpha_T}; \quad K_2 = \frac{A_L \rho_V U_\infty}{q(x_e)}; \quad K_4 = \frac{\rho^V}{\rho^L} \quad (21)$$

A point to note is that x_e is dependent on q via the dimensionless coefficient K_2 , therefore, in order to determine q and x_e it is necessary to solve equations 18 and 20 simultaneously by also taking into account the dependency between α_T and $\bar{\alpha}$. In ADAM, this is done by using an iterative procedure based on Brent's method (Numerical Recipes, 1992).

Case Side Venting

When the rupture is in the sidewall of the vessel, it is necessary to estimate the void fraction profile within the vessel. By assuming a simple linear profile, the local void fraction in correspondence of the rupture is given by (Britter, 2011):

$$\alpha_{hole} = \alpha_B + \frac{(\alpha_T - \alpha_B) H_{hole}}{H_L^{swell}} \quad (22)$$

where the void fraction at bottom, α_B is simply given by: $2\bar{\alpha} - \alpha_T$. In such a case the vapour quality at the vessel exit is related to Eq. 22 by the relation below, and the flow rate is calculate by using Eq. 18.

$$x_e = \frac{\alpha_{hole} \left(\frac{\rho^V}{\rho^L} \right)}{1 - \alpha_{hole} \left(1 - \frac{\rho^V}{\rho^L} \right)} \quad (23)$$

$H_L^{swell} \geq H_{vessel}$ (No VL Disengagement)

When the estimate of $\bar{\alpha}$ leads to a value of the swelled liquid height that is higher than the height of the vessel, since the liquid volume cannot expand to a level to exceed the vessel volume, it is assumed that the liquid reaches the vessel top and a homogeneous flow regime takes place. In such a case, the vapour quality at the rupture exit will be identical to that of the two-phase mixture within the vessel. The release flow rate is calculated by using eq. 18.

Vessel Dynamic during outflow

As for the previous cases, an iterative procedure is used to assess the process dynamic and the vessel response. At the process start, the initial conditions, the calculus of initial flow rate q_0 and the initial vapour quality at the exit are set. This is done according to the specific flow regime as described in the previous section. In addition, a first time step is set according to ratio between the initial mass outflow and the total mass contained in the vessel (<0.2%).

For each time step, the temperature decrease $\Delta T = T_{i+1} - T_i$ due to the liquid evaporation within the vessel is estimated. This is done by assuming mass conservation:

$$\begin{aligned} Q_{i+1}^L &= Q_i^L - q_{e_i}(1 - x_{e_i})\Delta t - Q_{ev_i} \\ Q_{i+1}^V &= Q_i^V - q_{e_i}x_{e_i}\Delta t + Q_{ev_i} \end{aligned} \quad (24)$$

and volume invariance, i.e.:

$$\frac{Q_{i+1}^L}{\rho_{i+1}^L} + \frac{Q_{i+1}^V}{\rho_{i+1}^V} = \frac{Q_i^L}{\rho_i^L} + \frac{Q_i^V}{\rho_i^V} \quad (25)$$

where Q_i^L , Q_i^V , and Q_{ev_i} are respectively liquid mass, vapour mass, and evaporated mass present in the vessel at time t_i . By combining the above equations and assuming that the vapour and liquid density do not vary significantly within the concerned temperature range, the following expression holds true:

$$Q_{ev_i} = q_{e_i}x_{e_i}\Delta t + q_i\Delta t \frac{1}{\frac{\rho^L}{\rho^V} - 1} \quad (26)$$

which, is used to assess the temperature decrease, by assuming an adiabatic outflow:

$$\Delta T = Q_{ev_i} \frac{h_v(T_i)}{c_p(T_i) m_i} \quad (27)$$

where h_v (J kg⁻¹) and c_p (J kg⁻¹K⁻¹) are the latent heat of vaporisation and the specific heat, respectively.

Whence the temperature at step $i+i$ -th is obtained, all parameters are recalculated and the iteration continues until the exit conditions are reached (i.e. the internal pressure approaching the ambient pressure).

Hole-down procedure ($H_{hole} < H_L$)

When the rupture is below the liquid level, the depressurisation within the vessel will not occur, and the outflow at the orifice exit will appear as a metastable liquid, i.e. it is superheated since its temperature, close to ambient, is higher than its normal boiling point. After rupture, the pressurised liquid is released into the atmosphere by intersecting the vapour-pressure saturation curve. The flashing process resulting from the rapid liquid boiling leads to the formation of a two-phase jet with vapour and droplets. Smaller droplets will stay airborne and then evaporate as air is entrained into the two-phase jet. By contrast, greater droplets might rainout on the ground forming a boiling pool that would spread and consequently evaporate.

The specific development of the jet spread after flashing and the air entrainment is addressed in the next section. Here it is described the release at the exit orifice or pipe and the corresponding vessel dynamic.

For release from a hole in a vessel, since the outflow is a metastable liquid, the flow rate at the orifice is simply given by the following relation:

$$q_e^{hole} = C_d A_h \sqrt{2(P_h - P_a)\rho_L} \quad (28)$$

where P_h is the stagnation pressure within the vessel (Pa), which includes the hydrostatic head, P_a is the atmospheric pressure (Pa), and ρ_L is the density of the pressurised liquid. The vapour quality at the orifice exit will be simply equal to zero.

The situation is much more complex if the release is occurring from a pipe leak or a pipe rupture, connected to the vessel. This because after the opening, the pressurised liquid will start flashing even within the pipe, and the meta-stable assumption cannot be made. In order to estimate the release flow rate and the vapour quality at the pipe exit, ADAM implements the TPDIS model (Two Phase DIScharge of liquefied gases through a pipe) introduced by Kukkonen (Kukkonen, 1990). According to this model, the release flow rate from a horizontal pipe, after a first transient phase, can be assessed by estimating the pressure P_e at the downstream point of the pipe where the rupture is located, by considering the critical flow condition:

$$\frac{\partial q_e^{hole}}{\partial P_e} = 0 \quad (29)$$

where:

$$q_e^{pipe} = A_h \sqrt{\frac{2(P_h - P_e)\rho_e^{2ph}}{f_D \left(\frac{L_p}{D_p}\right) \alpha_R + \sum_i \tau_i K_i}} \quad (30)$$

In which:

A_h	orifice area (m ²)
P	stagnation pressure within the vessel, which includes the hydrostatic head (Pa)
P_e	pressure at the downstream point of the pipe (Pa)
ρ_e^{2ph}	density of the two-phase mixture at pipe exit (Kg/m ³)

L_p	Distance from pipe inlet to rupture (m)
D_p	inner pipe diameter (mm)
f_D	Darcy friction factor (-)
K_i	i-th loss term (pipe inlet, pipe exit, fittings) (-)
τ_i	density ratio, ρ_e^{2ph} / ρ_i being ρ_i is the fluid density at i-th loss term location(-)

the volume ratio parameter α_R of eq. 30 is estimated via the following correlation (Van den Bosch, 2005 Chapter 2):

$$\alpha_R = \begin{cases} 1 - \frac{L_p}{10} & (0 \leq L_p < 3m) \\ 0.7 - (L_p - 3m) \frac{0.2}{17} & (3m < L_p \leq 20m) \\ 0.5 & (L_p > 20m) \end{cases} \quad (31)$$

The critical flow condition and, in turn, P_e , is estimated numerically by considering the following expression for the density of the two-phase mixture at pipe exit:

$$\rho_e^{2ph} = \frac{1}{\frac{x_e(P_e)}{\rho_e^v(P_e)} + \frac{1 - x_e(P_e)}{\rho_e^L(P_e)}} \quad (32)$$

where the vapour quality x_e of the two-phase mixture at the pipe exit is calculated by assuming the isentropic condition:

$$x_e(P_e) = \frac{T_e}{h_v(T_e)} \Delta S \quad (33)$$

Being T_e the saturated temperature of the two-phase at pressure P_e , and ΔS the entropy variation of the fluid between stagnation and exit conditions, i.e., $S(P_h) - S(P_e)$.

Darcy friction factor f_D , which is also dependent on P_e , is calculated from eq. 8 and the loss terms using the two-K method (i.e., eq. 10) for using the fittings' values of the ADAM database.

Vessel Dynamic during outflow

Also for this case, an iterative procedure is used to assess the vessel dynamic. By following the same approach as in the previous case, the temperature decrease at time step t_i is given by equation (27), with the following expression for the evaporated mass within the vessel:

$$Q_{ev_i} = q_{e_i}^{orifice} \Delta t \frac{1}{\frac{\rho^L}{\rho^v} - 1} \quad (\text{from orifice from vessel})$$

$$Q_{ev_i} = q_{e_i}^{pipe} x_{e_i} \Delta t + q_i^{pipe} \Delta t \frac{1}{\frac{\rho^L}{\rho^v} - 1} \quad (\text{from pipe}) \quad (34)$$

At each iteration step, all parameters are recalculated until the exit condition is met. This is achieved when the liquid level reaches the rupture exit. From this point on, the *hole-up* procedure described in the previous section will be activated, since depressurisation within the vessel takes place. A point to note is that the flow rate is significantly higher during the *hole* down process. Thus, an automatic assessment of the flow regime (i.e. vapour, bubbly or churn) is conducted only if the released mass, during the time preceding the arrival of the liquid level to the hole, is 10% smaller than the total mass of the substance within the vessel (i.e. when the initial liquid level is relatively close to the rupture). Otherwise, a vapour flow regime is imposed because the complete calculation would be an unnecessary sophistication. For pipes, due to the complexity of the phenomenon involved, a vapour flow regime is always considered.

Jet flashing, droplet formation and rainout

This chapter describes the behaviour of the liquid, gaseous or two-phase jet after loss of containment. It includes the calculus performed by ADAM to estimate the post-expansion parameters of flashing substances that follow the rapid depressurisation and expansion to atmosphere before air entrainment (see Figure 3). In addition, this section describes the mechanisms of droplet formation and the different droplet correlations used by ADAM to estimate the droplets' average size after jet release. Droplet average size, together with the droplets' distribution, are then employed to assess the mass fraction of droplets reaching the ground and that of those remaining airborne (rainout). This is particularly important because rainout reduces the airborne concentration and leads to an extended cloud duration due to the evaporation of the rained-out pool.

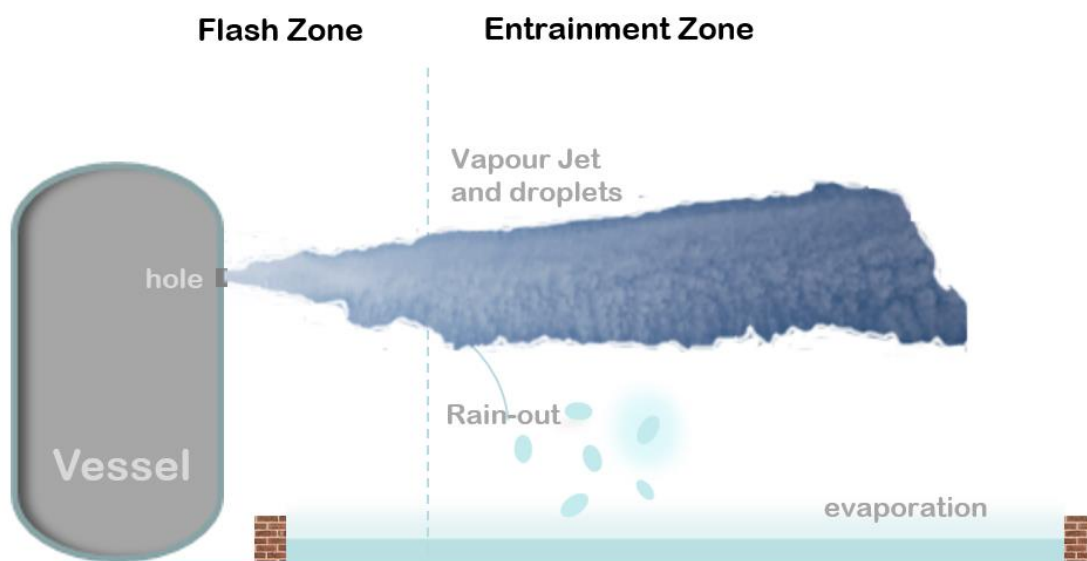


Figure 3: Release of a pressurised liquid: flashing, droplet formation and rainout.

Post-expansion parameters

A specific calculus module in ADAM addresses the depressurisation from the rupture plane to the environment (i.e., flashing). This phenomenon is typical of outflows involving pressurised liquids or compressed gases. By assuming one-dimensional flow behaviour together with the usual conservation laws, flashing is described by assessing the jet parameters on the ideal plane that separates the entrainment-non entrainment zone. This is where the final jet pressure reaches the atmospheric pressure P_a and the temperature is close (or equal) to the normal boiling temperature. In order to model this phenomenon, the jet is considered homogeneous (i.e. no phase-slip) and thermal equilibrium is assumed. Turbulence related effects, which may occur especially for high flash velocities, are here neglected.

The main output of this calculus module is the release post-expansion parameters, i.e.:

- jet velocity after flash v_f (m/s), i.e. a fictitious velocity, generally larger than the discharge velocity v_e (m/s), i.e. jet velocity at the orifice exit);
- flash temperature T_f (K);

- vapour quality after flash x_f (-);
- expanded cross-sectional area of the jet after flash A_f (m²) that is larger than the orifice area A_h (m²).

Two main different approaches have been followed to address the post-expansion process and the calculation of relevant parameters (Britter, 1994 and Britter, 1995). The first is based on the combination of conservation of *mass, momentum and energy* whilst in the second the energy conservation equation is replaced by assuming an *isentropic expansion*.

Although some attempts have been done to assess which of these two approaches is the best (Britter, 1994), a definite conclusion has yet not been established. In ADAM, both approaches are used for two-phase jets, in accordance to the corresponding droplet correlation, as selected from the literature (see next section). For compressed gases, we use always the isentropic assumption since it seems to provide better results (Witlox, 2002).

Calculation via conservation of mass, momentum and energy

Post-expansion jet velocity (flash velocity) v_f (m/s) is determined by combining mass and momentum conservation equations:

$$v_f = v_e + \frac{(P_e - P_a)}{q_e} \quad (35)$$

where the discharge velocity v_e (i.e., the outflow velocity at exit plane) is related to the flow rate and the fluid density at exit plane by:

$$v_e = \frac{q_e}{C_d A_h \rho_e} \quad (36)$$

The vapour quality of the jet after flash x_e can be obtained from energy conservation, i.e.:

$$H_f - H_e = -\frac{1}{2} (v_f^2 - v_e^2) \quad (37)$$

where H_f and H_e (J/kg) are the post-expansion jet enthalpy and the jet enthalpy at plane exit, respectively, which can be expressed as follows:

$$\begin{aligned} H_f &= x_f H_f^V + (1 - x_f) H_f^L \\ H_e &= x_e H_e^V + (1 - x_e) H_e^L \end{aligned} \quad (38)$$

By combining equations 37 and 38, the following expression for the flash quality x_f holds true:

$$x_f = 1 + \frac{(H_f^V - H_e^V) + (1 - x_e)(H_e^V - H_e^L) + \frac{1}{2} (u_f^2 - u_e^2)}{H_f^L - H_f^V} \quad (39)$$

which can be rewritten as follows:

$$x_f = 1 - \frac{\Delta H - (1 - x_e) h_v(T_e) + \frac{1}{2} (u_f^2 - u_e^2)}{h_v(T_f)} \quad (40)$$

where $h_v(T_e) = H_e^V - H_e^L$ and $h_v(T_f) = H_f^V - H_f^L$ are the latent heat of evaporation, at exit temperature and after flashing, respectively, whilst the enthalpy variation is given by:

$$\begin{aligned} \Delta H &= (H_f^V - H_e^V) = H^V(T_f, P_a) - H^V(T_e, P_e) = \\ &= - \int_{T_f}^{T_e} c_p^V dT \end{aligned} \quad (41)$$

In ADAM, ΔH is calculated from the specific heat data valid for ideal gases and using the residual enthalpy Abbot's correction (Green, 2007), i.e.:

$$\Delta H = H_f^R - H_e^R - \int_{T_f}^{T_e} c_p^{V \text{ id.gas}} dT \quad (42)$$

where $c_p^{V \text{ id.gas}}$ is the specific heat for ideal gases and H_f^R and H_e^R the residual enthalpy after post expansion and at the plane exit, respectively.

Whence the post expansion vapour quality is known, it is possible to calculate the jet density after flash ρ_f by considering the density of the jet single phases, and the expanded jet cross-sectional area A_f , by applying the conservation of mass:

$$\rho_f = \frac{1}{\left(\frac{x_f}{\rho_f^V} + \frac{1 - x_f}{\rho_f^L} \right)} \quad (43)$$

$$A_f = A_h C_d \frac{\rho_e v_e}{\rho_f v_f} \quad (44)$$

It was observed that the application of the current method might lead to an over estimate of the flash velocity (supersonic) due to turbulence effects (Witlox, 2002). In order to address this aspect ADAM introduces an optional cut-off velocity (i.e. speed of sound)

Calculation via Isentropic assumption (mass/momentum/entropy)

Post-expansion vapour quality is estimated first, via the isentropic assumption, i.e.:

$$S_f = S_e \quad (45)$$

where S_f and S_e ($\text{J K}^{-1} \text{ kg}^{-1}$) are the post-expansion jet entropy and the jet entropy at plane exit, respectively, which can be expressed as follows:

$$\begin{aligned} S_f &= x_f S_f^V + (1 - x_f) S_f^L \\ S_e &= x_e S_e^V + (1 - x_e) S_e^L \end{aligned} \quad (46)$$

that combined to eq. 45 leads to:

$$x_f = \frac{x_e (S_e^V - S_e^L) + (S_e^L - S_f^L)}{S_f^V - S_f^L} \quad (47)$$

For scenarios involving the releases of a pressurised liquid from a hole in a vessel, since the outflow is a meta-liquid at the plane exit, x_e can be assumed as equal to zero and eq. 47 becomes:

$$x_f = \frac{S_e^L - S_f^L}{S_f^V - S_f^L} \quad (\text{pressurised liquid}) \quad (48)$$

By contrast, in the case of compressed gases the vapour quality at plane exit is always equal to unity and eq. 47 becomes:

$$x_f = 1 - \frac{S_f^V - S_e^V}{S_f^V - S_f^L} \quad (\text{compressed gases}) \quad (49)$$

For scenarios involving the release from a pipe, eq. 47 in full has to be considered.

ADAM performs the calculation of the previous equations from the values of the specific heat as shown below. Abbot's correction is used for the case involving the specific heat of vapours (Green, 2007):

$$\begin{aligned} S_f^L - S_e^L &= S^L(T_f, P_a) - S^L(T_e, P_e) = - \int_{T_f}^{T_e} \frac{c_p^L}{T} dT \\ S_f^V - S_e^V &= S^V(T_f, P_a) - S^V(T_e, P_e) = - \int_{T_f}^{T_e} \frac{c_p^V}{T} dT \end{aligned} \quad (50)$$

with:

$$\begin{aligned} S_e^V - S_e^L &= \frac{h_v(T_e)}{T_e} + \int_{T_b}^{T_e} \frac{c_p^V}{T} dT - \int_{T_b}^{T_e} \frac{c_p^L}{T} dT \\ S_f^V - S_f^L &= \frac{h_v(T_f)}{T_f} + \int_{T_b}^{T_f} \frac{c_p^V}{T} dT - \int_{T_b}^{T_f} \frac{c_p^L}{T} dT \end{aligned} \quad (51)$$

All other parameters are calculated as in the previous case, i.e. combining mass and momentum conservation. It should be mentioned that the isentropic assumption is sometimes combined with the mass and energy conservation law without accounting for the momentum conservation law (e.g. in PHAST). This is not implemented in ADAM that adopts always the mass/momentum/entropy conservation laws for this case.

Aerosol droplets' formation and rainout

After post-expansion (or simply after release for non-boiling liquids), the liquid mass fraction of the jet (i.e., $1-x_f$) will break into aerosol droplets by two main mechanisms:

1. *mechanical brake-up*, independent of the jet thermodynamic state, which is normally produced on subcooled liquids relative to ambient conditions, which are also under enough pressure as they share forces resulting from the velocity difference between liquid and air;
2. *flashing brake-up*, which is very much dependent on the jet thermodynamic state and which is typically produced on superheated liquids (i.e. pressurised) during a depressurisation process.

The understanding of the formation of aerosol droplets and their entrainment in a vapour cloud is particularly important since aerosols increase cloud density and influence cloud dispersion behaviour. In addition, droplet size is directly associated with liquid mass fraction falling onto the ground after release (rainout), due to airborne concentration reduction and extended time duration of the dispersion phenomenon. The modelling of this process is rather complex, and the main influencing parameter is the initial mean diameter of droplets, which is estimated using empirical correlations. In actuality, droplets will have different diameters, which will follow a certain distribution. ADAM uses different correlations for the estimate of the Sauter Mean Diameter (SMD or d_{p32}) of droplets, which is defined as follows:

$$SMD = \frac{\int_0^{\infty} D^3 dD}{\int_0^{\infty} D^2 dD} \quad (52)$$

where D is the droplet diameter. The choice on SMD with respect to other means is because droplet size distributions with the same SMD have the same volume to surface ratio, which is very important in the rainout process. The different correlations, used by ADAM to determine the value of SMD for a determined release scenario, make use of the post expansion data, which were presented in the previous section. They can be selected in the option menu from a list of four, as briefly described hereunder.

1) TNO Yellow Book correlation

The first correlation is that proposed in the TNO Yellow Book and it is based on the work of Appleton (Appleton, 1984) and Wheatley (Wheatley, 1997), which describes a two-break up mechanism. Post expansion data are calculated by assuming mass/momentum/energy conservation laws and the following value for the droplets' mean diameter, SMD (m) is proposed:

$$SMD = \begin{cases} 1.89 d_f \sqrt{1 + 3 \frac{We_{cr}^{0.5}}{Re_f}} & \text{when } (We_{cr} < 10^6 Re_f^{0.45} \text{ and } T_e < 1.11 T_f) \\ \frac{We_{cr} \sigma_L(T_f)}{v_f^2 \rho_a} & \text{otherwise} \end{cases} \quad (53)$$

where the Weber and the Reynolds liquid numbers after expansion are given by:

$$We_{cr} = d_f \frac{v_f^2 \rho_f}{\sigma(T_f)} \quad \text{and} \quad Re_f = \frac{d_f v_f \rho_f}{\mu(T_f)} \quad (54)$$

with the post expansion parameters:

- d_f jet diameter (m)
- v_f jet velocity (m²/s)
- ρ_f jet density (kg/m³)
- ρ_a air density (kg/m³)
- $\sigma(T_f)$ surface tension between liquid and vapour (N/m)
- $\mu(T_f)$ jet dynamic viscosity (Pa s)
- We_{cr} critical Weber number, with a recommended value of 15 (-)

Since the Weber number is a measure of the ratio of the disruptive hydrodynamic forces to the stabilising surface tension forces, the critical number We_{cr} is a value below which mechanical break-up does not occur.

2) CCPS correlation

The second droplet size correlation used in ADAM is that proposed in the CCPP book by Johnson and Woodward (Johnson, 1999), which uses the isentropic assumption for the assessment post expansion parameters. The meta-stable liquid assumption for the expansion from stagnation to the orifice conditions is combined with the conservation of *mass/momentum/entropy* during jet expansion into the atmosphere, without assuming flashing at the orifice. The proposed approach assumes simultaneous mechanical and flashing break-up mechanisms with a droplet mean size given by:

$$SMD = \min[SMD_m, SMD_f] \quad (55)$$

where the first term is associated with the mechanical break-up:

$$SMD_m = \frac{We_{cr} \sigma_L(T_f)}{v_f^2 \rho_a} \quad (56)$$

The second term, SMD_f is given by the flashing break-up mechanism. The correlation to estimate this term was done by comparing rainout experimental data with a number of different parameters by concluding that the most relevant is the partial expansion energy, E_p (J/kg) given by:

$$E_p = -\Delta H - \frac{P_{sat} - P_a}{\rho_e} + \frac{|P_e - P_{sat}|}{\rho_e} \quad (57)$$

where:

$\Delta H = H_f - H_e$ (J/kg) is the enthalpy difference from exit to post expansion, ρ_e is the jet density at exit, P_{sat} is the saturated vapour pressure at exit temperature (i.e., $P_V(T_e)$), P_a is the external ambient pressure and P_e is the jet pressure at exit, which equals P_{sat} when

the stored liquid is under saturated conditions. The flashing term of the initial droplet mean size SMD_f (m) is then given by the following correlation that highlights the negative dependence of the initial droplet size with the partial expansion energy:

$$SMD_f = 833 \cdot 10^{-6} - 73.4 \cdot 10^{-6} \ln(E_p) \quad (58)$$

3) Modified CCPS

With regard to the CCPS correlation, a recent study argued that such a correlation tends to under predict the initial mean droplet size (Witlox, 2013). This would be mainly due to the fact that, being the correlation based on the minimum value of the mechanical and flashing brake-up contributions, it does not account for the degree of superheat that is a key parameter in the droplet formation mechanism. To cope with this potential drawback, the same study proposed a modified version of the original CCPS correlation consisting of assigning the mechanical break-up term to subcooled jets whilst using the flashing brake-up term for superheated jets, i.e.:

$$SMD_m = \begin{cases} SMD_m & P_a \geq P_{sat} \\ SMD_f & P_a < P_{sat} \end{cases} \quad (59)$$

It was shown that this correlation provides better results on the rainout estimate (Witlox, 2013).

4) JIP Phase III

This correlation is based on the work conducted in the framework of the Joint Industry Project (JIP) on liquid jets and two-phase droplet dispersion, which aimed at increasing understanding of the behaviour of subcooled and superheated liquids, and to improve the prediction of release flow rate, droplet formation, dispersion and rainout (Witlox, 2007, Witlox, 2010, Witlox, 2013). Final post expansion conditions are obtained via *mass/momentum/energy* conservation laws, and the initial mean droplet diameter, SMD is defined as a tri-linear function of the initial superheat, ΔT_{sh} (K). For lower values of ΔT_{sh} , the main regime governing the droplet formation is the mechanical break-up. For intermediate values of ΔT_{sh} there is a transition regime whilst for higher values of ΔT_{sh} flashing break-up dominates (Witlox 2010).

The initial superheat is defined as:

$$\Delta T_{sh} = T_0 - T_{sat}(P_a) \quad (60)$$

where T_0 is the stagnation temperature, and T_{sat} is the saturated temperature at the ambient pressure.

The mean droplet size is determined via the tri-linear function shown in Figure 4, which depicts the three regimes of mechanical brake-up (prior to point A), transition to flash (from point A to point B), and fully flashing (after point B). In the mechanical break-up zone the following SMD correlation is applied:

$$SMD = 74 d_h W e_{cr}^{-0.85} R e_e^{0.44} \left(\frac{L}{d_h}\right)^{0.114} \left(\frac{\mu_e}{\mu_w}\right)^{0.97} \left(\frac{\sigma_e}{\sigma_w}\right)^{-0.37} \left(\frac{\rho_e}{\rho_w}\right)^{-0.11} \quad (61)$$

where d_h is the diameter of the exit orifice (i.e. hole or pipe diameter), L is the vessel thickness in case of release from vessel hole or the pipe length in case of release from pipe, and all other parameters are defined as in the previous sections with the difference that they are not post expansion data (i.e., the 'e' subscript refers to the exit conditions). The subscript 'w' refers water, which properties are taken at standard temperature and pressure (i.e., 273.16K and 1atm). Cut-off values of the L/d_h ratio are taken as: 0.1 for $L/d_h < 0.1$ and 50 for $L/d_h > 50$.

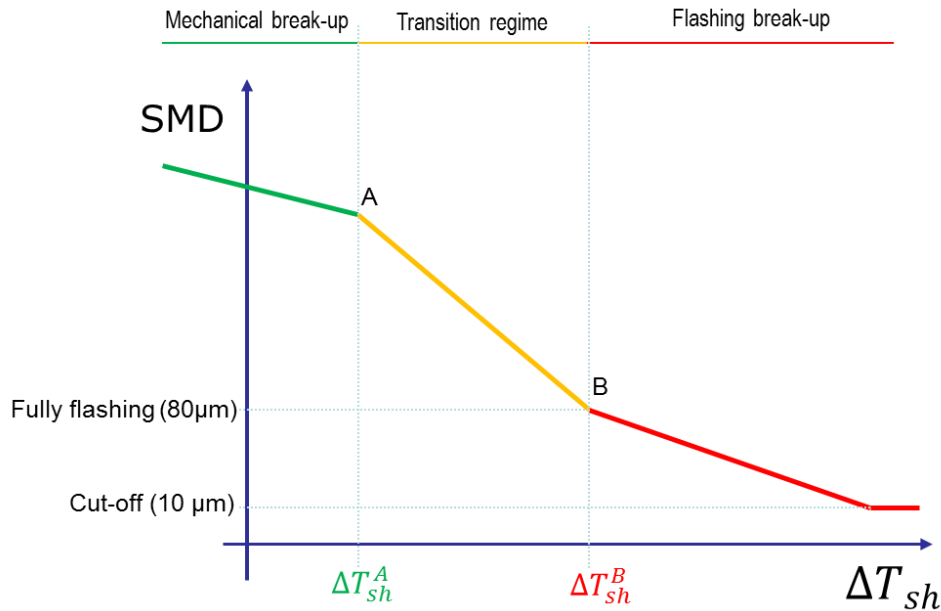


Figure 4: JIP correlation, tri linear function to determine SMD as a function of the superheat (from Witlox, 2010)

The determination of transition regime points A and B is conducted by using the following criteria to calculate the corresponding ΔT_{sh}^A and ΔT_{sh}^B values:

$$\text{Point A: } Ja^A \varphi = 48 We_{cr}^{-1/7} \quad (62)$$

$$\text{Point B: } Ja^B \varphi = 108 We_{cr}^{-1/7}$$

where the corrector factor φ is defined by Kitamura (Kitamura, 1986):

$$\varphi = 1 - \exp\left(-2300 \frac{\rho^V}{\rho^L}\right) \quad (63)$$

with ρ^V and ρ^L , the density of the vapour and liquid phase, calculated at the orifice temperature. The Jacob number, Ja is directly to the superheat through the following relationship:

$$Ja = \frac{c_p^L \Delta T_{sh}}{h_v} \frac{\rho^L}{\rho^V} \quad (64)$$

Where c_p^L ($J \text{ kg}^{-1} \text{ K}^{-1}$) is the specific heat of the liquid phase at constant pressure, and h_v ($J \text{ kg}^{-1}$) the latent heat evaporation, both calculated at the orifice temperature. By combining equations 62 and 64 it is possible to get ΔT_{sh}^A and ΔT_{sh}^B , respectively. A point to note is that

the We_{cr} number of eq. 62 is calculated from eq. 54, but using the parameters calculated at the orifice temperature (i.e., with 'e' subscript) instead of the post expansion data (i.e., with 'f' subscript).

Once the x-coordinates of points A and B are determined (i.e. ΔT_{sh}^A and ΔT_{sh}^B), the y-value of point A is determined by using eq. 61 whilst the y-coordinate of point B, which defines the start of fully flashing regime, is fixed at a value of 80 μm . Later on the SMD dependence on ΔT_{sh} is assumed to be characterised by a slope of - 0.1 $\mu\text{m}/\text{K}$ until it reaches at a cut-off value of 10 μm .

In ADAM the JIP Phase II correlation has been implemented by taking the vapour density at equilibrium ambient pressure, as suggested by Bitter et al. (2011)

Rainout

The calculus of the rainout, i.e. the total mass fraction that falls on the ground after release, is conducted in ADAM by following two main steps:

1. Determination of the single droplet mass fraction falling on the ground, as a function of the initial droplet diameter D .
2. Calculus of the total mass fraction after release by considering the overall droplet distribution with initial mean size diameter SMD and taking into account the result of the first step.

The rainout calculation is directly based on the droplets correlations, provided in the previous sections. For completeness, ADAM incorporates also some empirical correlations, which were developed using rainout data directly by DeVaul & King (DeVaul, 1992) and Lautkaski (Lautkaski, 2008). These have anyhow some inherent limitations of lacking generality obtained under specific conditions.

Single droplet rainout

The mass fraction of a single droplet reaching the ground after release is estimated by taking into account the motion equation of the droplet, which is assumed to be a liquid sphere with diameter $D(t)$, combined with the evaporation process and the related mass flux from the droplet surface to ambient air.

The overall phenomenon can be described by the following dimensionless numbers: the droplet Reynolds number, Re , the Schmidt number Sc (i.e. the ratio of viscosity to mass diffusion), and the Prandtl number Pr , (i.e. the ratio of viscosity to and heat diffusion), the Sherwood number Sh (i.e. the ratio of the total mass transfer to the purely diffusive mass transfer), and the Nusselt number Nu (i.e., the ratio of the total heat flux to the purely conductive heat flux) :

$$Re = \frac{\rho_a v_d D}{\mu_a}; \quad Sc = \frac{\mu_a}{\rho_a D_v}; \quad Pr = \frac{c_p^L \mu_a}{\lambda_a} \quad (65)$$

$$Sh = 1 + 0.276 Re^{1/2} Sc^{1/2}; \quad Nu = 1 + 0.276 Re^{1/2} Sc^{1/2}; \quad (66)$$

where ρ_a ($\text{kg} \cdot \text{m}^{-3}$), μ_a ($\text{Pa} \cdot \text{s}$), and λ_a ($\text{W} \cdot \text{m}^{-1} \text{K}^{-1}$) are density, dynamic viscosity and thermal conductivity of air, respectively. c_p^L ($\text{J kg}^{-1} \text{K}^{-1}$) is the droplet specific heat at constant pressure, v_D ($\text{m} \cdot \text{s}^{-1}$) droplet velocity relative to the surrounding air, and D_v ($\text{m}^2 \text{s}^{-1}$) binary diffusion coefficient of the vapour through air, which can be assessed using Graham's law of effusion (Thibodeaux, 1979):

$$D_v = D_v^{water} \sqrt{\frac{M_W^{water}}{M_W}} \quad (67)$$

where M_W and M_W^{water} are the molecular weights of the substance and water, respectively, and the binary diffusion coefficient of water vapour in air, D_v^{water} ($\text{m}^2 \text{s}^{-1}$) can be expressed as a function of ambient temperature (Tuve, 1976, Nellis, 2008) as follows:

$$D_v^{water} = -2.775 \cdot 10^{-6} + 4.479 \cdot 10^{-8} T_a + 1.656 \cdot 10^{-10} T_a^2 \quad (68)$$

A rainout criteria can be established by analysing the time dependence of the single droplet size with initial diameter $d_0 = SMD$. The rate of decrease of the diameter D of spherical droplets in air due to evaporation can be described by (Williamson and Threadgill, 1974):

$$\frac{dD(t)}{dt} = -\frac{k_B}{D(t)} Sh \quad (69)$$

where:

$$k_B = -4 D_v \frac{\rho_d^V}{\rho_d^L} \ln \left(\frac{1}{1 - \frac{P_v(T_D)}{P_a}} \right) \quad (70)$$

with ρ_d^V and ρ_d^L as the density of the vapour and liquid phases of the droplet substance and $P_v(T_D)$ is the saturation pressure of the released substance at droplet temperature T_d .

A point to note is that Eq. 69 is transcendental, since k_B and Sh depend on the droplet diameter D , and it has to be coupled with the equation of the droplet motion to determine the droplet velocity v_D (needed to assess the droplet Reynolds number) and with the heat balance to determine the droplet temperature T_D .

The droplet velocity can be obtained from the equation of motion (Holterman, 2003):

$$\frac{dv_D(t)}{dt} = -\frac{3}{4} \frac{\rho_a v_D^2 C_D}{\rho_d^L D(t)} \quad (71)$$

where C_D is the drag coefficient given by (Melhem, 1992):

$$C_D = \begin{cases} \frac{24}{Re} & (Re < 0.1) \\ 24/Re \left(1 + \frac{3}{16}Re + \frac{9}{160}Re^2 \ln(2Re)\right) & (0.1 \leq Re < 2) \\ \frac{24}{Re} (1 + 0.15 Re^{.687}) & (2 \leq Re < 500) \\ 0.56 & (500 \leq Re < 200000) \end{cases} \quad (72)$$

Droplet temperature T_d can be assessed from the heat balance by assuming that no kinetic energy is converted into thermal energy (Van den Bosch, 2005 Chapter 2):

$$T_d = T_a + h_v(T_d) k_B \rho_d \frac{Sh}{4 \kappa_a Nu} \quad (73)$$

ADAM is able to numerically solve the equations above in order to assess the droplet dynamic and in turn to estimate the droplet lifetime, t_{fl} (s), the stopping distance S_{dist} (m), and the droplet diameter $D(t_{fl})$ when the droplet falls into the ground (if ever). . Whence the final droplet diameter is known, the mass fraction of the droplet that remains airborne is simply given by:

$$x_{rain}^{sd} = 1 - \frac{D(t_{fl})^3}{D_0^3} \quad (74)$$

where x_{rain}^{sd} stands for the mass fraction of the single droplet (*sd*) that remains airborne. This quantity represents the vapour quality resulting from the single droplet after partial or total evaporation.

In order to save calculus time, a cut-off criterion is applied in ADAM: droplets that have an initial diameter greater than 5000 μm are considered to rainout entirely, whilst those having an initial diameter smaller than 20 μm are supposed to remain airborne. These assumptions are fully justifiable for release height of the order of few meters, typical of common industry.

Droplet distribution and rainout

Since the droplets formed after the release do not all have the same initial size, but they follow a distribution with an initial mean value expressed by the *SMD* parameter, in order to estimate the total amount of rainout mass, the procedure described hereunder is applied within ADAM.

For *M*-droplets, total mass of the jet that remains airborne, x_{rain} is given by:

$$x_{rain} = 1 - \frac{\sum_{i=1}^M n_i(D_i) x_{rain}^{sd}(D_i) D_i^3}{\sum_{i=1}^M n_i(D_i) D_i^3} \quad (75)$$

where $n_i(D_i)$ is the number of droplets having initial diameter equal to D_i with $\sum_{i=1}^M n_i(D_i) = M$, and $x_{rain}^{sd}(D_i)$ the vapour quality resulting from the single droplet after partial or total evaporation. If the distribution of droplets is known, Eq. 75 becomes:

$$x_{rain} = 1 - \frac{\int_{-\infty}^{\infty} p(D) x_{rain}^{sd}(D) D^3 dD}{\int_{-\infty}^{\infty} p(D) D^3 dD} \quad (76)$$

where $p(D)$ is the droplets' density function and D the initial droplet size, and $p(D)dD$ the probability that the droplet initial average size is within the $(D, D+dD)$ range.

Another relevant parameter is given by the centre of the evaporating pool, which corresponds to the average impact point of the jet portion that rainouts. This is determined by calculating the average ground distance of the impinging jet from the release point, i.e.:

$$X_{offset} = \int_{-\infty}^{\infty} p(D) X_{offset}^{sd}(D) dD \quad (77)$$

where X_{offset}^{sd} is the falling distance of the single droplet of diameter size D that is calculated by solving the droplet motion equation.

For the calculus of x_{rain} and X_{offset} , ADAM makes use the log-normal and the Rosin-Rammler distributions that can be selected in the option menu. These are given hereunder:

Log-normal (Woodward, 2014)

$$p(D) = \frac{1}{\sqrt{2\pi} \ln(\sigma_D) D} e^{-0.5 \left(\frac{\ln(D) - \ln(SMD)}{\ln(\sigma_D)} \right)^2} \quad (78)$$

where σ_D is the standard deviation of the normalised drop size distribution. Normally this parameter is in the range 1.3-1.9 (Norkus, 2010) and it can be inserted in the option menu. According to Johnson (Johnson, 1999bis), the recommended value in ADAM is 1.4, which is set as a default value.

Rosin-Rammler (Kay, 2010)

$$p(D) = a_{RR} \left(\frac{D}{SMD} \right)^{b_{RR}-1} e^{-a_{RR} \left(\frac{D}{SMD} \right)^{b_{RR}}} \quad (79)$$

where the two distribution coefficients a_{RR} and b_{RR} can be set to 0.422 and 5.32, respectively according to the work of Elkotb (Elkotb, 1982) or by using the suggested values following the JIP projects (Kay, 2010) as presented below:

$a_{RR} = \left\{ \begin{array}{l} 0.4 \\ \text{Linear between the two extremes} \\ 0.79 \end{array} \right.$	0.4	<i>if</i> $\Delta T_{sh} \leq \Delta T_{sh}^A$	(80)
	<i>Linear between the two extremes</i>		
	0.79	<i>if</i> $\Delta T_{sh} > \Delta T_{sh}^B$	
$b_{RR} = \left\{ \begin{array}{l} 5.32 \\ \text{Linear between the two extremes} \\ 0.97 \end{array} \right.$	5.32	<i>if</i> $\Delta T_{sh} \leq \Delta T_{sh}^A$	(81)
	<i>Linear between the two extremes</i>		
	0.97	<i>if</i> $\Delta T_{sh} > \Delta T_{sh}^B$	

ΔT_{sh} is the superheat and ΔT_{sh}^A and ΔT_{sh}^B are calculated, as for the procedure in the JIP droplet correlation (see previous section).

DeVaull and Lautkaski correlations

As previously mentioned, ADAM incorporates DeVaul and Lautkaski correlations (DeVaull, 1992; Lautkaski, 2008) to determine rainout, which can be selected in the ADAM option menu as an alternative approach to that described in the previous section. Both approaches refer to empirical calculations that are based on the CCPS rainout experiments of the AIChE (Johnson, 1999 bis) and that bypass modelling droplet size, droplet evaporation and motion.

The *DeVaull correlation* is based on uncorrected CCPS rainout data. It makes use of the adiabatic mixing curve for an air/aerosol mixture and depends on the substance volatility. More specifically, by defining *non-volatile substance* as having $(T_a - T_{as})/T_a < 0.14$, being T_a is the ambient temperature and T_{as} the adiabatic saturation temperature the rainout fraction x_{rain} is:

$$x_{rain} = 1 - \frac{1}{h_v} \int_{T_{as}}^{T_0} c_p^L dT \quad (82)$$

The adiabatic saturation temperature T_{as} is the minimum temperature reached by an equilibrium air/aerosol mixture, which occurs as the liquid dry out.

For *volatile substances*, defined when $(T_a - T_{as})/T_a \geq 0.14$:

$$x_{rain} = x^* \begin{cases} 1 - \left(\frac{x_f}{0.145}\right)^{1.8} & \text{if } x_f \leq 0.145 \\ 0 & \text{if } x_f > 0.145 \end{cases} \quad (83)$$

with the scaling factor defined as:

$$x^* = 1 - 2.33 \frac{T_a - T_{as}}{T_a} \quad (84)$$

The *Lautkaski correlation* is based on CCPS corrected rainout data. It does not depend on the volatility of the substance and in turn on T_{as} , and provides the following expression for the rainout fraction x_{rain} :

$$x_{rain} = 0.6 \left[1 - \left(\frac{Ja}{93}\right)^{1.36} \right] \quad (85)$$

where the Jacob number Ja is the dimensionless ratio of the substance superheat to enthalpy of vaporisation with an adjustment for the ratio of liquid and vapour densities:

$$Ja = \frac{c_p^L \Delta T_{sh}}{h_v} \frac{\rho^L}{\rho^V} \quad (86)$$

Discharge Coefficient

The discharge coefficient C_d (-) accounts for the phenomenon of *vena contracta* consisting of the reduction of the cross-sectional area flow with respect to the rupture area. As a result, the flow rate and, in turn, the discharge velocity will be smaller than their theoretical values. The main mechanisms involved consist of the frictional losses occurring in proximity of the rupture and the fluid contraction due to velocity components of the flow perpendicular to the rupture axis. The discharge coefficient depends on the type of orifice and on the flow's Reynolds number. For sharp edged orifices, C_d is approximately about 0.6 in the incompressible flow case (i.e. unchoked flows with low pressure drops) and slightly below 0.9 in the compressible case (choked flows with high pressure drops). For rounded orifices, the above mechanisms play a less relevant role and the discharge coefficient approaches to one. This last value should always be taken when the orifice shape is unknown or when the flow is characterised by a small Reynolds number.

In ADAM, the default discharge coefficient for the outflow of *non-boiling liquids* (i.e. incompressible fluids) is taken as $C_d^L = 0.61$. For *compressed gases*, since in most practical releases gases are under choked conditions, the recommended value is $C_d^V = 0.88$, which is a more conservative choice. However, it is possible also to set an automatic procedure by which the discharge coefficient can be calculated as a function of the outlet-to-inlet pressure b (Kostowski, 2012):

$$C_d^V = \begin{cases} 0.8674, & b \leq 0.3024 \\ 0.8236 + 0.4927b - 1.375 b^2 + 0.7443 b^3, & b > 0.3024 \end{cases} \quad (87)$$

For *pressurised liquids*, the flow is two-phase and the discharge coefficient is calculated by using the method proposed by Lenzing et al. (Lenzing, 1998) consisting of estimating C_d via a linear combination between the values valid for compressible and incompressible fluids by using the void fraction at inlet conditions $\alpha = x_e \rho_e / \rho^V$, i.e.:

$$C_d = \alpha C_d^V + (1 - \alpha) C_d^L \quad (88)$$

Catastrophic Releases

The total rupture of a vessel leads to the instantaneous release of its content into the atmosphere, possible ejections of fragments, and creation of a blast wave due to the expansion of the vessel content. The main reasons that are at the basis of a catastrophic rupture of the vessel are: (i) failure of its structural integrity (due to corrosion, fatigue, overheating, impact of an object, etc.) and (ii) overpressure due to possible run-away reactions, internal explosion, overheating, overfilling, and failure of pressure measuring units. The following sections provide information on the procedure employed in ADAM to assess all relevant parameters associated with the release of hazardous substances stored as compressed gases or pressurised liquefied gases due to instantaneous loss of containment resulting from the catastrophic failure of a vessel. For hazardous substances stored as non-boiling liquids (i.e. pure liquids), the main physical phenomenon involved is described by the pool evaporation resulting from the release, which will be addressed in the following chapter.

The sudden depressurisation of a compressed gas or a pressurised liquefied liquid, which results from a sudden loss of containment is modelled as an isentropic expansion. For pressurised liquids, the final temperature T_f of the expanded mixture is assumed to equal the substance's normal boiling temperature T_b . For compressed gases, the expansion is modelled as a series of isentropic sub-expansions for which temperature and pressure at the i -th expansion step can be estimated by using the corresponding values at the proceeding step $i-1$ -th:

$$T_i = T_{i-1} \left(\frac{z_{i-1}}{z_i} \right)^{\frac{\zeta-1}{\zeta}} \left(\frac{P_i}{P_{i-1}} \right)^{\frac{\zeta-1}{\zeta}} \quad (89)$$

where $\zeta(-)$ and $z(-)$ are the Poisson ratio and the gas compressibility factor, respectively. The reason why in ADAM the overall expansion is described as a series of sub-expansion is because the direct application of eq. 89 on the initial and final states would lead to a quite inaccurate value of ζ , since this is averaged within the initial and final states.

Post-expansion vapour quality x_f is estimated first, via the isentropic assumption, i.e.:

$$S_f = S_{st} \quad (90)$$

where S_f and S_e ($\text{J K}^{-1} \text{kg}^{-1}$) are the substance entropy after expansion and under storage conditions, respectively. These can be expressed as follows:

$$S_f = x_f S_f^V + (1 - x_f) S_f^L \quad (91)$$

$$S_{st} = x_{st} S_{st}^V + (1 - x_{st}) S_{st}^L$$

that combined together leads to:

$$x_f = \frac{x_{st} (S_{st}^V - S_{st}^L) + (S_{st}^L - S_f^L)}{S_f^V - S_f^L} \quad (92)$$

For compressed gasses the storage vapour quality is simply equal to unity ($x_{st} = 1$), whilst for pressurised liquids it can be estimated from the vessel fill level φ , and the densities of the liquid and vapour phases of the substance calculated at the storage pressure and temperature:

$$x_{st} = \frac{1}{\left(1 + \frac{\rho_{st}^L}{\rho_{st}^V} \frac{\varphi}{(1 - \varphi)}\right)} \quad (93)$$

Eq. 92 is calculated by using the following expressions, in which Abbot's correction is used for the case involving the specific heat of vapours (Green, 2007):

$$\begin{aligned} S_{st}^V - S_{st}^L &= \frac{h_v(T_{st})}{T_{st}} + \int_{T_b}^{T_{st}} \frac{c_p^V}{T} dT - \int_{T_b}^{T_{st}} \frac{c_p^L}{T} dT \\ S_{st}^L - S_f^L &= \int_{T_f}^{T_{st}} \frac{c_p^L}{T} dT \\ S_f^V - S_f^L &= \frac{h_v(T_f)}{T_f} + \int_{T_b}^{T_f} \frac{c_p^V}{T} dT - \int_{T_b}^{T_f} \frac{c_p^L}{T} dT \end{aligned} \quad (94)$$

The expansion energy E_p (J kg⁻¹) is calculated from energy, momentum, and mass conservation:

$$E_p = \Delta H - \frac{P_{st} - P_a}{\rho_{av}(T_{st})} \quad (95)$$

where ρ_{av} is substance average density within the vessel that, in the case of pressurised liquids accounts also for the presence of a vapour phase. The Enthalpy variation ΔH (J kg⁻¹) from the initial state (i.e. storage conditions) to post expansion is calculated from:

$$\Delta H = H_{st}^L - H_f^L + x_{st}h_v(T_{st}) - x_f h_v(T_f) \quad (96)$$

with:

$$H_{st}^L - H_f^L = \int_{T_f}^{T_{st}} c_p^L dT \quad (97)$$

In alternative, the following equivalent expression for ΔH holds true:

$$\Delta H = H_{st}^V - H_f^V - (1 - x_{st})h_v(T_{st}) + (1 - x_{st})h_v(T_f) \quad (98)$$

with:

$$H_{st}^V - H_f^V = \int_{T_f}^{T_{st}} c_p^V dT \quad (99)$$

using Abbot's correlation to account that the gas is not ideal.

Whence the expansion energy is obtained, the post-expansion velocity v_f (m/s) is calculated from the following relationship:

$$v_f = (2E_p)^{\frac{1}{2}} \quad (100)$$

which does not take into account for turbulence. In ADAM a quite arbitrary cut-off speed limit of 1.5Mach -which is substance specific- is introduced (upper bound).

Droplets are calculated for completeness by using the CCPS correlation.

Rainout is not calculated by using the procedure described in the previous chapter, valid for continuous releases.

Pool spreading and vaporisation

The release of a non-boiling liquid or a pressurised liquefied gas that partially rainout after flashing will produce a liquid pool. The formation of the liquid pool will allow the released substance to spread from the release point to create an expanded source of vapour through vaporisation. In order to model the source term it is necessary to understand the pool spread mechanism and the pool vaporisation process. Pool spread is driven by the gravity force, the resistance effect, and the vaporisation process. The spreading will often be limited by the presence of a bund or dike, which are typically designed to contain all possible release content. The pool vaporisation process is governed by the heat transfer to the pool from the surrounding and heat removal mechanisms that depends greatly on the substance volatility and status (i.e., boiling or non-boiling).

ADAM uses GASP (*Gas Accumulation over Spreading*) to analyse pool spreading and vaporisation, which is a quite established model developed at the UKAEA (nowadays ESR Technology) on behalf of the UK Health and Safety Executive (HSE) (Webber, 1990; Webber and Jones, 1987; Webber and Jones, 1989). GASP is based on the numerical solution of a series of differential equations for the integral properties of the pool and is applied to both continuous and catastrophic releases.

More specifically, GASP describes the spreading and the evaporation rate of a circular liquid pool on a flat, horizontal, and uniform surface. The differential equations describing the model refer to: (i) pool spreading, in terms of the pool radius and the front velocity, (ii) mass conservation, (iii) energy balance, and (iv) evaporation model. A point to note is that these equations are coupled, as the main parameters governing the phenomenon, such as pool size temperature and evaporation rate, are present simultaneously in more than one equation. The following sections describe the coupled models that refer to pool spreading and pool vaporisation, respectively.

Spreading model

The spreading pool model includes a gravity driving term acting on the pool together with a flow resistance contribution. The GASP spreading model is based on the analytical solution of the shallow water equations generalised to include the effect of friction in laminar and turbulent conditions, which was introduced to overcome the negative inertia limitation typical of similar integral models.

The pool spreading is governed equations based on the conservation of mass, momentum and energy. For catastrophic releases, the pool spreads until it reaches a minimum layer depth (h_{min}). Afterwards the pool is assumed to shrink as the volume decreases for vaporisation with a constant depth (i.e., h_{min}). For continuous releases, the spread can continue even when the pool depth reaches the limit value due to the presence of mass spill. However when the release ceases, the pool start shrinking as the volume decreases by vaporisation as for the catastrophic case. In any case, the pool depth cannot be smaller than h_{min} . The minimum layer depth is very much influential on the pool spread dynamic and it is strongly influenced by the terrain roughness.

According to the GASP model, by assuming the pool being of circular shape with radius R (m) and with radial flow U (m²/s), the spreading of the pool on a horizontal solid surface which is pitted in a statistically uniform way is described by the following equations (Webber, 1990):

$$\frac{dR}{dt} = \left(1 - 2 \frac{\Phi_1(\epsilon)}{\epsilon}\right) \cdot U \quad (101)$$

$$\frac{dU}{dt} = 4g \frac{\gamma(s) h_e}{R} - F$$

where g (m/s²) is the acceleration due to gravity, h_e (m) = $(V/\pi R^2 - h_{min})$ is the depth of the dynamic part of the pool of volume V (m³) spreading over the a stagnant part of average depth h_{min} , and F accounts for the effect of friction. The h_{min} value represents the minimum layer thickness of the spreading pool, and has a strong impact on the pool dynamic, as the spreading ceases when the pool depth h reaches such a value. In ADAM h_{min} is calculated by using the relation given by Kapias and Giffiths (Kapias, 2001), which is determined by the surface roughness where the spreading takes place:

$$h_m = \begin{cases} 0.005 + 5 z_0 10^{-3} & (z_0 \leq 0.0001 \text{ m}) \\ 0.01 + z_0 10^{-2} & (0.0001 \text{ m} < z_0 \leq 0.1 \text{ m}) \\ 0.02 + 3 z_0 10^{-2} & (0.1 \text{ m} < z_0 \leq 10 \text{ m}) \\ 0.05 \text{ m} & (10 \text{ m} < z_0) \end{cases} \quad (102)$$

The parameter ϵ of eq. (101) is given by $\epsilon = 8U^2/gh_{min}$ and $\Phi_1(\epsilon) = (1 + \epsilon)^{1/2} - 1$, which accounts for the retarding effect of a rough ground if compared to a flat surface (i.e. $h_{min} = 0$ and $dR/dt = \cdot U$).

The shape factor s and the γ function of eq. (101) are given by:

$$s = \Phi_1(\epsilon) \frac{h_{min}}{h_e} \quad (103)$$

$$\gamma(s) = \begin{cases} 1 - s, & s < 2 \\ -s^2/4, & s \geq 2 \end{cases}$$

The friction factor F can be established from the turbulent and laminar friction terms as follows:

$$F = \frac{U|U|}{U^2} \max(|F_T|, |F_L|) \quad (104)$$

where:

$$F_L = 2.53 j(s)^2 \frac{3 \nu U}{h_e^2}$$

$$F_T = 4.49 j(s) \frac{1.5 \cdot 10^{-3} U |U|}{h_e} \quad (105)$$

$$j(s) = \begin{cases} 1, & s < 2 \\ 2/s, & s \geq 2 \end{cases}$$

With ν (m²/s) the kinematic viscosity of the liquid pool.

In presence of a containment, which is assumed circular with radius R_{max} , ADAM treats the pool as spreading until $R \leq R_{max}$. Afterwards eq. (101) is replaced by: $\dot{R} = 0$ and the radius is calculated according to volume conservation, i.e.:

$$R = \sqrt{\frac{V}{\pi h_{min}}} \quad (106)$$

The pool radius remains constant until the evaporation/vaporisation starts depleting the volume whilst the pool depth is maintained at its minimum level. This situation is very common for accident in chemical plants where vessel and columns are often surrounded by bunds in order to limit the consequences of the loss of containment.

Concerning the initial conditions, the following procedure is applied in ADAM. For catastrophic releases, the initial pool radius is estimated by assuming it being equal to the radius of a hypothetical sphere containing the whole amount released. For continuous releases, the initial pool radius will be that of the released 'cylinder' at the first iteration step of the source term modelling. In both cases, the initial pool depth is calculated by mass balance, accordingly.

Alternative spreading model

ADAM incorporates also an alternative and simpler model for the pool spreading, which can be selected in the option menu. It consists of the model provided by Opshoor (Opshoor, 1979):

$$\frac{dR}{dt} = \sqrt{2g(h - h_{min})} \quad (107)$$

However, this equation does not accurately take account of the effect of ground friction (Brambilla, 2009; Webber, 2012). For this reason, it is not recommended and it was added as an option for comparison purposes with other models, only.

Mass conservation

Mass conservation is described by a rather trivial equation, which accounts for mass balance between the discharged outflow and the vaporised mass that is described in terms of the variation of pool volume V , i.e.:

$$\frac{dV}{dt} = \frac{q}{\rho^L} - \pi R^2 q_{ev} \quad (108)$$

where q is the liquid source flow rate (kg s⁻¹), ρ^L is the pool density (kg m³), and q_{ev} the evaporation rate per unit surface (kg s⁻¹ m⁻²).

Evaporation model

The evaporation rate is the source term for the physical effect models. This strongly depends on the pool size and temperature, the properties of the involved substance and the properties of the environment. ADAM does not adopt the well-known correlation of MacKay and Mastugu (Mackay, 1973), on which several evaporation models are based. This because the scaling up of this correlation to the associated laboratory experiments has seriously been questioned (Brighton, 1985). By contrast as suggested in the GASP methodology, ADAM makes use of Brighton model to estimate the evaporation rate (Brighton, 1985).

The evaporation/vaporisation behaviour of a liquid pool is normally in between the two limit phenomena: the *boiling limit*-typical of liquid cryogen-where the vaporisation rate is entirely controlled by the heat exchange with the environment, and the *evaporation limit* -typical of liquids at ambient temperature- where the evaporation rate is controlled by the wind stream.

The expression providing the evaporation/vaporisation rate per unit surface q_{ev} ($\text{kg s}^{-1} \text{m}^{-2}$) from a plane liquid surface into a turbulent boundary layer is given by:

$$q_{ev}(T) = \begin{cases} -\frac{M_w P_v(T)}{RT} u_* \cdot \bar{j} \cdot \frac{\ln(1-y)}{y}, & y < 1 \text{ (non boiling)} \\ \frac{H_{Tot}}{h_v}, & y \geq 1 \text{ (boiling)} \end{cases} \quad (109)$$

where:

M_w molecular weight of the liquid pool (kg mol^{-1})

R gas constant (i.e. $8,314472 \text{ JK}^{-1}\text{mol}^{-1}$).

$P_v(T)$ substance vapour pressure above the pool (Pa)

u_* atmospheric friction velocity above the pool (m s^{-1})

\bar{j} spatially averaged mass transfer coefficient (-)

y partial pressure relative to atmospheric, which equals the mole fraction of vapour at the surface, and is given by $y = P_v(T)/P_a$

A point to note is that the above expression was developed for pool of fixed area, and its application to expanding and contracting pool is an approximation (Brambilla, 2009).

Non-boiling pools (Evaporation)

For non-boiling liquids ($y < 1$) the first formula of eq. (109) allows estimating the evaporation rate using Brighton's model and is valid under the assumption that the vapour acts as a passive containment in the atmosphere. This equation typically applies to cryogen (e.g. LNG, ammonia) but also to less volatile substances such as oil related products (e.g., petrol, kerosene). The validity of the above assumption does not hold true anymore when the vapour pressure approaches the atmospheric pressure (i.e. y close to 1).

Once the evaporating substance and its properties are known, eq. (109) can be calculated by using appropriate values for the atmospheric friction velocity above the pool u_* and the spatially averaged mass transfer coefficient \bar{j} .

ADAM estimates the atmospheric friction velocity by using the procedure described by van der Bosch (Yellow Book, 2005), which takes account the difference between friction velocity above the pool that well upwind. The latter is directly influenced by the terrain roughness z_0 , whilst the former depends on the aerodynamic pool roughness z_{0p} . ADAM allows the use of different aerodynamic pool roughness values, as listed in the table below:

z_{0p} (mm)	Reference
0.2 (default)	Brighton, 1985
0.5	Hanna and Britter, 2002
Terrain roughness	
Manual setting	

The spatially averaged mass transfer coefficient \bar{j} is a dimensionless quantity that depends essentially on the atmospheric wind profile -described by the n parameter- the turbulent Schmidt number, and a rather complex function³ of the dimensionless distance X_1 , evaluated at the downwind edge of the pool, and the parameter Λ defined hereunder:

$$\bar{j} = \frac{\kappa}{Sc_T} (1 + n)G(e^\Lambda X_1) \quad (110)$$

$$X_1 = \frac{n \kappa^2 D_p}{Sc_T z_{0p} e^{\frac{1}{n}}} \quad (111)$$

$$\Lambda = \frac{1}{n} + (1 - 2\gamma) + 2 \ln(1 + n) + \frac{\kappa}{Sc_T} (1 + n) \beta(Sc_L) \quad (112)$$

where:

- κ von Karman constant (i.e. 0.4)
- D_p pool diameter (m²)
- Sc_T turbulent Schmidt number of the vapour in air (i.e. 0.85)
- Sc_L laminar Schmidt number of the vapour in air (i.e. the ratio of viscosity to mass diffusion $\mu_a/(\rho_a D_v)$ (-))
- z_{0p} aerodynamic pool roughness (m)
- γ Euler's constant (i.e. 0.5772)

and β a function of the laminar Schmidt number Sc_L of the vapour in air [$\mu/(\rho D_v)$] given by:

³ $G(\xi) = \frac{1}{2} - \frac{1}{\pi} \operatorname{atan}\left(\frac{\ln(\xi)}{\pi}\right) + \frac{0.4228}{\ln^2(\xi) + \pi^2} + \frac{2.824 \ln(\xi)}{(\ln^2(\xi) + \pi^2)^2} + 1.025 \frac{(\ln^2(\xi) - \pi^2/3)}{(\ln^2(\xi) + \pi^2)^3} + \dots$

$$\beta(Sc_L) = \begin{cases} 7.3 Re^{0.25} Sc_L^{0.5} - 5Sc_T, & Re > 2 \text{ (Rough)} \\ \left(3.85 Sc_L^{\frac{1}{3}} - 1.3\right)^2 + \frac{Sc_T}{K} \ln(0.13 Sc_L), & Re < 0.13 \text{ (Smooth)} \\ \text{interpolated between Rough and Smooth} & 0.13 \leq Re \leq 2 \end{cases} \quad (113)$$

with Re , the roughness Reynold number, which is constructed from the aerodynamic pool roughness and the friction velocity, i.e.:

$$Re = u_* z_0 \rho_a / \mu_a \quad (114)$$

ADAM estimated the n index describing the atmospheric wind profile via a least-square analysis procedure between the power law approximation and the logarithmic profile law in the range z_{0p} and z_{10} , being the latter the measuring height of the wind speed (normally 10 m). For this purpose, the full expression of the logarithmic profile, which accounts for the Monin-Obukhov length, is considered (Paulson, 1970).

Boiling pools (Vaporisation)

For boiling pools ($\gamma \geq 1$), typically resulting from the release of pressurised liquefied gases, the Brighton model is not applicable and the vaporisation rate is assessed by considering the overall energy balance via the second formula in eq. (109).

Energy Balance

The pool temperature T is a key parameter in the pool evaporation process and is governed by the overall heat balance:

$$\frac{dT}{dt} = \frac{A}{C_p^L \rho^L V} (H_{Tot} - q_{ev} h_v) + \frac{q}{\rho^L V} (T_0 - T) \quad (115)$$

where:

- A pool area = πR^2 (m²)
- C_p^L specific heat (J kg⁻¹ K⁻¹)
- ρ^L pool density (kg m³)
- V pool volume (m³),
- h_v latent heat of vaporisation (J kg⁻¹)
- q liquid source flow rate (kg s⁻¹)
- T_0 temperature at which the liquid is discharging into the pool (K).

The term H_{Tot} (W m⁻²) represents the overall heat (per unit time and unit surface) exchanged between the pool and the external environment (W/m²). Three main heat transfer mechanisms take place: heat exchange from the ground/dike by conduction H_c , heat from ambient air by convection H_a , and radiative heat transfer H_r , which can be represented in such a way:

$$H_{Tot} = H_c + H_a + H_r \quad (116)$$

Heat from the ground/dike

Under the pool spreading, due to the temperature difference between the pool and the ground, heat exchange will take place. In order to account for the different temperatures

of the surface positions beneath the dynamically spreading pool, Webber has proposed a different expression of the heat exchange from the common case (Webber, 1987):

$$H_c = -\lambda \frac{\Phi(t)}{\sqrt{\pi\alpha t}} - \frac{\kappa}{A(t)\sqrt{4\pi\alpha}} \int_0^t (t-t')^{-\frac{3}{2}} [\Phi(t) A(t) - \Phi(t') A(t')] dt \quad (117)$$

where $A(t)$ is the pool area and $\Phi(t) = T(t) - T_g$ is the normalised pool temperature to the temperature ground T_g ; λ ($\text{Wm}^{-1}\text{K}^{-1}$) and α (m^2s^{-1}) are the ground thermal conductivity and diffusivity, respectively.

The second term of eq. 117 is associated with the spreading mechanism of the pool and is zero for a confined pool. This integration has to be conducted for each iterative step of the ordinary equation call. A simpler approximated expression of eq. 117 is also available in the literature (Brambilla, 2009), but in ADAM the Webber expression is used.

Heat from the ambient air

The heat transfer from the air is given by the following equation:

$$H_a = h A (T_a - T) \quad (118)$$

where T_a is the air temperature and the heat transfer coefficient h is modelled similarly to Brighton's (Brighton, 1985) mass transfer model described in the "Evaporation model" section, by changing the appropriate scalar quantity involved in the transfer mechanism process (i.e. heat exchange rather than mass) and by replacing the laminar Schmidt number Sc_L with the Prandtl number Pr (i.e. the ratio of viscosity to and heat diffusion).

Heat radiation

The radiative heat flux from the atmosphere is considered constant and give by:

$$H_r = H_{sr} + \varepsilon \sigma (T_a^4 - T^4) \quad (119)$$

being H_{sr} the contribution due to solar radiation, which can be either uploaded in ADAM or calculated via the following expression (Raphael, 1962):

$$H_r = C (1 - 0.0071 C_L^2)(\sin(\varphi_s) - 0.1) \quad (120)$$

where:

- C solar constant (i.e. 1111 W m^{-2})
- C_L Dimensionless cloudiness index (0 for clear day, 10 for complete cover)
- φ_s solar altitude above the horizon (rad)

The second term is the long-wave radiation heat exchange between the pool surface and the surrounding, with the emissivity ε of the pool is set to 0.95 and σ is the Stefan-Boltzman constant ($5.67 \cdot 10^{-8} \text{ W m}^{-2} \text{ K}^{-4}$).

PHYSICAL EFFECTS CALCULATION (Module 2)

General

Module 2 of ADAM is intended to calculate the physical effects of an industrial accident following an unintended release of substance and/or system failure. Physical effects can be subsequently used to assess the potential to produce damage (e.g. lethality) by using appropriate vulnerability models (Module 3). This provides an estimate of the accident severity level (i.e. consequences).

After having assessed the accident source term (i.e. substance release amount and overall dynamic of the release process), the calculus of physical effects depends on the type of accident. Thus, the associated model has to be selected accordingly. For Seveso-type establishments, different accident types might occur as shown in Table 4, which are associated with different physical effects:

OUTCOME CATEGORY	RELATED PHYSICAL EFFECT
FIRE	thermal radiation
EXPLOSION	overpressure
TOXIC DISPERSION	toxic concentration

Table 4: List of possible accident outcome typologies

Each accident type is characterised by several sub-categories. These correspond to quite different phenomena that have to be modelled separately. The sub-category list is given hereunder:

OUTCOME CATEGORY	SUB-CATEGORIES
FIRE	POOL FIRE/ROOF FIRE FLASH FIRE JET FIRE FIREBALL
EXPLOSION	VAPOUR CLOUD EXPLOSION (VCE)
TOXIC DISPERSION	HEAVY GAS CONTINUOUS RELEASE HEAVY GAS CATASTROPHIC RELEASE

Table 5: List of possible accident outcome sub-categories

In order to perform all involved calculations, it is necessary to provide a detailed description of the accident scenario, which includes the dangerous substance involved, the storage or operating conditions, the source term outcome, and the relevant meteorological and environmental data. In addition, some modelling assumptions have to be made, as specified in the ADAM 'option menu'.

For each accident scenario uploaded in the system, ADAM identifies all possible accident outcomes that might occur by activating the corresponding icons to run the case (see Figure 5). Depending on the selected substance, operating conditions and failure type, different accident outcome will be present. For instance, for toxic and non-flammable substances (e.g. chlorine), the only active icon is TOXIC DISPERSION. Clearly, if the toxic material is also flammable, the FIRE related and VCE icons will also be displayed.

ICON	Accident Outcome	ICON	Other moduli
	POOL FIRE		SOURCE TERM
	JET FIRE		POOL EVAPORATION
	FLASH FIRE		
	FIREBALL		
	VCE		
	TOXIC DISPERSION		

Figure 5: Different accident outcomes and source term calculation menu

The failure mechanism plays a key role: if the outflow of a flammable and pressurised substance (e.g. LPG) is due to a hole in a vessel or a pipe, the associated accident outcome sub-categories will be: JET FIRE, FLASH FIRE, POOL FIRE or VCE. By contrast, if the release is due to a catastrophic release of the vessel containing the same substance, the only possible outcome are POOL FIRE, FIREBALL or VCE. In summary, ADAM has an automatic system, which, depending on the substance, operating conditions (i.e. substance state) and failure mode, identifies all possible outcomes. The user is only asked to select the specific accident outcome of interest to run the case.

Upon selection, the Physical Effect Module associated to the selected accident subcategory is opened.

At present, the scope of ADAM relates to the consequence effects on humans. The relevant physical effects for this case are: (i) the thermal radiation produced by a fire due to the ignition of a flammable liquid or vapour, (ii) the overpressure produced by the blast of a vapour cloud ignited in the presence of some physical obstruction, and (iii) the airborne propagation of a toxic cloud into the atmosphere. Other outcomes, such as chronic effects associated with the pollution by released substances, environment contamination of land and water due to possible releases of liquid substances, and projection of solid fragments that might result from the blast of a vessel, are not included in the scope of ADAM.

The following sections describe the different models and assumptions employed by ADAM to describe the physical effects of accidents involving fires, explosions of flammable clouds, and releases of toxics.

Fire accidents due to the combustion of liquid and gases

Major fires are typical industrial accidents and are produced by the release of flammable substances from plant installations such as tanks, drums, pipeworks, reactors, etc. The unintended release can result either from equipment spills or because of the catastrophic failure of the substance containment. In the both cases, the overall development of possible accidental events depends on the state of the substance following the release (i.e. vapour, pure liquid or two-phase material).

When the released substance is a *flammable vapour*, in absence of immediate ignition, a cloud is formed in the surrounding atmosphere, by dispersing toward the wind direction. When the gas-air mixture of the cloud is within the flammability limits, following an ignition, a premixed flame will propagate, which will turn later on into a diffusive flame by involving also the cloud portion with concentration above the upper flammability limit. If the characteristic time of the energy release within the combustion process is not short enough to create an explosion, a *flash fire* will take place, by burning in everything that is present inside the cloud. If the release is coming from a leak, in presence of immediate ignition a *jet fire* will occur, consisting of a high momentum turbulent diffusion flame.

When the release contains also a *liquid phase*, depending on the temperature of the liquid, two different situations may occur. If the liquid temperature is below the normal boiling point (i.e., subcooled), a slow evaporation will take place. In the case of delayed ignition, a flammable cloud will be formed by the evaporated substance, which will develop as previously described. By contrast, in the case of immediate ignition, a *pool fire* will occur. When the temperature of the substance is above its normal boiling point and pressurised (i.e., superheated) the release will undergo to a sudden depressurisation (i.e., *flashing*) as soon as in contact with the atmosphere. The resulting vapours and aerosols might disperse in the atmosphere if not immediately ignited. However, in presence of immediate ignition, the flashing substance might form a *jet fire* (outflow from a leak/pipe), or a *fireball* (catastrophic release), with a significant amount of substance involved. The latter consists of the flame formation from the cloud ignition, which will suddenly be lifted upward for the density drop induced by the heating produced by the flame starting at the cloud surface. The consequences associated to this phenomenon are often characterised by a very high level of thermal irradiation.

The release involving superheated substances will often have a pure-liquid portion, which generally results from both the liquid component of the release and the aerosols' rainout. This will form a dispersing cloud of the evaporated substance or a *pool fire* if directly ignited.

The block diagram describing a fire development following the release of a flammable substance and depending the specific accident conditions is depicted in Figure 6. Other indirect effects caused by the dispersion of combustion by-products in the atmosphere can have also detrimental effects on humans and the environment but are not in the scope of ADAM.

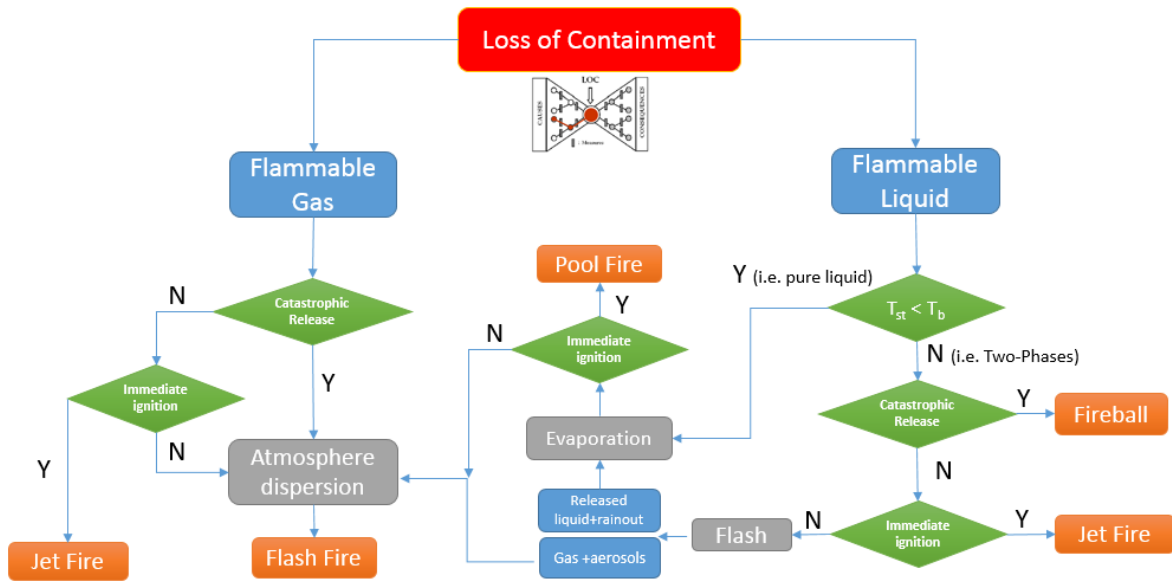


Figure 6: Fire development following loss of containment of a flammable substance

The thermal effects associated with fire related scenarios can be direct, when the flame impinges on the receptor, or indirect, when the mechanism for injury and/or damage is due to *thermal radiation*. Direct effects are assumed being lethal in all cases for humans and they produce extreme consequences for the affected infrastructures or equipment. The thermal radiation effects depend on both the energy reaching the receptor and the duration of exposure. Usually, severe damage to people is expected for high levels of radiation. Lower intensity radiations have significant damage potential only for longer exposure times, which allow people to escape or protect themselves.

According to Rew and Hulbert (Raw, 1996) there are two different approaches to thermal radiation modelling: semi-empirical approaches based on correlation formulas validated against experimental data and Computational Fluid Dynamics (CFD) models. Since ADAM focus in on real-time simulation, the first approach was selected.

In all cases and with the exception of flash fires, ADAM is based on solid flame semi-empirical models, which address the following aspects:

- *Fire flame*, which is normally represented by a simplified geometrical figure representing the flame (i.e. cylinder, sphere, frustum), which corresponds to the time-average of the visible flame envelope. The size and shape of the simplified flame is directly associated with the substance properties and the wind.
- *Radiative properties* of the flame, which are associated with the flame average surface emissive power, SEP (kW m^{-2}), which is specifically dependent on the substance properties, flame size, and temperature.
- *Calculation of the radiant flux at receptor* location, q_R (kW m^{-2}), which depends on the size, and shape of the flame and of the thermal radiation absorption in the atmosphere. This can be expressed from the average surface emitting power, SEP the view factor F_{view} (-), and the atmospheric transmissivity τ_a (-) as:

$$q_R = SEP F_{view} \tau_a \quad (121)$$

The view factor qualifies the geometry relationship between the model flame shape and the receiving surface, and it is defined as the fraction of the emitted radiation that reaches the receptor per unit area. It can be calculated using the following relationship (Mudan, 1984):

$$F_{view} = \iint_{A_i} \frac{\cos(\beta_i) \cos(\beta_j)}{\pi d^2} dA_i \quad (122)$$

where β_i and β_j are the angles to the surfaces and the line of sight for the emitter (flame) and the target respectively, and d the distance between the emitting elemental surface area dA_i and the target along the line of sight (see Figure 7).

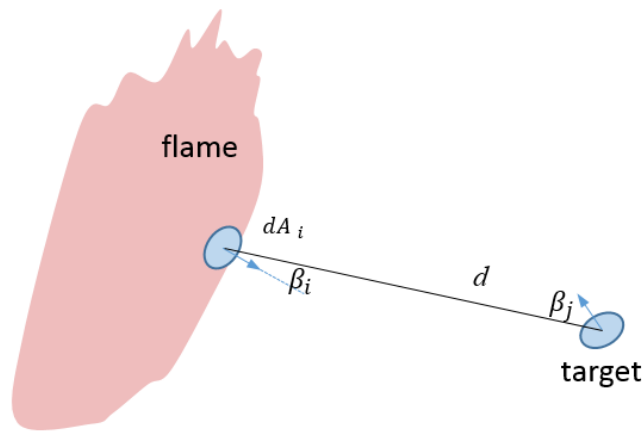


Figure 7: View Factor: elemental surface areas

In ADAM, the view factor is calculated from eq.122 numerically. The flame surface is divided in a number of radiant and axial meshes, which density is optimised on the distance d to the receptor, being higher for the near field and lower for the far field, for which the flame geometry plays a less relevant role. The view factor is calculated for horizontal F_H and vertical F_V targets, and under maximum conditions that are attained when the target is perpendicular to the line of sight.

The atmospheric transmissivity τ_a accounts for the thermal radiation absorption by the atmosphere, which reduces the overall effects on the target. ADAM employs the following relationship for atmospheric transmissivity:

$$\tau = \begin{cases} 1.53 (P_w d)^{-0.06}, & P_w d < 10^4 N \cdot m^{-1} \\ 2.02 (P_w d)^{-0.09}, & 10^4 \leq P_w d \leq 10^5 N \cdot m^{-1} \\ 2.85 (P_w d)^{-0.12}, & P_w d > 10^5 N \cdot m^{-1} \end{cases}$$

where P_w is the partial pressure of water in the atmosphere and d the distance between the surface of the flame and the receiver (Casal, 2008).

Pool Fires

A pool fire is a diffusion fire with turbulent behaviour burning over a pool of vaporising flammable liquid. The thermal radiation associated with a pool fire is strongly dependent on the size and shape of the emissive surface (flame), the heat produced in the combustion process, and by the presence of vapour water and carbon dioxide that partially absorb the radiation.

A pool fire is normally represented by a cylindrical flame originating by a circular puddle, which is tilt toward the wind direction (see Figure 8). The base of the cylinder might turn from circular to elliptical in presence of flame drag.

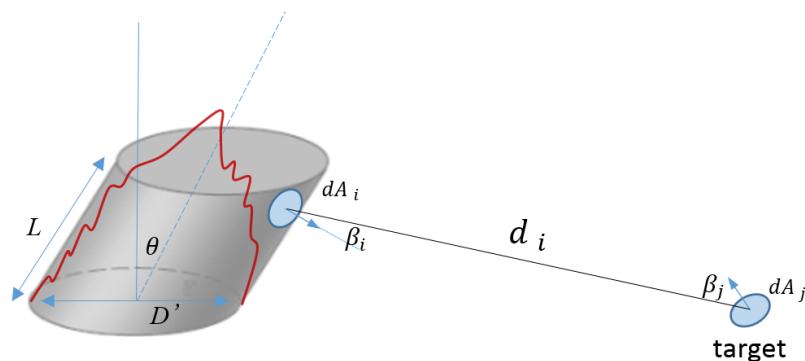


Figure 8: Pool fire geometry

Three different empirical methods are implemented in ADAM as listed in Table 6

CODE	MODEL	DESCRIPTION	REF
1	MODIFIED TNO	Originates from the TNO procedure but with diverse correlations to describe the flame geometry.	Engelhard, 2005 Pritchard, 1992
2	SHOKRI and BEYLER	Based on Heskestad's correlation for the flame length. There is no flame tilt and drag. It does not account for atmosphere transmissivity.	Shokri, 1989
3	MUDAN	Based on Thomas' correlation for the flame length and AGA correlation for flame tilt.	Mudan, 1988

Table 6: Pool fires. Empirical methods implemented in ADAM.

Model 1 is the recommended method in ADAM. It originates from the TNO method described in the Yellow Book (Engelhard, 2005) but with some modifications. In particular, since experimental evidence demonstrates that Thomas' correlation (used in the original TNO method) underestimates the mean flame length, it was decided to use the correlation proposed by Pritchard-Binding in their FIRE2 model (Pritchard, 1992). In addition, also the correlation for the flame drag was replaced with the one employed in the FIRE2 model.

Models 2 and 3 are the empirical models selected in the SFPE Handbook⁴ and were included in ADAM for completeness.

⁴ SFPE Handbook of Fire Protection Engineering, National Fire Protection Association, edition 4th, chapter 3 by Craig L. Beyler.

The three models differ amongst each other for the use of different correlations and assumptions. Independently of the model used, ADAM implements the same general procedure, which consists of estimating of the following parameters for the pool fire:

- Pool diameter;
- Burning rate;
- Flame length;
- Flame tilt;
- Drag diameter
- Surface Emissive Power (SEP);
- View factor;
- Atmospheric transmissivity.

ADAM addresses confined and/or unconfined pool fires on land.

Pool diameter D

Pool fires can be unconfined or confined when in presence of a bund. When the pool is confined, the pool is assumed to be circular with diameter equal to:

$$D = \sqrt{4 \frac{A_{bund}}{\pi}} \quad (123)$$

where A_{bund} is the area of the bund.

The situation is more critical for the case of unconfined pools, since the pool diameter is dependent on time. The pool-spreading model developed by Webber, which was described in detail in the previous section on pool evaporation, is not applicable in this case since it does not account for the contemporary burning process. For this reason, in ADAM it was implemented the Mudan and Croce procedure described by Casal (Casal, 2008). More specifically, for catastrophic releases, the pool diameter dependence on time t is given by:

$$D = D_{max} \sqrt{\frac{\sqrt{3}}{2} \left(\frac{t}{t_{max}}\right) \left[1 + \left(\frac{2}{\sqrt{3}} - 1\right) \left(\frac{t}{t_{max}}\right)^2\right]} \quad (124)$$

with a maximum pool size D_{max} reached at time t_{max} :

$$D_{max} = 2 \left(\frac{V^3 g \rho^2}{\dot{m}^2}\right)^{1/8} \quad t_{max} = 0.6743 \left(\frac{V \rho^2}{g \dot{m}^2}\right)^{1/4} \quad (125)$$

where g is the acceleration due to gravity, V the volume of the spilled liquid, ρ is the liquid density, and \dot{m} is the liquid burning rate ($\text{kg m}^{-2} \text{s}^{-1}$). ADAM uses the average value of the pool diameter calculated from eq. (124) as the input parameter for the pool diameter.

For unconfined pool fires resulting from a continuous release of a flammable with a flow rate q , ADAM uses the equilibrium diameter for the burning pool taken from the following relation (Casal, 2008):

$$D_{eq} = 2 \sqrt{\frac{q}{\pi \dot{m}}} \quad (126)$$

Burning rate, \dot{m}

The burning rate \dot{m} ($\text{kg m}^{-2} \text{s}^{-1}$) expresses the mass of the flammable substance supplied to the flame per unit time. According to the work of Babrauskas (Babrauskas, 1983), the burning rate depends on the diameter, the equivalent burning rate of an infinite-diameter pool \dot{m}_∞ , and the flammable substance as follows:

$$\dot{m} = \dot{m}_\infty (1 - \exp(-k \beta D)) \quad (127)$$

where the limit value \dot{m}_∞ , is taken for each flammable substance from the ADAM database. For those substances for which this parameter is not available, the Burgess-Strasser-Grumer relation is used (Burgess, 1961):

$$\dot{m}_\infty = 1.26 \cdot 10^{-6} \rho(T_b) \frac{\Delta H_c}{\Delta h_v + \int_{T_0}^{T_b} c_p dT} \quad (128)$$

where ρ is the fuel density calculated at the boiling temperature T_b , T_0 is the initial temperature, Δh_v (J/kg) the heat of vaporization at boiling point, and ΔH_c is the fuel heat of combustion (J/kg).

Values of the parameters k and β are available only for a few substances, however for typical accidents in an industrial setting the pool diameter size is such that in practice $\dot{m} = \dot{m}_\infty$.

Flame length L

The length of the visible flame is a function of the pool diameter. In actuality, the flame geometry is not uniquely defined, having normally a pulsing behaviour with a period of the order of one second. The empirical correlations used to define its length represent, therefore, average values in time, as well as all the other parameters used to describe the flame. The most known correlation is probably the one proposed by Thomas (Thomas 1963), which is based on laboratory experiments conducted on wood fires. It provides the following expression for the average flame length L :

$$\frac{L}{D} = 42 \left[\frac{\dot{m}}{\rho_a \sqrt{gD}} \right]^{0.61} \quad (129)$$

where ρ_a is the air density at ambient conditions and g is the acceleration due to gravity. The above equation is recommended when the influence of the wind is limited and in absence of soot. If wind is present, wind speed has to be accounted for, through the dimensionless wind velocity u^* :

$$u^* = \min[1, u_w/u_c]; \quad u_c = \left[\frac{g \dot{m} D}{\rho_v} \right]^{\frac{1}{3}} \quad (130)$$

and:

$$\frac{L}{D} = 55 \left[\frac{\dot{m}}{\rho_a \sqrt{gD}} \right]^{0.57} (u^*)^{-0.21} \quad (131)$$

where u_w is the wind speed measured at 10m above the ground, u_c is the characteristic wind speed, and ρ_v is the density of unburned fuel vapour (kg m^{-3}).

It was argued (Pritchard, 1992) that Thomas' correlation tends to underestimate the average flame length for the majority of large scale experiments conducted on typical industrial fuels and an alternative correlation was proposed:

$$\frac{L}{D} = 10.615 \left[\frac{\dot{m}}{\rho_a \sqrt{gD}} \right]^{0.305} (u^*)^{-0.03} \quad (132)$$

where the dimensionless wind speed u^* is defined as in eq. 130, but with u_w the wind speed measured at 9m above the ground.

Finally, the Heskestad correlation is also implemented in ADAM (Heskestad, 1984). This is given by:

$$L = 0.235 Q^{2/5} - 1.02 D \quad (133)$$

where the estimated flame length (m) is expressed in terms of the pool diameter and the heat of release of the pool fire Q (kW), but is independent of the wind speed, i.e.:

$$Q = \dot{m} \Delta H_c \pi D^2 \quad (134)$$

with ΔH_c the fuel heat of combustion (J/kg).

The three different models implemented in ADAM, make use of the different correlations described above as specified in Table 7.

CODE	MODEL	FLAME LENGTH	EQUATIONS
1	MODIFIED TNO	Pritchard-Binding's correlation	132
2	SHOKRI and BEYLER	Heskestad's correlation	133
3	MUDAN	Thomas' correlation	129-131

Table 7: Flame length correlations used in the different models.

Tilt angle, θ

In presence of wind, the flame may not remain vertical and tilt toward the wind direction with a certain angle θ .

The America Gas Association (AGA, 1974) proposed the following expression to determine the flame tilt:

$$\cos(\theta) = \begin{cases} 1, & u^* = 1 \\ u^{*\frac{-1}{2}}, & u^* > 1 \end{cases} \quad (135)$$

where u^* is the dimensionless wind speed calculated by using eq. 130 but with u_w the wind speed measured at 1.6m above the ground.

The main drawbacks of eq. 135 is that when the characteristic wind speed is higher than the wind speed, the tilt angle is zero. This led to in inaccurate predictions for large pool fires under low wind speed conditions as demonstrated by experimental evidence (Pritchard, 1992). For this reason, other correlations are proposed, which relate the tilt angle to the Froude (Fr) and the Raynolds (Re) numbers (Welker & Sliepcevich, 1966):

$$\frac{\tan(\theta)}{\cos(\theta)} = a Fr^b Re^c \left(\frac{\rho_v}{\rho_a}\right)^d \quad (136)$$

with :

$$Fr = \frac{u_w^2}{g D}; \quad Re = \frac{u_w \rho_a D}{\nu_a} \quad (137)$$

where ν_a is the air dynamic viscosity (Pa s) and ρ_v is the density of the unburned fuel vapour (kg m^{-3}).

The parameters a , b , c , and d of eq. 136 employed in ADAM are those proposed by Pritchard and Binding in FIRE2 model (Pritchard, 1992) i.e.:

$$a = 0.666, b = 0.333, c = 0.117, d = 0 \quad (138)$$

Table 8 provides detail on the correlation used in the three different models implemented in ADAM.

CODE	MODEL	TILT ANGLE	EQUATIONS
1	MODIFIED TNO	Welker and Sliepcevich correlation with Pritchard-Binding's coefficients	136-138
2	SHOKRI and BEYLER	No tilt considered	
3	MUDAN	AGA correlation	135

Table 8: Tilt correlations used in the different models.

Drag diameter

Experimental evidence shows that flame drag, (i.e. flame base extension) is normally present in industrial pool fires. The effect of drag on the pool diameter D makes the pool base component in the wind direction slightly bigger, which render the flame base of elliptical shape.

A correlation that was demonstrated to match well with experimental data on a number of different flammable substances is proposed by Pritchard and Binding in FIRE2 model (Pritchard, 1992):

$$\frac{D'}{D} = 2.506 Fr^{0.067} Re^{-0.03} \left(\frac{\rho_v}{\rho_a} \right)^{0.145} \quad (139)$$

This is the correlation implemented in model 1 of ADAM. The other two models do not consider the Drag flame effect and they model the flame with circular shape base.

Surface Emitting Power, SEP (kW m⁻²)

The radiative properties of the flame are normally represented by an average surface emissive power (SEP). This values, which is associated with the energy produced by the burning process, is therefore dependent on the specific flame geometry assumed in the model. According to the model used, SEP might be based on the actual area of visible flame or represent the averaged radiant emission on the whole surface of the flame, which accounts also for those portions of the flame that are shielded by soot or smoke.

In the model proposed by Shokri and Beyler (Model 2 in ADAM), the SEP value was obtained by fitting experimental measurements of radiant heat flux from pool fire flame. In practice, it represents the average surface emissive power over the whole surface of the flame, and by implicitly containing the effect of soot, this value is significantly lower than the emissive power obtained locally. The following empirical relation is given for this case (Shokri, 1989):

$$SEP = 58 \cdot 10^{-0.000823 D} \quad (140)$$

A different approach was proposed by Mudan and Croce (Mudan, 1988). This is mainly applicable to smoky flames produced by heavy hydrocarbons and it accounts for the effect of soot explicitly, via the following empirical expression:

$$SEP = SEP_{max} e^{-0.12 D} + SEP_{soot} (1 - e^{-0.12 D}) \quad (141)$$

where SEP_{max} is the maximum surface emissive power from a flame without soot production, which is set to 140 kW/m², whilst SEP_{soot} is the soot equivalent set to 20 kW/m². For lighter hydrocarbons and other flammables, the pool burns with a luminous flame and the SEP is given by (Moorhouse, 1982):

$$SEP = \frac{0.3 \dot{m} \Delta H_c}{1 + 4 L/D} \quad (142)$$

Model 1 and Model 3 implemented in ADAM (Modified TNO and Mudan, respectively) make use of these last two equations for the evaluation of SEP.

The SEP value calculated according the above procedure is always limited to a reference maximum cut-off value that is selected in the ADAM option menu (400 kW by default).

View Factor

The procedure implemented in ADAM to evaluate the view factor, F_{view} (-) via eq. 122, to be solved numerically, consists of using a property algorithm to generate a rectangular mesh on the cylindrical surface and considering the approximation of the double integral of Riemann as follows:

$$F_{view} = \sum_{i=1}^N \frac{\cos \beta_i \cos \beta_j}{\pi d_i} dA_i \quad (143)$$

with the parameters of the equation as in Figure 8.

A point to note is that the flame geometry of Method 1 differs from that of Methods 2 and 3. Contrary to the last two methods that represent the flame as a pure cylinder, due to the effect of flame drag, the first method is characterised by a flame with elliptical base. This requires two separate algorithms to generate the mesh in the case of circular or elliptical bases.

Jet Fires

A Jet Fire is the result of turbulent dispersion due to the combustion of a flammable substance released continuously in a specific direction and with high momentum. The calculus of heat radiation is performed by assuming the jet as a solid flame with the shape of a conical frustum (see Figure 9).

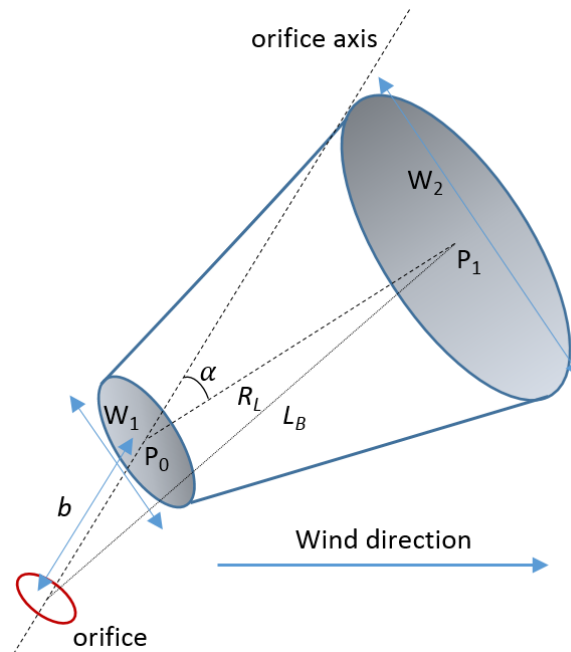


Figure 9: Jet fire solid flame model

As for the pool fire, the calculus algorithm consists of assessing the flame length, SEP, and view factor. The implemented methodology in ADAM is the Chamberlain model (Chamberlain, 1987), with Johnson's variant for horizontal jets (Johnson, 1994). In the model, the flame shape is represented as a tilted frustum of cone, radiating as a solid body with a uniform surface emissive power. In particular, the following parameters are relevant for the modelled flame shape:

- the flame lift-off distance b from the orifice,
- the flame length L_B is defined as the distance between the orifice and the frustum tip at the flame axis (i.e. flame end)
- the frustum length, R_L , is the length of the burning flame
- the width of the of the frustum bases, W_1 and W_2 , are the width of the burning flame near the orifice and the flame end, respectively
- the angle α by which the flame is deflected from the orifice axis toward the wind direction

Chamberlain model was developed by Shell for gaseous substances for vertical and inclined flares. In order to extend its validity to two-phase releases (i.e. LPG), Cook's correction was applied (Cook, 1990).

A relevant parameter for the modelling of jet fires is the effective diameter D_s of the source. This expresses the diameter of a hypothetical orifice through which air at normal

ambient density ρ_a (kg m^{-3}) is released at a flow rate and velocity equal to the actual flow rate and velocity of the jet i.e., q (kg s^{-1}), and u_j (m s^{-1}), respectively:

$$D_s = \sqrt{\frac{4q}{\pi \rho_a u_j}} \quad (144)$$

where q and u_j are taken from the ADAM source term output module. A point to note is that the velocity of the jet is considered after flashing, if the outflow is choked.

The original expression for the equivalent diameter provided by Chamberlain is valid for a gaseous outflow. For two-phase and liquid jets, Cook's correction is applied (Cook, 1990), which consists of multiplying eq. 144 by the factor $\sqrt{(\rho_v/\rho_a)}$ where ρ_v is the pure vapour density of the jet.

In ADAM, the following reference system is considered. The origin is at the orifice exit, the plane (xy) represents the horizon, and the z-axis is the vertical direction. The x-axis is oriented in such a way that the plane (xz) contains the orifice axis. The wind direction, which is assumed horizontal, is represented by the versor \hat{w} . By construction, this lays in the plane (xy) and it forms an angle of α_1 with the x-axis. The orifice axis, described by the versor \hat{j} , forms an angle of α_2 with the horizon:

$$\hat{w} = (\cos \alpha_1, \sin \alpha_1, 0); \hat{j} = (\cos \alpha_2, 0, \sin \alpha_2) \quad (145)$$

The angle θ between the orifice axis and the horizontal wind direction plays a key role in the determination of some of the flame parameters. This angle can be expressed as follows as a function of the previously introduced versors, and in turn of α_1 and α_2 . In ADAM these two angles are set in the input menu and θ is calculated accordingly.

$$\theta = \cos^{-1}(\hat{w} \cdot \hat{j}) = \cos^{-1}(\cos \alpha_1 \cos \alpha_2) \quad (146)$$

As for the case of pool fire, the procedure implemented in ADAM to evaluate the view factor numerically (see eq. 122), consists of using a property algorithm to generate a mesh on the frustum. The main difficulty consists on expressing the equation of frustum in the appropriate reference coordinates. In particular, the frustum is uniquely determined when the following parameters are known (see Figure 9):

- Position of the centre of the base and of the tip (points P_0 and P_1)
- Base and tip diameters (W_1 and W_2)

Point P_0 is obtained from geometrical considerations, i.e:

$$P_0 = b \hat{j} \quad (147)$$

where b (m) is the lift-off distance of the frustum.

whilst P_1 can be obtained by solving the following relations, i.e. :

$$\begin{cases} (\mathbf{P}_1 - \mathbf{P}_0) (\widehat{\mathbf{w}} \times \widehat{\mathbf{j}}) = 0 \\ (\mathbf{P}_1 - \mathbf{P}_0) \cdot \widehat{\mathbf{j}} = R_L \sin \alpha \\ |\mathbf{P}_1 - \mathbf{P}_0| = R_L \end{cases} \quad (148)$$

where R_L is the frustum length and α is the angle by which the flame is deflected from the orifice axis toward the wind direction. All these parameters are obtained through correlations as described in the next sections.

Whence points \mathbf{P}_0 and \mathbf{P}_1 are determined, the generic point on the frustum \mathbf{P}_s can be expressed as follows (see Figure 10):

$$\mathbf{P}_s = \mathbf{P}_0 + d \widehat{\mathbf{n}}_F + r(d)[\widehat{\mathbf{s}}_1 \cos \varphi + \widehat{\mathbf{s}}_2 \sin \varphi] \quad (149)$$

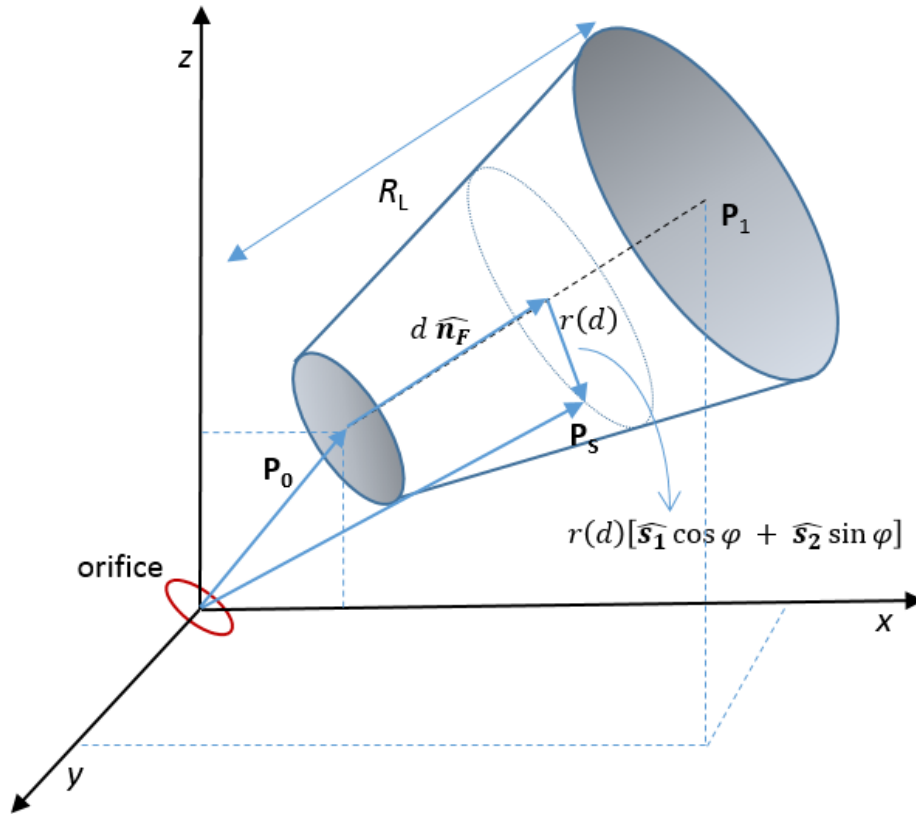


Figure 10: Frustum: main vectors

in which:

$\widehat{\mathbf{n}}_F$ frustum axis versor, i.e., $\mathbf{P}_0\mathbf{P}_1 / \|\mathbf{P}_0\mathbf{P}_1\|$

d distance between point \mathbf{P}_0 and the centre of the generic frustum circular section containing \mathbf{P}_s

$\widehat{\mathbf{s}}_1, \widehat{\mathbf{s}}_2$ perpendicular versors, which are orthogonal to frustum axis. i.e.: $\widehat{\mathbf{s}}_1 \cdot \widehat{\mathbf{s}}_2 = 0$ and $\widehat{\mathbf{s}}_1 \times \widehat{\mathbf{s}}_2 = \widehat{\mathbf{n}}_F$

φ is the generic angle ranging within $[0, 2\pi]$.

The view factor is calculated by an integration process along the annular rings build by varying d in the range $(0, R_L)$. The contribution due to the side areas is calculated separately.

Vertical and inclined Flames

ADAM makes use of the Chamberlain methodology to address vertical or inclined jet fires with an angle to the horizon α_2 that is greater the 10 deg.

Wind presence has an important effect on flame geometry. At slow wind speeds, the flame tilt is limited but the air engulfment is high since all lateral surface of the flame is exposed to the wind. This increase the combustion and the consequent reduction of the flame length. For higher wind speeds, the flame tilt increases and the flame tends to move toward the wind direction. The flame length starts increasing because of the wind drag and then decreasing again for the dilution effect.

Flame Shape

The *flame length* L_B (m) is calculated from the empirical formula (Kalghatgi, 1983, 1984):

$$L_B = L_{B0} (0.51 e^{-0.4 u_w} + 0.49)[1 - 0.00607(\theta - 90^\circ)] \quad (150)$$

where u_w is the wind speed whilst the *flame length in still air*, L_{B0} is given by:

$$L_{B0} = D_s Y \quad (151)$$

with Y the root of the equation:

$$0.024 \left(g \frac{D_s}{u_j^2} \right)^{\frac{1}{3}} Y^{\frac{5}{3}} + 0.2 Y^{\frac{2}{3}} - \left(\frac{2.85}{W} \right)^{\frac{2}{3}} = 0 \quad (152)$$

and

$$W = \frac{M_w}{(15.816 M_w + .0395)} \quad (153)$$

being M_w the molecular weight of the substance (kg mol^{-1}).

The angle α (°) between the orifice axis and the flame axis, i.e. the angle by which the flame is deflected from the orifice axis toward the wind direction can be expressed in terms of the Richardson number ξ (Kalghatgi, 1983, 1984):

$$\alpha = \begin{cases} \frac{8000 R + \xi(L_{B0})(\theta - 90)(1 - e^{-25.6 R})}{\xi(L_{B0})}, R \leq 0.05 \\ \frac{1726\sqrt{R - 0.026} + 134 + \xi(L_{B0})(\theta - 90)(1 - e^{-25.6 R})}{\xi(L_{B0})}, R > 0.05 \end{cases} \quad (154)$$

where R is the ratio of the wind velocity to the jet velocity:

$$R = \frac{u_w}{u_j} \quad (155)$$

and the Richardson number based on L_{B0} , which represents the importance of buoyancy in calculating the size of the flame is given by:

$$\xi(L_{B0}) = L_{B0} \left(\frac{g}{D_s^2 u_j^2} \right)^{1/3} \quad (156)$$

The lift-off distance b (m) of the frustum of the flame depends on the flame length and is calculated as:

$$b = \begin{cases} 0.015 L_B & \text{(two – phase and liquid jets)} \\ L_B \frac{\sin K\alpha}{\alpha} & \text{(gases)} \end{cases} \quad (157)$$

where the following empirical correlation provides a value of the K parameter:

$$K = 0.185 e^{-20R} + 0.015 \quad (158)$$

The frustum length R_L can be calculated from geometrical considerations (see Figure 9):

$$R_L = \sqrt{L_B^2 - b^2 \sin^2 \alpha} - b \cos \alpha \quad (159)$$

The frustum base width can be calculated from empirical relations. In the case of gas jets (Chamberlain, 1987):

$$W_1 = D_s (13.5 e^{-6R} + 1.5) \left(1 - \left[1 - \frac{1}{15} \sqrt{\frac{Q_a}{Q_j}} \right] e^{-70 \xi(D_s) R \cdot C} \right) \quad (160)$$

with:

$$C = 1000 e^{-100R} + 0.8 \quad (161)$$

and:

$$\xi(D_s) = D_s \left(\frac{g}{D_s^2 u_j^2} \right)^{1/3} \quad (162)$$

whilst in the case of liquid and two-phase jets, the Cook's correlation applies (Cook, 1990):

$$W_1 = D_s (13.5 e^{-6R} + 1.5) \left(1 - \left[1 - \frac{1}{15} \sqrt{\frac{Q_a}{Q_j}} \right] e^{-7R} \right) \quad (163)$$

The width of frustum tip is given by (Chanberlain, 1987):

$$W_2 = L_B (0.18 e^{-1.5 R} + 0.31) (1 - 0.47 e^{-25 R}) \quad (164)$$

Finally the total area of the frustum $A(m)$ which includes the end discs is:

$$A = \frac{\pi}{4} (W_1^2 + W_2^2) + \frac{\pi}{2} (W_1 + W_2) \sqrt{R_L^2 + \left(\frac{W_2 - W_1}{2}\right)^2} \quad (165)$$

SEP of vertical or inclined jets

For jet fires, the fraction of the surface that is covered by soot is considered very small, and the surface emitting power, SEP (kW m^{-2}) is practically the flame emitting power in absence of soot. In the present case, it can be calculated as a function of the heat of combustion, ΔH_c (kJ kg^{-1}), the burning rate, \dot{m} (kg s^{-1}) and the total surface area of the frustum, A (m^2) as:

$$SEP = F_s \frac{q}{A} \Delta H_c \quad (166)$$

where F_s (-) is the radiation fraction i.e, the fraction of the combustion energy radiated from the flame.

For large gas flames, the radiation fraction is given by an empirical expression as a function of the fuel velocity in the jet:

$$F_s = 0.21 e^{-0.00323 u_j} + 0.11 \quad (167)$$

where u_j (m s^{-1}) is the exit velocity of the flammable gas in the expanding jet. For smaller fires, the above expression overestimates the radiation fraction F_s , which is however conservative.

For liquid and two-phase jets, Cook's correlation applies and the above radiation fraction F_s has to be further multiplied by a factor that depends on the substance molecular weight as follows (Cook, 1990):

$$\left\{ \begin{array}{ll} 1 & M_w < 21 \\ \sqrt{\frac{M_w}{21}} & 21 \leq M_w \leq 60 \\ 1.69 & M_w > 60 \end{array} \right. \quad (168)$$

The SEP value calculated according the above procedure is always limited to a reference maximum cut-off value that is selected in the ADAM option menu (400 kW by default).

Horizontal Flames

For horizontal jets, ADAM applies the Johnson's variant to the Chamberlain method (Johnson, 1994). The flame is still modelled as a frustum of cone but some of the flame

shape parameters and the radiative properties are based on other correlations, which were obtained by large-scale experiments. Differently from Chamberlain, Johnson's variant account for the buoyancy lift effect.

Flame Shape

Johnson's model provides directly correlations to get the position \mathbf{P}_1 of the centre of the frustum tip as a function of the wind momentum flux (which lays in the xy-plane):

$$\boldsymbol{\Omega} = L_{B0} \frac{u_w}{u_j} \hat{\mathbf{w}} = L_{B0} \frac{u_w}{u_j} (\cos \alpha_1, \sin \alpha_1, 0) \quad (169)$$

where L_{B0} is the flame length in still air, calculated as in the previous section, u_w is the wind speed, u_j is the jet velocity after expansion and $\hat{\mathbf{w}}$ the wind versor that is placed on the xy plane (forming an angle α_1 with the x-axis). For two-phase and liquid jets, Cook's correction is applied (Cook, 1990), which consists of multiplying eq. 169 by the factor $\sqrt{(\rho_v/\rho_a)}$ where ρ_v is the pure vapour density of the jet.

The point \mathbf{P}_1 can be simply expressed through the relation:

$$\mathbf{P}_1 = \mathbf{P}_0 + (X, Y, Z) \quad (170)$$

where the co-ordinates X, Y, Z are provided by the correlations described hereunder:

$$X = L_{B0} F(\xi)(1 + R(\xi)\Omega_x) \quad (171)$$

with the condition that X cannot exceed L_{B0} , ξ is the Richardson number (see eq. 156), and $F(\xi)$ $R(\xi)$ expressed as:

$$F(\xi) = \begin{cases} 0.55 + (1 - 0.55)e^{-0.168\xi} & \xi \leq 5.11 \\ 0.55 + (1 - 0.55)e^{-0.168\xi - 0.3(\xi - 5.11)^2} & \xi > 5.11 \end{cases} \quad (172)$$

$$R(\xi) = \begin{cases} 0. & \xi \leq 3.3 \\ 0.082(1 - e^{-0.5(\xi - 3.3)}) & \xi > 5.11 \end{cases} \quad (173)$$

The Y variable, which accounts for the flame deflection by the wind:

$$Y = 0.178 (X - b) \Omega_x \quad (174)$$

with the lift-off b calculated using the following correlation:

$$b = 0.125 \sqrt{\rho_a \rho_j} u_j d_j \Omega_x \quad (175)$$

where the densities have to be expressed in (kg m^{-3}) , the velocity of the expanded jet u_j in m s^{-1} and the expanded jet diameter d in m.

Analogously:

$$Z = L_{B0} H(\xi)(1 - C(\xi)\Omega_x) \quad (176)$$

with the condition that it cannot exceed L_{B0} and with $H(\xi)$ $C(\xi)$ given by:

$$H(\xi) = \left(1 + \frac{1}{\xi}\right)^{-8.48}; C(\xi) = 0.02\xi \quad (177)$$

The frustum base width W_1 correlates the Richardson number ξ and the lift-off b :

$$W_1 = b(-0.18 + 0.081 \xi) \quad (178)$$

whilst the frustum tip width W_2 can be obtained as follows:

$$W_2 = \sqrt{X^2 + Z^2}(-0.004 + 0.0396 \xi - \Omega_x(0.0094 + 9.5 \cdot 10^{-7} \xi^5)) \quad (179)$$

W_2 must be greater or equal to frustum base width W_1 and less than the length of the projection of the vector (X, Y, Z) on the xz -plane, i.e. $\sqrt{X^2 + Z^2}$.

Finally, the frustum length can be simply calculated as:

$$R_L = \sqrt{X^2 + Y^2 + Z^2} \quad (180)$$

SEP of Horizontal jets

Also for horizontal jets eq. 166 applies, but Johnson suggested different values of the radiation fraction F_s for the ends and the side of the flame (Johnson, 1994). These values are given hereunder:

$$F_s^{SIDE} = (0.21 e^{-0.00323 u_j} + .14)(1 - e^{-0.4 W_2}) \quad (181)$$

$$F_s^{END} = (0.21 e^{-0.00323 u_j} + .14)(1 - e^{-0.4 R_L}) \quad (182)$$

The *SEP* value calculated according the above procedure is always limited to a reference maximum cut-off value that is selected in the ADAM option menu (400 kW by default).

Fireballs

A fireball is the result from a sudden release and immediate ignition of a pressurised flammable gas. The most common situation in which a fireball takes place is in the presence of a BLEVE (Boiling Liquid Expanding Vapour Explosion). This event consists of the collapse of a vessel containing a pressurised liquefied gas, which is due to the weakening of the vessel material from external heating (i.e. fire). This fact, in conjunction with the internal overpressure, is the cause of the failure of vessel structural integrity. The liquefied gas released undergoes to flashing, and is immediately ignited by the external fire. The flame is then lifted upward for the density drop of the cloud induced by flame heating. This phenomenon is always associated with high thermal radiation, which occurs for relatively short time.

In order to estimate the thermal radiation of a fireball, ADAM makes use of classical empirical models, which provide the geometry of the fireball, and the thermal radiation. The relevant parameters for the fireball effects are the fireball diameter, the duration of the fire, and the lift-off height of the fireball centre from the ground. Whence the geometry of the flame is determined, the thermal radiation impinging on an external target is determined by estimating the surface emissive power (SEP), the atmosphere transmissivity, and the view factor, which is calculated numerically as in the previous cases.

The substance amount involved in the burning process, M is not the whole content of the vessel but only the remained portion that remains airborne after flashing and rainout.

Sphere geometry

The sphere maximum diameter D_{max} (m) reached by the fireball, and the fire duration t_d (s) are directly associated with the mass M (kg) of remaining airborne involved in the fireball formation, via the following empirical relationships:

$$D_{max} = C_1 M^{C_2} \quad (183)$$

$$t_d = C_3 M^{C_4} \quad (184)$$

In ADAM, the values for the C_i coefficients are taken from the table below:

	n-BUTANE	PROPANE	n-PENTANE	HYDR.CARB. (other)
C_1	5.72	5.88	5.25	5.8
C_2	0.303	1/3	0.314	1/3
C_3	0.45	1.09	1.07	0.45
C_4	1/3	0.167	0.181	1/3
Ref.	Lihou and Maund (1982)	Williamson and Mann (1981)	Hasegawa and Sato (1977)	Roberts (1982)

Table 9: Coefficients used in eq. 183 and 184 and related references.

For very large quantities (i.e. $M > 37.000$ Kg) different coefficients are considered for the fire duration (i.e. $C_3 = 2.6$ and $C_4 = 1/6$) (IChemE, 1989).

The lift-off height of the fireball centre from the ground, H_f (m), is considered equal to the maximum diameter (Roberts, 1982), i.e.:

$$H_f = D_{max} \quad (185)$$

Surface Emitting Power, SEP (kW m⁻²)

By assuming no soot formation, the average surface emitting power can be calculated as a function of the net heat of combustion ΔH (kJ Kg⁻¹), the amount of the involved substance M (kg), the diameter of the fireball D_{max} (m), the burning time t_d (s), and the radiation fraction F_s (-) (Roberts, 1982):

$$SEP = F_s \frac{M \Delta H}{\pi D_{max}^2 t_d} \quad (186)$$

where F_s (-), i.e. the fraction of the combustion energy radiated from the flame surface is calculated from the following empirical relationship:

$$F_s = 0.00325 P_s^{0.32} \quad (187)$$

with P_s (Pa), the stagnation pressure inside the vessel just before the release (usually the vapour pressure if the substance is at saturation) and the net heat of combustion ΔH given by (Engelhard, 2005):

$$\Delta H = \Delta H_C - h_v - c_p^l \Delta T \quad (188)$$

where h_v (kJ kg⁻¹) and c_p^l (kJ kg⁻¹K⁻¹) are the latent heat of vaporisation and the specific heat of the fuel, and ΔT (K) the temperature difference between flame and ambient temperature, that is fixed at 1727 K.

The *SEP* value calculated according the above procedure is always limited to a reference maximum cut-off value that is selected in the ADAM option menu (400 kW by default).

Flash Fires

A flash fire is a nonexplosive combustion resulting from the ignition of a flammable cloud. Normally, this takes place when the cloud propagates in absence of obstacles or dispersion turbulence, which might accelerate the flame and produce a vapour cloud explosion. In presence of a flash fire, the shock wave is normally very small, and the fire duration will last for very few tens of second.

When the target is outside the flame front, due to the very short duration of the burning process, the thermal dose received is very small, and in such a case, the flash fire effects are negligible. This is also true when the target is in proximity of the flame itself, and it is the main reason why very little is reported about the thermal radiation of flash fires.

For this reason ADAM does not explicitly model the thermal radiation associated with flash fires but it focuses on the determination of the contour of the flame, within which the effects are extremely severe. In this sense, the analysis of the effects due to a flash fire is rather different if compared to the previous cases.

In order to identify the flame boundaries, the size and position of the flammable cloud has to be determined. For such a purpose, after having assessed the source term, ADAM applies atmospheric dispersion models to estimate the cloud size and position at the time of ignition. In particular, the flammable vapours will burn if the cloud is within the substance flammability limits. ADAM calculates the iso-concentration curve of the cloud at the time in which ignition is supposed to take place by determining the concentration level equal to the lower flammability limit (LFL). The iso-concentration curve is normally calculated at the height where the ignition is supposed to take place. All the area delimited by the iso-concentration curve is considered to take part in the burning process by including the inner part of the cloud with concentration above the upper flammability limit (UFL), since turbulence induced combustion mixes this material with air and burns it. In this area the lethality level is fixed to 100%. In order to account for the time averaging effect inherent to any dispersion model (in ADAM it is fixed at its minimum, i.e. 10s), the analysis is also extended to lower values of concentration (Rew, 1988). ADAM calculates a second iso-concentration curve at a fixed value of $\frac{1}{2}$ LFL.

In practice, since the ignition time is generally unknown, by assuming a certain value for the downwind distance of the ignition location, ADAM has an iterative procedure to calculate the LFL and $\frac{1}{2}$ LFL iso-concentration curves, with the cloud front at the ignition position.

For the calculus of the effects, it is assumed that 100% lethality will be present within the flame boundary (i.e. LFL concentration), and a probability of death decreasing linearly outside the flame to reach a value of 0 for the concentration of $\frac{1}{2}$ LFL.

Vapour Cloud Explosions (VCE)

Vapour cloud explosions (VCE) result from the ignition of flammable clouds travelling across structures, obstacles and partial confinements in such a way that the flame produced is accelerated to such high speed to generate a significant overpressure. However, a vapour cloud explosion may occur only if some specific conditions are met:

- the *flammable* substance should have been at certain storage or process conditions and the *total mass* should be large enough to create sufficient airborne air-substance mixture in the cloud;
- *ignition time* is very critical. It should take place after the cloud is formed to a sufficient size (i.e. with a concentration below UFL) and before the air-flammable mixture is diluted below the substance lower flammability limit (LFL).
- the level of *confinement, congestion or turbulence* in the area where the cloud propagates should be enough to sustain the explosion. Sufficient turbulence can be also induced in absence of external obstacles by the release itself (e.g., catastrophic rupture or high momentum jet) but pressure will drop as soon as the blast wave will enter the uncongested area.

For vapour cloud explosions typical of the petrochemical sector, the flame propagation occurs though deflagration. This because the volume of clouds is normally large and the rate of energy released is relatively slow. In such a case, the blast wave propagates at subsonic velocity and overpressures are much lower than those produced by detonations. Only in very rare occasions, detonations may result from flammable vapour clouds. These have to be driven by very high-power triggering events and are characterised by flame fronts and shock waves propagating together at supersonic velocity.

The damage effects of a vapour cloud explosion are mainly those associated with the *peak overpressure* produced by the blast wave. However, the overall dynamic process of the blast wave can play a significant role, which is described by the positive-phase blast-wave *duration* in which the blast persists and the *positive impulse*, defined as the area under the overpressure/time curve. ADAM implements the calculations of all these parameters to fully describe the vapour cloud explosion.

Free-air explosions occur when the explosive cloud is located far from the ground. In this case, the blast wave will be spherical. When the explosion take place *at ground*, the blast wave will be reflected by acting over a hemispherical volume. This case is much more common in industry. By neglecting the energy dissipation in the production of ground shock, a reflection factor of 2 is normally applied.

In order to predict the physical effects of vapour cloud explosions, ADAM makes use of empirical analytic methods, blast explosion models, which employ blast scaled curves to predict the blast overpressure and impulse at a given distance. These models are based on limited field data and accident investigations and are listed hereunder:

CODE	MODEL	DESCRIPTION	REF
1	Equivalent TNT	It assumes that all VCE are detonations and is based on a scaled curve where the explosive flammable equates an equivalent mass of TNT (i.e. tri-nitrotoluene).	Lees, 2005
2	TNO MultiEnergy	Based on 10 scaled curves for different strengths of explosion blast that depend on the layout where VCE takes place.	Van den Berg, 1985 Mercx, 2005
3	Backer-Strehlow-Tang (BTS)	Based on a continuum of numerically determined scaled curves obtained for different flame propagation speeds. (Default Method in ADAM)	Baker, 1996-Baker, 1996 - Tang, 1999 - Tang, 2000 Pierorazio, 2005

Table 10: VCE models used in ADAM

The *Equivalent TNT* mass method assumes that VCE are detonations and that the explosive substance involved behaves like a condensed explosive (i.e. tri-nitrotoluene). It is based on two single reference curves for the peak overpressure and positive impulse, respectively. In ADAM it was included for comparison purposes only.

The TNO Multi-Energy method is based on ten scaled curves for both peak overpressure and blast duration, referring to the associated blast severity.

The Backer-Strehlow-Tang method is based on a set of scaled curves for peak overpressure and positive impulse curves, which depends on the Mach number of the flame front speed.

Independently of the method used, ADAM estimates the amount of **explosive mass** M_{ex} by using dispersion models together with the values of the flammability limits of the substance under study. This is particularly relevant for the calculus of the combustion energy involved in the explosion, and it is an input requirement for all models. The explosive mass is determined by calculating the overall quantity of the flammable cloud within the flammability limits at the time of ignition. This can be obtained by calculating the following volume integral:

$$M_{ex} = \iiint_{V_{ULF/LFL}} C(\mathbf{r}, t_{ig}) dV \quad (189)$$

where C is the flammable concentration of the explosive cloud calculated at the time of ignition t_{ig} , whilst the volume integration is performed within the iso-concentration surfaces with concentrations equal to the flammability limits (i.e. UFL and LFL). For a more conservative approach, the integration can be done within the volume included within the LFL iso-concentration surface, by assuming that also the high concentration part of the cloud will take part in the explosion. This choice can be selected in the option menu. The integration procedure that is performed numerically allows obtaining also the *volume of the explosive cloud* V_c .

Since the cloud propagation is a dynamic process, it is necessary to input the ignition time t_{ig} to calculate the explosive mass. The calculus of the concentration distribution allows determining the LFL leading edge of the cloud at the ignition time, which identifies the ignition location. However, in practical situations ignition time is unknown and is more likely to identify the ignition location. For this reason, ADAM simulates the overall cloud propagation dynamic, and by fixing the ignition location, it calculates the front arrival time and, in turn, the ignition time necessary to fix the integration volume of eq. 189.

Since the dispersion model assumes the absence of obstacles to determine the extent of the cloud, for a more conservative approach, it is possible to assume that the whole amount of released vapours will be involved in the explosion. Thus, by assuming the mixture with air is stoichiometric, the volume of the flammable cloud V_c can be obtained as follows:

$$V_c = \frac{M_{ex}}{\rho c_s} \quad (190)$$

where ρ (kg m^{-3}) is the vapour density and c_s (vol.%) the stoichiometric concentration. In ADAM, the default procedure is based on the cloud dispersion modelling, however this alternative approach can be chosen in the option menu. If the stoichiometric option is selected, the vapour cloud dispersion is not considered, thus the results of the explosive mass is independent of the ignition location. Ignition time is required as an input data only for continuous releases for assessing the released mass at the time of explosion.

Finally, a point to note is that ADAM addresses only direct effects of the blast wave. Indirect effects, such as those associated with the presence of fragments or debris produced and accelerates by the explosion are outside the scope of ADAM.

TNT-equivalent mass method

The TNT equivalency model, described in detail by Lees (Lees, 2005) has been included in ADAM for comparison purposes only. This method is very simple and is based on the assumption of equivalence between the flammable substance involved in the VCE, and an amount of TNT, in terms of its potential blast effects.

The equivalent TNT mass M_{TNT} (kg) is obtained from the following expression:

$$M_{TNT} = f M_{ex} \frac{\Delta H_c}{\Delta H_{TNT}} \quad (191)$$

where the mass of the flammable involved in the explosion, M_{ex} , which is estimated by using eq. 189, is multiplied by the heat of combustion ΔH_c (kJ kg⁻¹) to get the equivalent energy of combustion, and then divided with the heat of combustion of TNT, ΔH_{TNT} (i.e., 4680 kJ kg⁻¹, HSE, 1986). The overall value is multiplied by an efficiency or yield factor f (-) that is the most critical, since it is very difficult to establish its actual value in practical circumstances. This is very much influenced by the reactivity of the substance and by the level of confinement and congestion where the explosion takes place. For hydrocarbons that are poor explosives, values in the range 0.01-0.1 were reported by several authors (Casal, 2008). In ADAM, according to the Health and Safety Executive (HSE, 1986), the selected reference value is associated with the reactivity of the involved substance as outlined in Table 11. These values have to be properly increased to 0.1, for high levels of congestion.

<i>f</i> (-)	<i>Reactivity</i>
0.03	Low
0.06	Medium
0.1	High

Table 11: Efficiency factor f (-) vs substance reactivity

The physical effect parameters that are necessary to determine the consequence of the explosion (i.e. peak overpressure and positive impulse) are represented in terms of the scaled distance \bar{r} (m kg^{-1/3}), i.e.:

$$\bar{r} = \frac{r}{M_{TNT}^{1/3}} \quad (192)$$

where r (m) is the distance from the centre of the explosion to the target where the effects have to be calculated. These parameters are normally obtained from normalised graphs. ADAM make use of the Kinney and Graham relations to calculate the peak overpressure ΔP_{peak} (Pa), the positive impulse i^+ (Pa s) and the positive-phase blast-wave duration t^+ (s) (Lees, 2005 vol 2 Chapter 17/124):

$$\Delta P_{peak} = P_a \frac{808 \left(1 + \left(\frac{\bar{r}}{4.5}\right)^2\right)}{\sqrt{1 + \left(\frac{\bar{r}}{0.048}\right)^2} \sqrt{1 + \left(\frac{\bar{r}}{0.32}\right)^2} \sqrt{1 + \left(\frac{\bar{r}}{1.35}\right)^2}} \quad (193)$$

$$i^+ = \frac{6.7 \sqrt{1 + \left(\frac{\bar{r}}{0.23}\right)^4}}{\bar{r}^2 \left[1 + \left(\frac{\bar{r}}{1.55}\right)^3\right]^{\frac{1}{3}}} \quad (194)$$

$$t^+ = \frac{0.98 M_{TNT}^{1/3} \left[1 + \left(\frac{\bar{r}}{0.54}\right)^{10}\right]}{\left[1 + \left(\frac{\bar{r}}{0.02}\right)^3\right] \left[\left(1 + \left(\frac{\bar{r}}{0.74}\right)^6\right)\right] \sqrt{1 + \left(\frac{\bar{r}}{6.9}\right)^2}} \quad (195)$$

Despite of the simplicity of the TNT-equivalent method, several aspects of a VCE are not addressed properly. First, there is no explicit reference to the level of confinement and the space configuration. In addition, differently from a TNT explosion, a VCE is normally characterised by very large clouds, which leads to a much lower overpressure at the centre of the explosion. For this reason, an upper limit of overpressure of 1 bar is considered in ADAM.

TNO Multi-Energy method

The TNO Multi-Energy method (Van den Berg, 1985; Mercx, 2005) is based on the assumption that the blast effect produced by a vapour cloud explosion is highly dependent on the level of confinement and congestion and less dependent on the overall amount of flammable. Severe blast effects are produced by the portions of vapour in partially confined or obstructed regions. The remaining unconfined parts will simply burn out without seriously contributing to the blast.

Since the layout of the space typical of industrial settings can be always split in areas of congestion of different size and shape, the Multi-Energy model defines a vapour cloud explosion as a number of sub-explosions, which take place inside these separate areas. Different sources of blast, which originate from these single areas, are therefore present in the cloud. The strength of each sub-explosion is directly associated with the level of congestion of the related area. These separate areas where the sub-explosions take place are named **obstructed regions**, which are regions with high density of obstacles resulting in the increase of spreading speed of the cloud.

Obstructed regions and sub-explosions

The Multi-Energy model is based on a specific procedure to separate the area surrounding each sub-explosion into obstructed regions. The part of the flammable cloud that is placed outside the congested area is called unobstructed region. The number and volume of obstructed regions are obtained by using series of empirical criteria, which are then compared with the volume occupied by the explosive cloud.

From this comparison, it is possible to estimate the number of the associated sources of blast that take part in the explosive process. This calculation has to be conducted before using ADAM, and the related information has to be uploaded accordingly.

A possible empirical approach to build up the obstructed regions is described in detail elsewhere (Mercx, 2005, Van den Berg, 2005). This consists of the break-down the plant structures into objects with simpler geometrical shapes (i.e., cylinder, boxes and spheres), and the separation of the different plant areas on the basis of the distance and shape of the different obstacles present. When the cloud covers more than one obstructed region, it is necessary to identify where the ignition takes place. The obstructed region where the ignition is located is indicated as '*donor*' and correspond to the location where the first explosion takes place. All the other regions are referred to as '*acceptors*' where subsequent explosions occur.

The overall blast effect produced by the contribution of all sub-explosions depends on the separation distance of the blast sources belonging to each obstructed region. Whence this distance is below a *critical separation distance* the sub-explosions will be considered practically simultaneous and their respective blast should be superimposed in the far field. Otherwise the separate explosions will be considered as occurring at different times and the overall peak overpressure will be considered as the maximum peak overpressure of the different sub-explosions. According to the results of the RIGOS test (van den Berg, 2005), in order to determine the critical separation distance (*CRD*) the following criterion is considered:

$$CRD = \begin{cases} \frac{1}{2}D_{donor} & \Delta P_{peak}^{donor} > 10^5 Pa \\ \frac{1}{4}D_{donor} & \Delta P_{peak}^{donor} < 10^4 Pa \end{cases} \quad (196)$$

where ΔP_{peak}^{donor} is the peak overpressure of the blast source belonging to the donor obstructed area and D_{donor} is the dimension of the donor obstructed area. For intermediate values of peak overpressure the *CRD* is obtained via linear interpolation of the above values.

As for the creation of the obstructed regions, the ADAM user has to apply this criterion as a separate exercise, and select whether the different sub-explosions have to be considered as simultaneous or occurring at separate times.

Effects parameters calculation

The scope of the Multi-Energy model should be clearly understood. It refers to vapour cloud explosions only, resulting from the release and following dispersion of a flammable cloud in a congested area of an industrial setting. The method is a simplification of reality and does not model directional blast effects due to the presence of inhomogeneous obstacles. VCE detonation is considered as extremely unlikely and the deflagration assumption is considered sufficiently conservative in any typical industrial setting.

The calculation of the peak overpressure and positive impulse are performed according to the procedure described in the TNO Yellow Book (Mercx, 2005) and herewith summarised:

1. Determine cloud mass and volume

The mass quantity contained within the flammable cloud at the time of the explosion is determined by using the ADAM dispersion modelling. This is obtained by integrating the concentration of the flammable within the cloud volume within the flammability limit surfaces (see eq. 189), which allows also obtaining the volume of the explosive cloud V_c . As an alternative option, ADAM allows considering the whole content of the released flammable mass, and the cloud volume is taken from the stoichiometric relationship as provided in eq. 190.

2. Identify potential blast sources

The potential blast sources present in the area covered by the flammable cloud have to be identified. Potential source of strong blasts are process equipment in chemical plants or refineries, stacks of crates or pallets, and pipe racks, the volume between parallel planes (beneath closely parked cars, multi-story parking garages), tubelike structures (i.e. tunnels, bridges, corridors), highly turbulent fuel jets, etc.

3. Define obstructed regions

The obstructed regions are defined according to the empirical criterion outlined in the previous section and described in detail in the TNO Yellow book (Mercx, 2005) and in the paper by Van den Berg and Mos (Van den Berg, 2005). The area where the VCE takes place will be therefore split in a series of boxes delimiting each identified obstructed region. At this stage, it is necessary to upload in ADAM the maximum part of the cloud that can be inside each of the identified boxes, which corresponds to the associated free space (i.e.

the volume of the box delimiting the obstruction region minus the volume of the associated obstacles). When all the obstructed regions results as completely filled in by the cloud, the portion of the cloud volume that remains, if any, is referred to as the *unobstructed part of the cloud*. This part still contributes to the blast but to a much lower extent. Finally, for each obstructed area it is possible to calculate the blast energy associated with each sub-explosion $E(J)$ by multiplying the flammable mass contained in each box by the heat of combustion per unit mass of the flammable, ΔHc ($J\ kg^{-1}$), which is taken from the ADAM database.

4. Estimate the source strength for each obstructed regions

To each source of blast, it is necessary to estimate its strength on a scale from 1 to 10, with the last referring to the highest explosion level (detonative strength).

For a safe and most conservative estimate of the strength of the sources of a strong blast can be made by assuming a strength of 10. However, a source strength of 7 seems more appropriate to represent actual experience in process plants (Crowl, 2003, CCPS, 2010).

The blast resulting from the remaining unobstructed parts of a cloud can be modelled by assuming a very low initial strength. In ADAM the allowed strength values are in the range 1-3, with 1 to be used for extended and quiescent parts, and 3 for more nonquiescent parts, which are in low-intensity turbulent motion (Crowl, 2003).

5. Calculate the blast effects parameters

Once the different obstruction regions, the cloud filling volume, the combustion energy and the initial blast strength are identified, the blast effect parameters (i.e. peak overpressure and the positive-phase blast duration) can be determined as a function of the distance r (m) between the explosion centres and the target. This is conducted by using the Multi-Energy **blast curves**, which can be extracted from the TNO Yellow book (Mercx, 2005), after calculation of the Sachs-scaled distance \bar{r} (-):

$$\bar{r} = \frac{r}{(E/P_a)^{1/3}} \quad (197)$$

where E (J) is the blast energy, and P_a (Pa) is the ambient pressure.

For each value of the target distance r and in turn of the associated scaled value \bar{r} , the blast peak overpressure ΔP_{peak} (Pa) and the positive-phase duration t^+ (s) are calculated from the corresponding Sachs quantities $\overline{\Delta P}$ (-) and $\overline{t^+}$ (-), which are obtained from the mentioned blast curves:

$$\Delta P_{peak} = \overline{\Delta P} P_a \quad (198)$$

$$t^+ = \overline{t^+} \frac{(E/P_a)^{1/3}}{c_0} \quad (199)$$

where c_0 ($m\ s^{-1}$) is the ambient speed of sound.

An approximate value of the positive impulse i^+ can be calculated by multiplying the peak overpressure with the positive-phase duration with a factor $\frac{1}{2}$, i.e.:

$$i^+ = \frac{1}{2} \Delta P_{peak} t^+ \quad (200)$$

If separate blast sources are located close to one another, the sub-explosions may initiate almost simultaneously. When it is not possible to exclude that the events occur simultaneously, the blasts should be superimposed. A possible criterion to establish this situation based on the determination of a minimum distance between potential blast sources so that their individual blasts may be considered separately is described in the previous sections and summarised in eq. 196.

Backer-Strehlow-Tang (BST)

The Baker-Strehlow-Tang method (BST) (Baker, 1996-1998; Tang, 1999-2000) is based on the assumption that only those parts of the flammable cloud that are in a confined and congested area contribute to the vapour cloud explosion. Within these regions, the obstacles are cause of an acceleration of the flame front. Differently from the Multi-Energy method, in which blast intensity depends on a generic parameter (i.e. blast strength), the BST method uses a continuum of numerically-determined pressure and impulse curves that are based on the flame propagation speed, expressed in terms of the **flame Mach number M_f** . This is the apparent flame speed divided by the ambient speed of sound, being the first the VCE flame front speed relative to the target.

In ADAM, the set of blast curves, providing the scaled blast intensity parameters, as a function as the scaled distance are those extracted from the work of Tang and Baker (Tang, 1999). Different curves are available for different flame Mach numbers. The blast energy $E(J)$, used to calculated the scaled parameters, and the cloud mass and volume are calculated as in the Multi-Energy case.

In order to apply the BST method and the associated blast curves, it is necessary to determine the flame Mach number associated with the VCE. This is dependent on: *a)* the **reactivity** of the flammable substance, *b)* the **confinement** (i.e., the way how flame expansion propagates), and *c)* the **congestion** (i.e., density of the obstacles).

Once these parameters are determined, the flame Mach number is obtained from the reference table provided by Pierorazio et al., which was obtained after a dedicated test programme (Pietorazio, 2005):

Confinement	Reactivity	Congestion		
		Low	Medium	High
2-D	High	0.59	DDT	DDT
	Medium	0.47	0.66	1.6
	Low	0.079	0.47	0.66
2.5-D	High	0.47	DDT	DDT
	Medium	0.29	0.55	1.0
	Low	0.053	0.35	0.50
3-D	High	0.36	DDT	DDT
	Medium	0.11	0.44	0.50
	Low	0.026	0.23	0.34

DDT: Deflagration-to-Detonation transition. In ADAM, for the application of the BST method, a Mach number 5.2 blast curve is associated to such a case.

Table 12: BST Flame speed correlations (Mach number) for different combinations of reactivity, confinement, congestion (Pierorazio, 2005)

In order to apply Table 12, it is necessary to determine the reactivity of the flammable involved in the VCE, the level of congestion, and the confinement type.

Reactivity is an inherent property of the substance providing a measure of the flame front tendency to accelerate and to create overpressures or potentially undergo a deflagration-to-detonation transition (DDT). For the purposes of the BST model,

reactivity is classified as low, medium or high depending on the laminar flame speed (LFS) according to the criterion reported in the table below (Baker, 1996):

Reactivity		Substances (examples)
High	$LFS > 75 \text{ cm s}^{-1}$	Acetylene, Ethylene oxide, Hydrogen, 1-3 Propylene Oxide, Ethylene
Medium	$45 \text{ cm s}^{-1} \leq LFS \leq 75 \text{ cm s}^{-1}$	Acetone, 1-3 Butadiene, Propane
Low	$LFS < 45 \text{ cm s}^{-1}$	Methane, Carbon monoxide

Table 13: Flammable reactivity by laminar flame front

Mixtures are classified according to the most reactive component in the mixture.

The effect of **confinement** refers to the number of dimensions involved in the flame expansion process. The following classification is used in the BST model:

Category	
3-D	Flame is free to expand in 3D (i.e., spherical or hemispherical). Flame surface increases with the square of the distance from the ignition. Flame expansion speed is normally low, and the disturbance to expansion due to the obstacles is relatively small. This represents an expansion into free space (i.e., no confinement)
2-D	2D expansion (i.e., cylindrical). This represents the case of expansion between two parallel planes. The overall surface of the flame is proportional to the distance from ignition. Disturbances of the flame expansion have a greater effect than the 3D case.
2.5-D	flame expansion in an area with limited 2D confinement. It represents the case of confinement that is made with frangible or partially confined panels (e.g., a closely paced pipe system). This category replaced the 1D category (hereunder described) by simply averaging the 2D and 3D flame speed results.
1-D	During a 1D expansion (e.g., expansion of a flame within a cylinder), the flame's surface is stable. A strong feedback mechanism is created for the increase of the flame's acceleration.

Table 14: Level of Confinement for the application of the BST method

As suggested by Pierorazio et al. (Pierorazio, 2005) category 1-D has to be removed, since it produces an excessive effect on flame acceleration by leading to DDT even under very low congestion. For this reason, ADAM addresses only the confinement categories: 3-D, 2.5-D and 2-D.

Congestion is represented by the obstacles density present where explosion takes place. This is classified as high, medium, or low based on the volume blockage ratio (VBR), i.e., the sum of all obstacle volumes divided with the total volume of the area under investigation. This parameter does indeed affect how the flame accelerates during propagation. In general, the following criterion can be used to assess the congestion category:

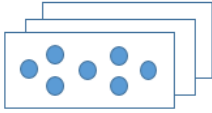
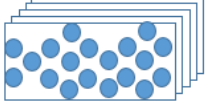
<i>Type</i>	<i>VBR</i>	<i>Geometry</i>	<i>Description</i>
Low	<10%		Easy to walk through, there are only 1-2 layers of obstacles
Medium	Between 10% and 40%;		Cumbersome to walk through. Often necessary to take indirect paths, 2-3- layers of obstacles
High	> 40%		Not possible to walk through, as there is insufficient space to pass between obstacles. 3 or more closely spaced obstacles

Table 15: Level of Congestion vs the volume blockage ratio (VBR)

Effects parameters calculation

The procedure employed in ADAM to determine the blast effect parameters (i.e., peak overpressure and positive-phase impulse) by using the BST method, is similar to the one presented in the section on Multi-Energy, and is summarised hereunder:

1. Determine cloud mass and volume

The amount of the flammable cloud involved in the explosion is determined by using ADAM dispersion modelling and by integrating the concentration of the cloud in the volume within the flammability limits' surfaces (see eq. 189). This allows obtaining also the size, i.e., the volume of the explosive cloud V_c . Alternatively, ADAM allows the whole content of the released flammable as taking part in the explosion. In such a case, the cloud volume is taken from the stoichiometric relationship provided in eq. 190.

2. Identify the congested or partially confined portion of the flammable cloud.

A plant walk through activity is necessary to define the level of Confinement (see Table 14) and the level of Congestion (Table 15). When several areas of confinement and congestion are present, these areas are averaged into a single area with average values of confinement and congestion.

3. Determine the suitable flame speed.

The apparent flame speed is expressed in terms of the **flame Mach number M_f** by using Table 12. Input parameters are the level of confinement and congestion, assessed in the previous step, and the reactivity of the flammable substance that is extracted from the ADAM database.

4. Determine the effects parameters from the selected BST blast curve.

The BST method provides different blast curves for the effect parameters as a function of the scaled distance, with the flame speed as a parameter. These curves include positive and negative peak overpressures, positive and negative impulses, and time durations for positive and negative phases. Amongst these, ADAM uses only the peak overpressure and positive-phase impulse as the reference effects parameters.

A point to note is that the blast curves provided by Tang and Baker (Tang, 1999) are obtained for nine different values of the flame Mach number ranging within 5.2-0.2. However, the flame speed correlations for different combinations of reactivity,

confinement, congestion provided in Table 12 (Pierorazio, 2005) yield to Mach number values that do not match with those associated with the blast curves. Thus, ADAM has implemented a procedure to interpolate from the original set (and in a few cases to extrapolate) the blast curves for all Mach number values of Table 12.

Whence a blast curve associated with the flame Mach number determined in the previous step is selected, the scaled effects parameters (i.e. $\overline{\Delta P}$ and \bar{t}^+ , normalised using Sach's scaling) can be obtained as function of the scaled distance \bar{r} .

From these values, the effect parameters (i.e., peak overpressure and positive impulse) are obtained as a function of the distance r of the target from the explosion centre, i.e.:

$$r = \bar{r} (E/P_a)^{1/3} \quad (201)$$

$$\Delta P_{peak} = \overline{\Delta P} P_a \quad (202)$$

$$i^+ = \bar{t}^+ \frac{E^{1/3} P_a^{2/3}}{c_0} \quad (203)$$

ΔP_{peak}	positive peak overpressure (Pa)
i^+	positive-phase impulse (Pa s)
P_a	ambient pressure (Pa)
c_0	ambient speed of sound (m s ⁻¹)

where the blast energy E (J) is calculated by multiplying the flammable mass contained in the cloud by the heat of combustion per unit mass of the flammable, ΔHc (J kg⁻¹), which is taken from the ADAM database. Since the BTS curves are based on a spherical explosion model, a suitable multiplication factor has to be considered to the calculus of the combustion energy E . In ADAM a factor of 2 is taken for ground explosions that accounts for the total reflection of the blast wave.

Atmospheric Dispersion of Toxic or Flammable Clouds

General

The term *Dispersion* is used in accident consequence analysis to describe the propagation of flammable or toxic cloud of vapour in the atmosphere. This propagation occurs by diffusion (i.e. turbulent eddy motion) and advection (i.e. wind) with the overall result of the cloud movement mainly toward the wind direction, but also perpendicular to the wind both in the horizontal and vertical directions. Atmospheric dispersion is a very complex phenomenon and its mathematical description requires some necessary simplifications.

When the release of a dangerous substance leads to the formation of a vapour cloud, foreseeing the behaviour of its concentration in the atmosphere is very important to estimate the potential consequences on people and on the environment. In particular, the purpose of the dispersion model is to predict how the concentration contaminant once released into the atmosphere varies with time and position. There are several parameters influencing the atmospheric dispersion process, which are input data for the ADAM-dispersion module. In particular:

- **release conditions**, which include (i) the type of substance, state and physical properties, (ii) the source term (exit velocity, exit temperature, flow rate, total amount, vapour quality rainout), and (iii) the source location. *All the parameters belonging to this category are provided as an output from ADAM module 1;*
- **meteorological conditions**, which include the wind speed and direction, the level of atmospheric turbulence, the ambient temperature and humidity, and the thermal inversion. All these variables are particularly critical since they affect the cloud dispersion significantly. In addition, they vary continuously with time, which requires taking average values of the associated variables in order to model the dispersion in a representative way;
- **surrounding environment**, which includes the terrain morphology, and the presence of obstacles. This aspect is probably the most difficult to model since it requires the full use of fluid dynamics calculations. For integral models, the influence of surrounding environment is reduced to the use of a few parameters. In ADAM we made use of the terrain roughness, Albedo and Bowen ratio.

The wind speed varies as a function of the altitude since the ground roughness produces air friction. Since the measurements are normally conducted at a certain altitude (i.e., typically 10m) it is necessary to correct the wind speed value to the geometric height of the source, i.e. the release height in the case of a jet, or the ground for catastrophic releases or pool evaporation vapour cloud formation. For this purpose, the logarithmic law, which provides the wind profile as a function of the Monin-Obukhov length, is commonly used.

ADAM uses an in-house modified version of the SLAB model for modelling atmospheric dispersion of toxic and flammable clouds. The SLAB model, applicable to denser-than-air and neutrally buoyant clouds, was developed by the Lawrence Livermore National Laboratory, with support from the US Department of Energy, US Air Force Engineering Center, and the American Petroleum Institute (Zeman, 1982; Ermak, 1990).

The present chapter summarises the main features of the model and the modifications implemented in ADAM. The description of the specific governing equations and sub-models of SLAB is provided in detail elsewhere (Ermak, 1990; Bakkum, 2005).

A point to note is that concentrations calculated using integral models such as SLAB or others available in the literature do not account of the removal mechanism by dry deposition at the surface and by chemical reactions in the cloud, which are present for many substances. For this reason, these models tend to over predict the consequences.

The SLAB dispersion model

The base model used by ADAM is SLAB, a widely used, validated and quality assured model to treat heavier-than-air clouds but that can be applied also to neutral buoyant or lighter-than-air clouds. In particular, SLAB addresses various types of releases, including a **ground-level evaporating pool**, an elevated **horizontal jet**, a stack or elevated **vertical jet**, and an **instantaneous volume source**. With the exception of the evaporating pool, in which the source term is assumed all vapour, the other sources may consist of either pure vapour or a mixture of vapour and liquid droplets.

The atmospheric dispersion is calculated by solving spatially averaged *conservation equations of mass, momentum, energy, species*. The conservation equations are spatially averaged in order to treat the cloud as a steady state plume, a transient puff, or a combination of the two depending on the duration of the release. In this respect, it should be considered that the solution to spatially averaged equations leads to spatially averaged cloud properties, as well as the description of the normal atmospheric advection and turbulent diffusion processes.

In general, the conservation equations used to calculate the spatially averaged effects of the dispersing cloud (i.e., toxic or flammable concentration) are expressed in two forms to represent two different dispersion modes: the *steady state plume* and the *transient puff*, depending whether the release source is *continuous* (i.e. with very long duration) or *instantaneous* (i.e. catastrophic). For *finite duration releases*, cloud dispersion is described by using the steady state plume mode until the source is active. Afterwards, when the release ceases, the cloud is treated as a puff and subsequent dispersion is calculated using the transient puff mode. Conservation of the half-plume width is applied in the transition point.

For completing the description of the normal atmospheric advection and the turbulent diffusion process, several submodules are added to the conservation equations. These sub-models are designed to assess the following issues:

- the *wind friction* and the *wind speed profile*, based on the logarithmic law, which includes the momentum Monin-Obukhov function;
- the *entrainment rates*, which includes the effect of friction, the differential air-cloud motion, the ground heating thermal convection, and the damping of air-cloud mixture due to stable density stratification within the cloud;
- *heat and momentum flux* terms;

- *Liquid droplets formation and evaporation* based on an equilibrium thermodynamics model that controls the liquid-vapour ratio. Droplets are those resulting from the release substance and from vapour water. SLAB assumes that the size of liquid droplets is sufficiently small so that the transport of the vapour-droplet mixture can be treated as a single fluid.

The solution of the set of conservation equations, together with the coupled sub-models, yields to the determination of the instantaneous spatially-averaged concentration, with the term “instantaneous” referring to the absence of *cloud meander*. The cloud meander effect is the random oscillation of the cloud centreline due to atmospheric turbulence and is responsible for an increase of the effective width of the cloud and a decrease of the centreline concentration. The 3D variation of the concentration distribution is then recaptured by applying similarity profile functions (Ermak, 1990). These functions give the concentration distribution about the cloud centre and are based on the calculated spatially-averaged parameters of the cloud (i.e. width, height and length). The result is an instantaneous concentration distribution in terms of the downwind distance from the source (x), the crosswind distance from the cloud centreline(y), and the height above the ground (z).

To obtain the time-average concentration distribution, as necessary to determine the dose absorbed after a certain exposure time, the following procedure is applied. First, the effective cloud width is recalculated from the instantaneous concentration by taking into account the cloud meander effect. Secondly, the actual time-average concentration is calculated from the recalculated instantaneous concentration distribution $C(\mathbf{r}, t)$, which includes the meander effect, as follows:

$$C_{av}(\mathbf{r}) = \frac{1}{t_{av}} \int_{t_{pk} - \frac{t_{av}}{2}}^{t_{pk} + \frac{t_{av}}{2}} C(\mathbf{r}, t) dt \quad (204)$$

where t_{av} and t_{pk} are the averaging time and the time of peak concentration, respectively.

In order to cope with the different possible types of releases, different calculus moduli are present in SLAB. These consists of instantaneous releases, when the formation time of the gas cloud is much smaller than the time to dissolve completely, continuous and finite duration releases, as described in the following sections.

Instantaneous releases (Transient Puff mode)

Instantaneous releases are typically those associated with a catastrophic failure of a vessel or when the formation time of the cloud is much smaller than the time required to dissolve the cloud (i.e., when the volume concentration of the dangerous substance is below the hazard threshold). These situations are modelled in SLAB using the Transient puff mode (see Figure 11), where the conservation equations are averaged over all three dimensions of the cloud leaving the downwind travel time of the puff (t) as the single independent variable.

The 3D-spacially averaged concentration is expressed in by using similarity profile functions (i.e. C , C_1 , and C_2) whose parameters (i.e. m , x_c , b_x , β_x , b_y , β_y , z_c , and σ) are

obtained from the solution of the governing equations (Ermak, 1990). The result is given by the following expressions:

$$C(r, t) = 4B_x B_y h C(t) C_1(x - x_c, b_x, \beta_x) C_1(y, b_y, \beta_y) C_2(z, z_c, \sigma) \quad (205)$$

$$C_1(x, b, \beta) = \frac{1}{4b_x} \left[\operatorname{erf} \left(\frac{x + b}{\sqrt{2}\beta} \right) - \operatorname{erf} \left(\frac{x - b}{\sqrt{2}\beta} \right) \right] \quad (206)$$

$$C_2(z, z_c, \sigma) = \frac{1}{\sqrt{2\pi}\sigma} \left[e^{-\frac{(z-z_c)^2}{2\sigma^2}} + e^{-\frac{(z+z_c)^2}{2\sigma^2}} \right] \quad (207)$$

where, the average puff volume concentration $C(t)$ is calculated from M_w^{air} and M_w^s , (air and substance molecular weights), and the average puff mass concentration m , obtained from the solution of the governing equations as a function of travelling time:

$$C(t) = \frac{M_w^{air} m(t)}{M_w^s + (M_w^{air} - M_w^s) m(t)} \quad (208)$$

The similarity profile functions (i.e., crosswind/horizontal C_1 and vertical C_2) are fully described by the following parameters that are obtained as a function of the travelling time t , from the governing equations' solutions:

- $b_x(t), \beta_x(t)$ puff half-width downwind parameters
- $b_y(t), \beta_y(t)$ puff half-width crosswind parameters
- $z_c(t), \sigma(t)$ puff height parameters

The puff half widths (B_x and B_y) and half height h can be determined from the mean square of the cloud profiles.

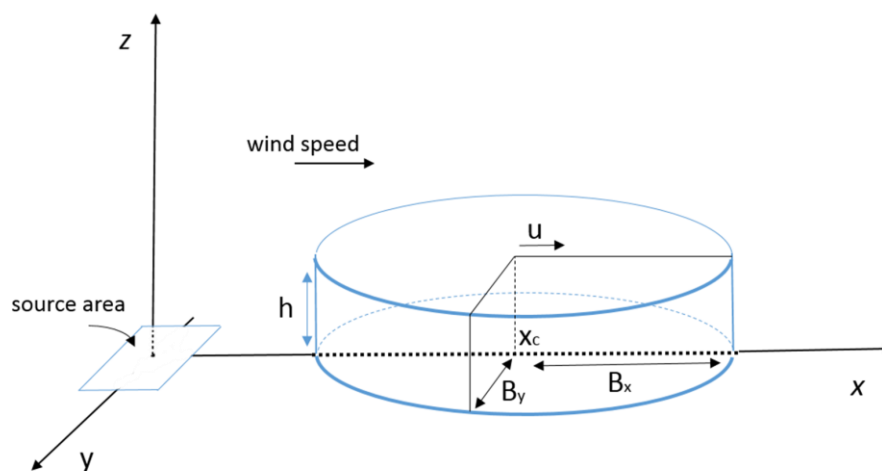


Figure 11: Dispersing cloud as depicted in the Puff dispersion mode

The similarity profile functions C_1 and C_2 are depicted in Figure 12 for different values of the width and height parameters.

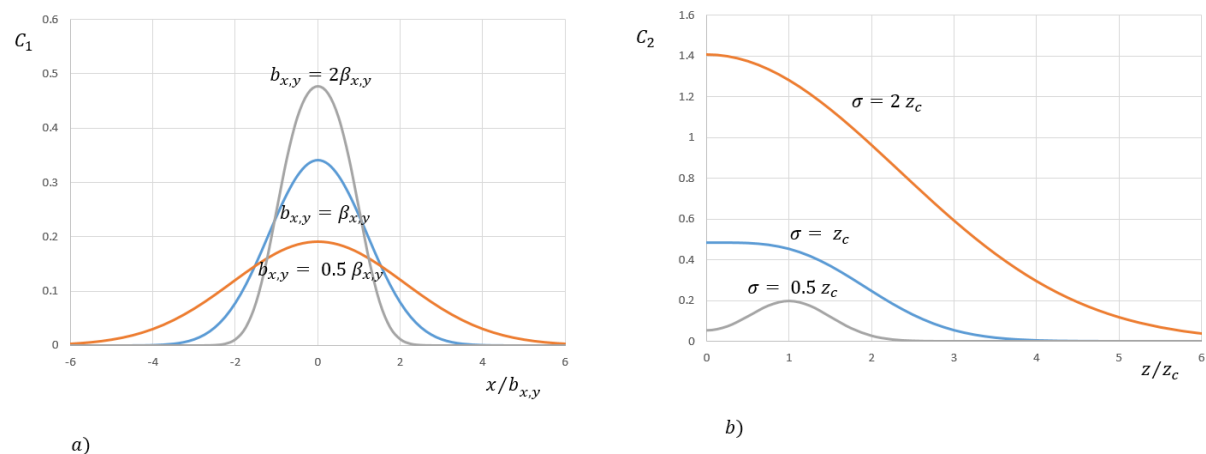


Figure 12: Cloud profiles for different values of the parameters a) Crosswind/horizontal profile, b) vertical profile

Continuous releases (steady state plume mode)

Continuous releases refers to all situations in which the outflow time scale is sufficiently large for settling a steady state plume, which is normally directed along the wind direction. The conservation equations are averaged over the crosswind plane of the plume leaving the downwind distance, x as a single independent variable.

Since this mode refers to a steady state, the 3D-plume concentration is independent of time and is expressed by the following expression:

$$C(\mathbf{r}) = 2 B_y h C(x) C_1(y, b_y, \beta_y) C_2(z, z_c, \sigma) \quad (209)$$

where:

$$C_1(y, b_y, \beta_y) = \frac{1}{4b_y} \left[\operatorname{erf}\left(\frac{y + b_y}{\sqrt{2}\beta_y}\right) - \operatorname{erf}\left(\frac{y - b_y}{\sqrt{2}\beta_y}\right) \right] \quad (210)$$

$$B_y^2 = b_y^2 + 3\beta_y^2 \quad (211)$$

$$C_2(z, z_c, \sigma) = \frac{1}{\sqrt{2\pi}\sigma} \left[e^{-\frac{(z-z_c)^2}{2\sigma^2}} + e^{-\frac{(z+z_c)^2}{2\sigma^2}} \right] \quad (212)$$

$$\sigma^2 = \begin{cases} \frac{h^2}{12}, & z_c > \frac{h}{2} \text{ (lofted)} \\ \frac{(h - z_c)^2}{3}, & z_c \leq \frac{h}{2} \text{ (grounded)} \end{cases} \quad (213)$$

with the crosswind-average volume concentration C is given by:

$$C(x) = \frac{M_w^{air} m(x)}{M_w^s + (M_w^{air} - M_w^s) m(x)} \quad (214)$$

where M_w^{air} and M_w^s , the air and substance molecular weight, respectively and m the mass concentration.

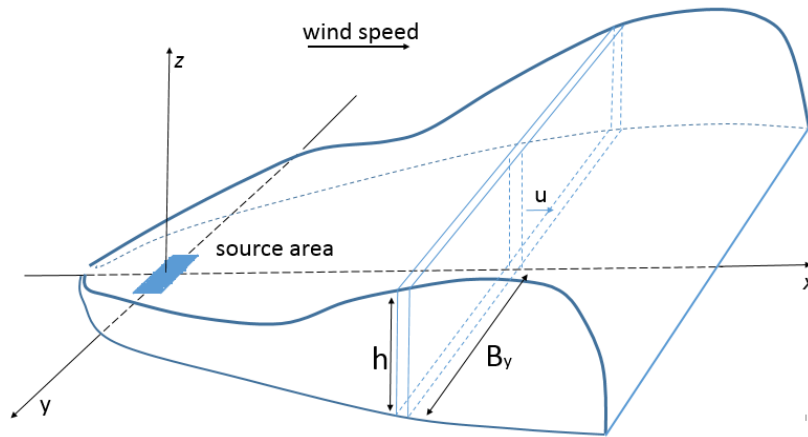


Figure 13: Dispersing cloud as depicted in the Plume dispersion mode

As for the previous case, C_1 and C_2 are the similarity profile functions describing the crosswind and vertical profiles of the plume. They are fully characterised following parameters that are obtained as a function of the downwind distance, x , from the equations' solutions:

- $m(x)$ mass concentration
- $b_y(x), \beta_y(x)$ plume half-width parameters
- $z_c(x), \sigma(x)$ plume height parameters

The plume half width (B_y) and the half height h can be determined from the mean square of the cloud profiles.

The main problem is that a purely continuous release does not exist, since in all practical cases, the release has always a finite time duration t_d . Under this condition, the cloud is modelled as steady state plume for times below the release duration t_d . Afterwards, the cloud is modelled as a puff. For this reason, there is a transition in the calculation of the specially-averaged cloud properties from the steady-state equations to the transient puff equations. The main difference is that whilst in the steady state plume mode the equations are specially-averaged over the crosswind plane of the cloud, in the transient puff mode, they are averaged over the entire volume of the cloud. To describe this

transition, SLAB defines a puff centre of mass x_T , in the downwind distance, and a cloud length at the time of transition t_a in order to ensure continuity of the cloud in the two different regimes. In such a way, the volume-averaged (puff) properties of the cloud will be equal to the crosswind-averaged (plume) properties at the time and the downwind location of the transition.

ADAM-SLAB model

General

In ADAM, the SLAB algorithm to model the airborne dispersion resulting from continuous, finite, and instantaneous releases from several source types, has been rewritten in a more efficient code by using the C++ language.

Differently from SLAB, which requires an external source term module to drive the physical effect calculation, ADAM makes use of its Module 1 to input all necessary data to run the algorithm. In addition, in order to ensure consistency and to compare the results between ADAM and SLAB, it was decided to maintain the same input data structure of the original SLAB software. Module 1 of ADAM produces an INPUT.txt file, containing the source term and the atmospheric release characteristics, as well as meteorological and terrain data, as described in the SLAB manual (Ermak, 1990, see also Table 16).

). Although ADAM Physical Effects (i.e. Module 2) receives the input data as an internal data structure, the INPUT.txt file is produced anyhow in order to allow the use of the original SLAB software with the same data set. This is mainly done for verification purposes and for exploring the differences between ADAM and SLAB.

After processing, ADAM produces concentration and lethality maps or iso-effect contours together with information on the centreline concentration, at the reference height, as set by the user. The original PREDICT.txt file of SLAB, providing the similarity function coefficients together with the concentration vs. downwind distance for some crosswind distances (i.e. $y = 0, 0.5B_y, B_y, 1.5 B_y, 2.5 B_y$) and for 4 different heights, has been therefore replaced with a more versatile output data structure. In addition, the output can also be transformed into a KML or GPX format in order to allow the visualisation in a GIS based system (e.g. Google Earth). As for SLAB, ADAM produces values for the *maximum concentration*, *average concentration* that is necessary to determine the absorbed dose, and *instantaneous concentration* that is necessary when dispersions involving flash fires or explosions are involved.

The original SLAB program has a special algorithm to execute the calculus of similarity function coefficients, and in turn the 3D-concentration, for a fixed number (i.e. 61) of downwind centreline points, with relative distances that are optimised to the specific dispersion under investigation. As a result, the output data have higher substance concentration at the source and nearby regions and lower substance concentration as one moves away from the source. The same algorithm has been used in ADAM; however, the number of points in the centreline has been increased by a factor of 20 (i.e. 1220). With such an increased number of points, the calculus time is still very short and the obtained concentration maps have good spatial resolution.

Whilst in SLAB, some environmental data, such as the ambient pressure and the thermophysical properties of air and water, are coded in the software, ADAM uses the values extracted from the database that correspond to the specific environmental conditions (i.e. temperature and pressure) of the scenario under study.

The above differences between ADAM and SLAB are general character, resulting in faster and more accurate calculation of the results. In addition to these modifications, ADAM

introduces some more specific modelling improvements, which cover the following aspects:

- alternative calculus of the *average concentration* for instantaneous releases;
- calculus for time-varying releases;
- inclusion of the contribution from pool evaporation in case of rainout;
- modification of the SLAB routine for the calculus of plume velocity.

Parameter	Description	Note
IDSPL	Spill source type	1-evaporating pool 2-horizonta1 jet 3-vertical jet 4-istantaneous
NCALC	Numerical SubStep parameter	Number of calculus substeps (1to3) for accuracy
<i>Source Properties</i>		
WMS	Molecular weight of substance (kg)	
CPS	Vapour heat capacity (J kg ⁻¹ K ⁻¹)	
TBP	Boiling point temperature (K)	
CMEDO	Initial liquid mass fraction	Liquid phase in the form of droplets
DHE	Heat of vaporisation (J kg ⁻¹)	
CPLS	Liquid heat capacity (J kg ⁻¹ K ⁻¹)	
RHOSL	Liquid density of substance (kg m ⁻³)	
SPB	Saturation pressure constant	Antoine parameters
SPC	Saturation pressure constant	
<i>Source Term</i>		
TS	Temperature of source Material (K)	Exit temperature. For flashing substances, temperature after flash
QS	Mass source rate (kg s ⁻¹)	Relevant for continuous (finite duration) releases only
AS	Source area (m ²)	IDSPL = 1 (pool area) IDSPL = 2,3 (fully expanded jet area) IDSPL = 4 (area of the volume source in the ground plane)
TSD	Source duration (s)	Relevant for continuous (finite duration) releases only
QTIS	Instantaneous source mass (kg)	Relevant for instantaneous releases only
HS	Source height (m)	IDSPL = 1 (zero) IDSPL = 2 (height of the jet centre) IDSPL = 3 (actual height of the jet) IDSPL = 4 (Volume source/AS)
<i>Field Parameters</i>		
TAV	Averaging time (s)	
XFFM	Maximum downwind distance (m)	
ZP	Height of concentration calculation (m)	
<i>Meteorological Parameters</i>		
ZO	Surface roughness height (m)	
ZA	Ambient measurement height (m)	
UA	Ambient wind speed (m s ⁻¹)	
TA	Ambient temperature (K)	
RH	Relative humidity (%)	
STAB	Pasquill Stability class	A to F (1 to 6)
ALA	Inverse Monin-Obukhov length (m ⁻¹)	Alternative to STAB

Table 16: Input data structure of the original SLAB programme (i.e. INPUT.txt file format)

Alternative calculus of the average concentration

The calculus of the time-average concentration is performed by using the following equation:

$$C_{av}(\mathbf{r}) = \frac{1}{t_{av}} \int_{t_{pk} - \frac{t_{av}}{2}}^{t_{pk} + \frac{t_{av}}{2}} C(\mathbf{r}, t) dt \quad (215)$$

where C is the instantaneous concentration, recalculated to account the meander effect, t_{av} is the travelling time and t_{pk} the time of peak concentration.

The calculus of the integral of eq. 215 is rather trivial for the steady state plume regime, as the concentration is assumed to rise to the steady state value (C_{max}) by remaining at this value for the whole duration of the release, and drops to zero afterward. Therefore the average concentration is equal to C_{max} if the average time is less than the release duration t_d , and is $t_d/t_{av}C_{max}$ otherwise.

By contrast, the case of the transfer puff dispersion, typical of instantaneous releases, is more complicated since the full integration has to be done. SLAB simplified this process by converting the time integration into the downwind distance x , with the puff centre-of-mass located at the downwind distance of interest X_c , i.e.:

$$C_{av}(\mathbf{r}) = \frac{1}{U(t_{pk})t_{av}} \int_{X_c - \frac{U(t_{pk})t_{av}}{2}}^{X_c + \frac{U(t_{pk})t_{av}}{2}} C(\mathbf{r}, t_{pk}) dx \quad (216)$$

where U is the velocity of the puff centre-of-mass at time of peak concentration. In such a way and by solving the above integral analytically, it is possible to reduce the calculus time significantly. However, this approximation has the inherent error that since the centre-of-mass of the puff will never be located for negative values of x (i.e. it propagates downwind), the average concentration backwind is always assumed to be zero by SLAB. This cannot be obviously true for catastrophic releases, as part of the toxics will also diffuse backwind.

The main problem associated with the SLAB assumption is that, despite of what intuition may suggest, the peak concentration time at a certain distance X_c from the source, does not necessarily occur when the centre-of-mass of the puff is centred in X_c as indicated in Figure 14. Since the puff decreases in intensity when travelling downwind, the maximum concentration at $x = X_c$ might occur when the puff centre-of-mass is still below X_c .

In general, the SLAB approximation leads to a diverging average concentration at the source, a lower concentration in the near region and it tends to be valid only further. Thus, in ADAM the SLAB approximation is not applied and the full integral of eq. 215 is calculated by using a special algorithm that makes use of both Romberg and Gaussian methods to optimise the calculus time.

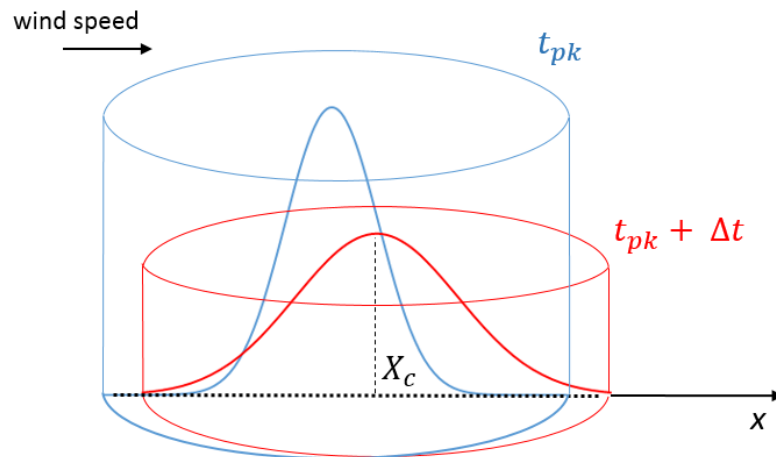


Figure 14: Puff at two separate instances, showing that the peak of concentration vs time in point X_c does not necessarily occur when the puff has centre of mass in X_c .

Calculus for time-varying releases

For scenarios involving finite duration release (i.e. horizontal/vertical jets, and pool evaporation), SLAB is based on the assumption that the flow rate (or evaporation rate) is constant within the release time range, and zero outside. Since ADAM calculates the actual source term, which includes its time dependence, it is necessary to couple the time-varying release with the dispersion model. In order to achieve this, the time-varying release is divided into a number of discrete time segments, and the dispersion associated therewith is calculated accordingly.

Figure 15 shows how this split is conducted on a typical source term, where the mass flow rate is depicted as a function of the release time. The release depicted in the figure is the typical jet outflow from a vessel containing compressed gas. As suggested in the Purple Book (RIVM, 1999), the segments used to approximate the flow rate are characterised by constant values, which correspond to the outflow average in the selected time segment. The segment duration is defined in such a way that all segments have equal areas (i.e. the released mass is equal in each segment time) and the sum of all segment areas is the same as the area under the flow rate curve (i.e., the total released mass). ADAM allows splitting the time-varying release source term into a maximum number of twenty segments, with a default value of five.

In addition to the multi segment approach, ADAM allows also approximating the time-varying source term with a single segment (see the green and red segments in Figure 15). In such a case, the constant value is equal to the outflow maximum value (“PEAK”) or alternatively, to the value of one of the different segments (“AVERAGE”). In both cases, the time duration is considered in such a way to produce a segment area that is equal to area under the flow rate curve (i.e., the total released mass). If the “AVERAGE” procedure is chosen, according to the Purple Book (RIVM, 1999), after having approximated the time-varying source term with five segments, the reference flow rate is set to the value of the first segment, whilst for toxics, the reference flow rate the 2nd segment value (as in the case of Figure 15). The ADAM users can change this criterion in the option menu (i.e., number of segments and reference segment).

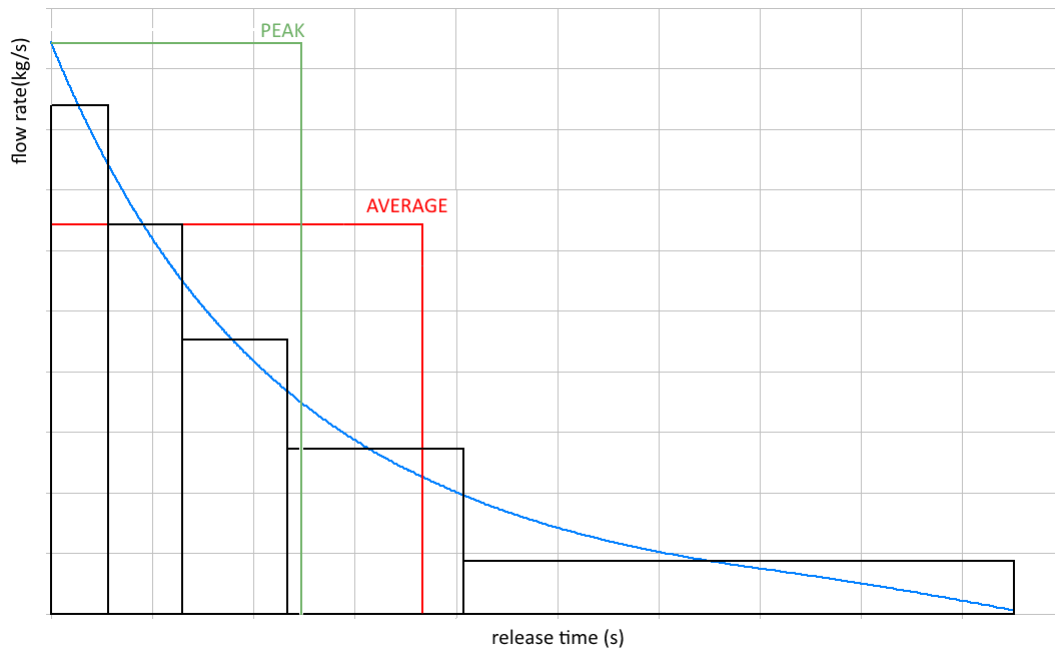


Figure 15: Time varying source term (blue curve) split in five finite segments together with the peak (green) and average (red) approximations.

If a single segment is used, the outflow value is fed directly to the dispersion model. By contrast, when the multi segment approach is considered (*default*), the following procedure is applied to calculate the maximum and the average concentrations:

- 1) The release is replaced by N segments with outflow rates q_i (i refers to the i -th segment) and time duration $t_i = Q_{tot} / (N q_i)$, where Q_{tot} is the total mass released.
- 2) N different dispersion calculations are separately conducted for hypothetical releases with outflow rates q_i and durations $t_{D_i} = \min(\sum t_i, Q_{tot}/q_i)$, where $\sum t_i$ is the total duration of the release. Please note that these values do not correspond to the single duration of time segments (see also simplified example with two segments in Figure 16).
- 3) Since the concentration produced by the time varying release, has to be in between the concentrations produced by the hypothetical releases with higher and lower outflow rates, the overall concentration is estimated by a weighted average of those associated to the single releases, with the released masses Q_i as the reference weights.

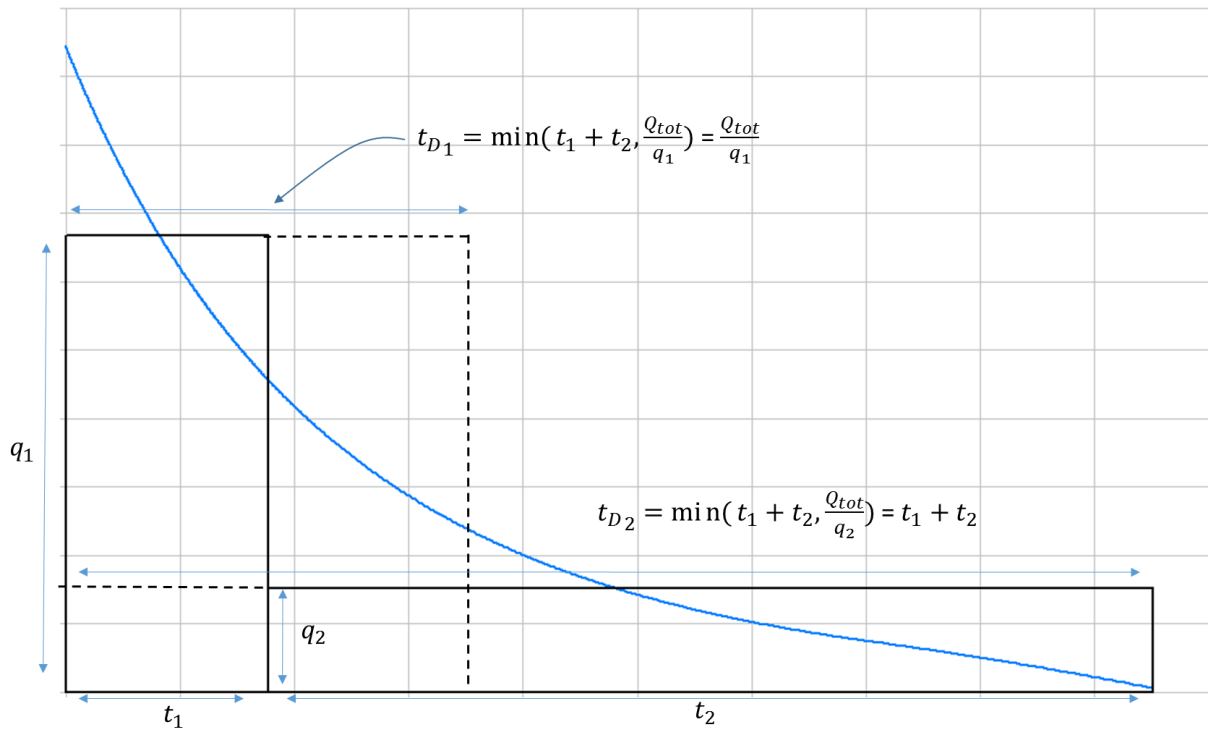


Figure 16: Simplified scheme with two segments.

A point to note is that the above procedure is applicable to calculate the *maximum* and *average concentrations*, but it is inappropriate to determine the *instantaneous concentration*. For this reason, it cannot be applied to those dispersion phenomena associated with a flash fire or an explosion of flammable clouds, which require the determination of the concentration distribution at a certain instant of time (i.e., ignition time). These two cases require more complex calculations, such as the cloud front position and the cloud volume, respectively, and the single segment approach is employed (i.e., “PEAK” or “AVERAGE”).

Inclusion of the contribution from Pool Evaporation in case of Rainout

In SLAB, liquid droplets formation and evaporation is modelled by assuming local thermodynamic equilibrium, where the droplet size is assumed sufficiently small so that the transport of the vapour-droplet mixture can be considered as a single fluid, which in turn allows neglecting gravitational settling and ground deposition of droplets (i.e. rainout).

Since the ADAM source term module allows estimating the mass fraction of the droplets falling on the ground and those remaining airborne, the dispersion is calculated by using a recombination process. In particular, the dispersion effect of the vapour jet (or the vapour part in a catastrophic release) is combined with the vapour resulting from the evaporation of the rainout pool. These two phenomena are considered as independent, and ADAM separately estimates the effects associated with each.. The overall concentration is conservatively estimated by adding up each contribution.

In order to apply the recombination method, the SLAB model is applied twice. The first calculus is applied to the primary phenomenon i.e. the one associated with the direct vapour source (i.e., the vapour jet of the vapour fraction in the case of an instantaneous

release), whilst the second calculus is associated with the secondary and less relevant phenomenon (i.e. the evaporation for the pool resulting from the rainout). When the release involves a pure liquid, the primary calculus refers to the vapours produced via evaporation from the pool, whilst the secondary is the one associated with the airborne vapours produced by the mechanical brake-up of droplets (see table below).

Stored substance	Primary dispersion	Secondary dispersion
Compressed vapour	From direct vapour or jet	From pool evaporation (often negligible)
Non-boiling liquid (i.e. pure liquid),	From pool evaporation	From direct vapour or jet (often negligible)
Pressurised liquid	From direct vapour or jet	From pool evaporation

Table 17: Primary and secondary dispersion phenomena recombined in ADAM

The input parameters to apply are selected according to the scheme depicted in Figure 17, which typically refers to a two-phase catastrophic release. Since after rainout, the droplets that remain airborne will be added to the vapour phase in the dispersion related phenomenon, the masses used as SLAB input variables for the primary and secondary dispersions are:

$$Q_{SLAB}^V = x_{rain} Q \quad (217)$$

$$Q_{SLAB}^L = (1 - x_{rain}) Q \quad (218)$$

where Q is the total mass released, and x_{rain} is given by:

$$x_{rain} = [1 - X_{rain}^L (1 - x_f)] \quad (219)$$

where X_{rain}^L the liquid fraction after rainout (i.e. Q_{pool}/Q_L in the figure), and x_f the vapour quality after flash.

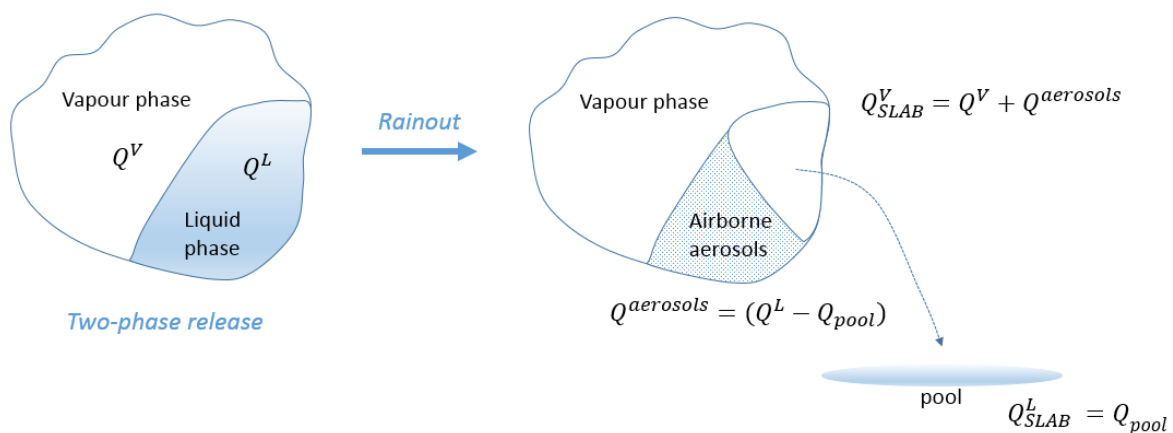


Figure 17: Catastrophic releases in presence of rainout. The total mass released Q is given by the sum of a vapour, $Q^V = x_f Q$ and a liquid, $Q^L = (1 - x_f) Q$, phase. After rainout a pool is formed, $Q_{pool} = X_{rain}^L Q^L$, whilst part of the liquid droplets remain airborne $Q^{aerosols} = (1 - X_{rain}^L) Q^L$.

Since in the SLAB model the substance droplets are considered as embedded/transported by the cloud, the liquid fraction to be fed to SLAB in the recombination process is provided by ADAM as follows:

$$X_{SLAB}^L = \frac{Q^{aerosols}}{Q_{SLAB}^V + Q^{aerosols}} = x_{rain} - x_f \quad (220)$$

Clearly for the part of the dispersion associated with the pool evaporation mechanism (i.e. generally the secondary dispersion), this parameter will be fixed to zero.

For continuous releases, the above relations are also valid, with the condition of substituting the mass with the flow rate.

A point to note is that the recombination process is applied to pure dispersion phenomena only. Flash fires and explosions are modelled by using the original SLAB approach.

Modification of the SLAB routine for the calculus of plume velocity

The extension of SLAB algorithm to a greater number of downwind points has shown a problem in the eval() routine of the original SLAB code. This routine involves the calculus of the plume velocity via the solution of a cubic equation, which was found to lead to wrong results for certain values of the involved parameters.

By implementing a novel procedure with the analytical solution of the root equations we get very consistent results (i.e. practically the same results for a different number of downwind points, as expected). In general, this correction leads to slightly higher concentration in proximity of the source and slightly lower concentration further away.

Dispersion and explosion of Flammable Clouds

The dispersion model is used in ADAM to assess the effects of Flash Fires and to evaluate the explosive mass of Vapour Cloud Explosions. The first case consists of a classical calculation of the concentration distribution of flammable at a certain height, whilst the second consists of the calculus of the flammable mass contained in the vapour cloud. In both cases, the calculus is conducted at a certain instance of time (i.e. ignition time), which corresponds to the instance in which the cloud front reaches the ignition location. Thus, differently from toxics, there is no interest in calculating the maximum or the time average concentration, as in the case of toxics.

Time dynamic is self-evident for the instantaneous releases, for which the puff propagates and spreads in the downwind direction. For finite duration releases (i.e. vertical/horizontal jets and evaporating pools), whence the plume reaches a certain target at downwind distance x , the concentration is constant for all the release duration if x is below a critical distance x_c (transition distance). For higher values of x , the cloud behaves as a puff. Since the SLAB requires the use of a minimum average time, a value of 10s is used for the calculation of the instant concentration. In addition, the multi segment and recombination procedures are not applicable because they are specifically addressed to calculate the maximum or the average concentrations and not the concentration at a specific instance.

Flash Fire contours

The flame contour is obtained by using the dispersion model to estimate the cloud size and position at the time of ignition. ADAM calculates the iso-concentration curves of the cloud at the time in which ignition is supposed to take place, by determining the level of cloud concentration equal to lower flammability limit, LFL and $\frac{1}{2}$ LFL. The inner part of the cloud having concentration above the upper flammability limit (UFL) is also supposed to take part in the fire, since turbulence induced combustion mixes this material with air and burns it. The ignition time is calculated by assuming that the ignition location takes place at a certain downwind distance from the release, which should match with the cloud front.

Explosive mass

In order to calculate the explosive mass at the time of ignition, ADAM has to calculate the volume of the cloud contained within the substance flammability limits (see eq. 189). In order to conduct the volume integration, the 3D concentration of the cloud has to be determined at the time of ignition. Since the cloud propagation is a dynamic process, it is necessary to input the ignition time to calculate the explosive mass. The calculus of the concentration distribution allows determining the LFL leading edge of the cloud at the ignition time, which identifies the ignition location. However, in practical situations ignition time is unknown and is more likely to identify the ignition location. For this reason, ADAM simulates the overall cloud propagation dynamic, and by fixing the ignition location, it calculates the front arrival time and, in turn, the ignition time necessary to fix the integration volume.

The integration procedure allows determining of the volume of the cloud. Thus, in order to determine the explosive mass, a conversion of the concentration values from ppm to mg/m^3 has to be done. This conversion requires the density, and in turn, the temperature in each point of the cloud. SLAB provides this information in all cases, with the exception

of the vertical jet, and specifically in the part that models the vertical rise. In such a case, the cloud temperature was estimated by interpolating between the ambient and the jet temperatures.

The overall integration was tested by calculating the cloud obtained by fixing a very low value of LFL (i.e. .001). The calculated value of the explosive mass should be the same as the overall mass released. A very good correspondence was found for catastrophic releases. For the jets releases, this procedure tends to slightly underestimate the mass for little ignition times.

VULNERABILITY (Module 3)

Introduction

As explained in this report, chemical accidents can result from emissions, fires or the explosion of chemicals during transportation, storage or industrial activities, leading to serious immediate or delayed damage to human beings, the environment and or to structures involving one or more chemical substances.

Bankoff et al. (Bankoff, 2014) described the vulnerability as associated with the multi-dimensionality of disasters by focusing attention on the totality of relationships in a given social situation, which constitute a condition that, in combination with environmental forces, produces a disaster. In practice, this means that a disaster is never a stand-alone event and numerous factors covering a broad scale of occurrences are needed prior to the accident to occur. Research on vulnerability can be traced back to the 1970s in natural hazard studies (Fengying, 2010). Since then, many papers appeared in the literature from a wide range of different perspectives. The estimation of the vulnerability is related to the type of chemical accident involved.

In the previous sections, the first two modules of ADAM have been described being Module 1 'Source term' and Module 2 'Physical effects'. The present and last section explains ADAM's third Module entitled 'Vulnerability'.

What is vulnerability

Vulnerability is a rather broad concept and is a specific risk factor of the subject of the system, which is exposed to a certain physical effect of an accident, and corresponds to its inherent tendency to be affected, or susceptible to damage. The first step of the vulnerability assessment process consists of identifying the potential targets that may be affected by the accident, and specifically: the population; the build and natural environment. Different vulnerability models apply to the different targets. The outcome of the vulnerability assessment is the estimate level of harm produced by the exposure to the effects produced by the hazardous substance accident development.

ADAM focusses on the effect of an accident on the population, vulnerability is normally expressed in terms of the likelihood a person will die as the consequence of a chemical accident, and the available vulnerability models specifically refer to this type of damage. However, ADAM is designed in such a way to allow the user to upload other vulnerability models, which may refer to other type of damages and targets, when needed.

Vulnerable populations

People are considered as society's most important asset. A point to note is that certain population groups may be more vulnerable to disasters due to age, poverty, race, disability or language barriers (Berke, 2016). These socially vulnerable groups often face greater challenges preparing for, coping with and recovering from disasters. In addition, people that stay for shorter periods at a certain location might also be at greater risk being less familiar with the local environment and hazards and less prepared to protect themselves during an accidental event. These include students, tourists, second homeowners, migrant farm workers, and visitors for special events (e.g. large sporting events, festivals, concerts).

Built Environment

The built environment includes existing structures, infrastructure systems, critical facilities, and cultural resources. Areas of future growth and development are also an important component when assessing the building environment for vulnerability purposes (Berke, 2016). All structures are exposed to risk, but certain buildings or concentrations of buildings may be more vulnerable because of their location, aging, construction type, condition or use. Infrastructure systems are critical for life safety and important for economic stability and include transportation, power, communication, and water and wastewater systems. Many critical structures depend on a good infrastructure to function. For example, hospitals need electricity, water, and sewer to continue serving the community. As with critical facilities, the continued operations of infrastructure systems during and following a disaster are key factors in the severity of impacts and the speed of recovery. Critical structures are necessary for a community's response to and recovery from accidental emergencies. It is therefore important that critical structures continue to operate during and following a disaster in order to reduce the severity of potential impacts and to accelerate recovery. When identifying vulnerability, both the structural integrity and content value of critical facilities and the effects of interrupting their services to the community are important factors to consider as part of risk prevention and risk management.

Natural Environment

Examples of environmental and natural resources are fields suitable for the production of food or the production of life-stock. Also a park, lake, playground or holiday park are examples. Environmental assets and natural resources are important to local communities and consequently to the quality of life and support to the (local) economy through agriculture, tourism and recreation, and a variety of other ecosystem services, such as clean air and water. The natural environment also provides protective functions that reduce hazard impacts and increase resiliency (Berke, 2016) e.g., trees can reduce the impact of an explosion and water can stop the spread of a fire. Protection of the environmental and natural resources are therefore important and also present opportunities to mitigate the impact of a possible accident such as developing parks, canals, trails, etc.

Vulnerability models

As previously mentioned, the level of harm produced by the physical effects of the accident (i.e. thermal radiation, overpressure, or concentration of toxics) resulting by the uncontrolled release of the hazardous substance, is the outcome of the vulnerability model. This depends on the intensity and duration of the exposure to this physical effect, which can be expressed in terms of the received dose. In particular, the dose is estimated as the product of the intensity I of exposure (to a certain exponent n) and the exposure duration t , i.e. $I^n t$.

In ADAM, vulnerability is primarily estimated on the basis of the probability of death of an individual or group of individuals as a consequence of the received dose. The dose-lethality relationship can be described using a number of statistical models including (log) probit, (log) logit and Weibull models. These models all make assumptions about the underlying statistical distribution of the dose, and describe the relationship between the data associated with this variable and the acute lethality rate data. In general, the outcome of this analysis is normally valid within the actual experimental exposure range (interpolation and limited extrapolation). A point to note is that, for risk assessment applications that tend to require predicting the impact also outside the actual experimental exposure range, the models are likely to produce widely different health outcomes for equal exposure-response scenarios (Ruijten, 2015).

In ADAM, the log-probit has been selected as the most simple and straightforward model to describe the human vulnerability distribution. In order to express the lethality for any accident type, specific vulnerability probits are used for each of the following exposure route: fire, explosion and inhalation of toxics.

In addition to the probit approach, ADAM allows the possibility of expressing the level of harm by also using reference thresholds of exposure intensity above which, the received dose corresponds to a certain identified level of damage.

Vulnerability to Fires

In order to estimate the consequences of fires on people, thermal radiation dose-response curves are usually employed. These correlate the level of harm with the related dose. This applies to all type of fires with the exception of flash fires, for which the radiative effect is considered negligible. For flash fires the vulnerability is assessed by assuming 100% lethality within the flame boundary (i.e. LFL concentration), and a probability of death decreasing linearly outside the flame to reach a value of 0 for concentrations of flammable equal to $\frac{1}{2}$ LFL.

The main consequence of intense thermal dose on people is the production of burns on the skin, with different degrees of severity depending on the type of fire, radiation intensity, time exposure, and the extension and depth of burning. For instance, pool fires are generally less effective than jet fires to produce damage, since exposed individuals have generally more time to escape from the affected area. The thermal radiation dose D ($W^{4/3}s \cdot m^{-8/3}$) received by a receptor, is defined in terms of the radiant flux at receptor location, q_R ($W m^{-2}$), as given by eq. (121) and the exposure time t_{exp} (s) to this flux:

$$D = \Phi t_{exp} q_R^{4/3} \quad (221)$$

The correction coefficient Φ accounts of any protection measure that is cause of a reduction of the effective dose due to e variation in skin area exposed. For normally clothed individuals $\Phi \cong 0.5$ (Lees, 1994). In ADAM, this corrector coefficient is set to unity by default.

The exposure time depends on the type of fire, and the reaction and escape times of the receptor i.e.:

$$t_{exp} = t_r + \frac{\Delta r}{u} \quad (222)$$

where t_r (s) is the reaction time, Δr (m) is the distance of the receptor from a safe point (e.g., a position with a radiation flux $< 1kW/m^2$) and u (m^2/s) is the escape speed. In ADAM, the default value for the exposure time is 20s.

The probit model used for the calculation of the probability, P (-), of injury (1st and 2nd degree burns) or death, as a consequence of a specified dose, is expressed by the following relationship:

$$P = \frac{1}{2} \left[1 + erf \left(\frac{P_r - 5}{\sqrt{2}} \right) \right] \quad (223)$$

in which erf is the "error function" and the probit, P_r (-), is given by the empirical expression,

$$P_r = a + b \ln D \quad (224)$$

where the probit coefficient a is strictly dependent on the measuring unit of the thermal dose, i.e. either $(kW m^{-2})^{4/3} \cdot s$ or $(W m^{-2})^{4/3} \cdot s$.

In eq. (223), the probability, $P(-)$, refers to injury or death, depending on the values of the coefficients a and b that are provided in Table 18 and Table 19, respectively.

Damage	$a[kW m^{-2}; s]$	$a[W m^{-2}; s]$	b	Reference
1 st degree burn	-11.65	-75.66	6.95	Sánchez Pérez (2010)
2 nd degree burn	-13.87	-77.88	6.95	

Table 18: Probit coefficients for injury with dose expressed in $(kW m^{-2})^{4/3} s$ (Sánchez Pérez, 2010)

$a[kW m^{-2}; s]$	$a[W m^{-2}; s]$	b	Reference
-14.9	-38.48	2.56	Eisenberg, 1975
-12.8	-36.38	2.56	Tsao & Perry, 1979
-10.7	-29.03	1.99	Lees, 1994
-13.65	-37.23	2.56	TNO, Opschoor, 1992 (recommended in ADAM)

Table 19: Probit coefficients for death with dose expressed in $(kW m^{-2})^{4/3} s$, from different sources

Probit coefficients provided by Sánchez Pérez et al. of Table 18 (1st and 2nd degree burn) were obtained from the original coefficients reported in the “Green Book” (TNO, 1992), but adjusted to take into account of new empirical information. They are used in ADAM since they seem being more consistent than the TNO equations. They are definitely more conservative.

Concerning the death related probit coefficients uploaded in ADAM (Table 19), the Eisenberg model is based on nuclear data (i.e. Hiroshima and Nagasaki) and describes the effect of thermal radiation with prevalence in the UV spectrum. Tsao & Perry model is based on the Eisenberg model but adjusted for experiments carried out at hydrocarbon fires and accounts for the infrared component of the radiation. The Lees probit is based on burn mortality data with radiations with also prevalence in the UV spectrum, and accounts for clothing. The TNO model (Opschoor, 1992) is based on the Tsao & Perry probit function and it is modified to account for clothing (i.e. 14%). This is used as the recommended probit in ADAM.

Vulnerability to Vapour Cloud Explosions

The expansion mechanism of a vapour cloud explosion consists of in five main stages:

- 1) cloud ignition and movement away from the point of ignition;
- 2) increase in the burning rate and its speed caused by the unstable nature of the flame and large turbulent eddies;
- 3) further increase of burning rate and speed due to the presence of obstacles;
- 4) formation of a shock wave due to increased flame speed, compression of the combustion products and zone and temperatures;
- 5) spread of a shock wave transmitting the transformed chemical energy into mechanical energy.

The shock wave induces significant changes in the surrounding space by altering its pressure and all associated properties. In a first phase this produces a peak overpressure followed by a pressure decrease below the ambient value (negative phase), to then return slowly to the original conditions (see Figure 18).

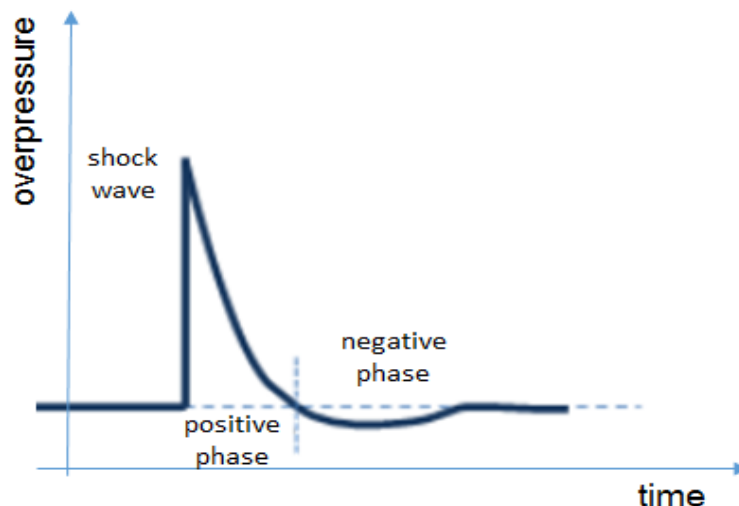


Figure 18 Final stage of the expansion mechanism of a vapour cloud explosion; the spread of a shock wave.

In order to assess the consequences of a vapour cloud explosion due to the shock wave, two main physical effects have to be considered:

- the initial peak overpressure as a function of the distance from the ignition source (i.e. centre of explosion);
- the time duration of the positive phase of the blast, or alternatively the blast impulse, which are simply related in eq. (200): i.e. $i^+ = 0.5 \Delta P_{peak} t^+$.

The probit model used for the calculation of the probability of death, as a consequence of the blast is equivalent to the previously described one for fires, and is expressed by the following probit function:

$$P_r = a + b \ln S \quad (225)$$

where S is a function of the dangerous effect (i.e. the peak overpressure (barg), the impulse (Pa s), or a function of the two), whilst a and b are the probit coefficient. Table 20 reports the probit functions included in ADAM to address the damage to affected population:

S	a	b	Reference
Peak overpressure (barg)	5.13	1.37	Hurst (1989) <i>(recommended in ADAM)</i>
Impulse (Pa s)	-46.1	4.82	Eisenberg (1975)

Table 20: Probit coefficients for explosions.

The first used as the default probit in ADAM for outdoor exposure, is the one proposed by Hurst, Nussey and Pape, which associates the blast effects to the peak overpressure. The second probit that can be selected is the one obtained with reference to the blast effect to body translation to impulse by Eisenberg, Lynch and Breeding, reported also in Lees, 2005 (vol 2 Chapter 17/226).

Other probit functions, which are based in the combination of peak overpressure and impulse and that differentiate the consequence amongst lung damage, head impact, and whole body displacement (Bowen, 1968), are not yet implemented in ADAM.

Vulnerability to inhalation of toxics

ADAM addressed the lethality effects on an average population, immediately or shortly after a single airborne exposure. In general, the toxic response of a human or animal population to a chemical exposure is determined by (Ruijten, 2015):

1. the chemical substance (chemical, physical and toxicological properties);
2. the exposure route (inhalation, dermal, oral or parenteral);
3. the exposure concentration of the chemical in the contact medium (air, water, food, etc.);
4. the duration of exposure (minutes, hours, days, months, years, life-time);
5. the species (test animals or humans);
6. physiological characteristics of the individuals in the exposed population (test animals or humans).

The dose D absorbed by inhalation by an individual, often referred to as ‘toxic load’, is calculated from the following expression:

$$D = C^n t_{exp} \quad (226)$$

where C is the concentration of the toxic at a particular point in space, which is normally expressed either in ppm volume or in mg m^{-3} , and t_{exp} is the exposure time expressed in minutes. This expression is valid when the concentration is constant for the whole exposure duration; therefore, in practice C is normally substituted with the average concentration C_{av} for the reference period.

The probit model is a standard bivariate probit model for concentration-time-lethality:

$$P_r = a + b \ln(D) \quad (227)$$

This probit function can also be extended with the use of a covariate for e.g. gender. In that case, the basic version of the probit model with interaction term X is the covariate (log-transformed, if appropriate, or 0/1 in case of sex) and described as:

$$P_r = a + b \ln(D) + c \ln(X) \quad (228)$$

In some cases, the model fit of the data can be improved by adding cross-terms for interactive effects between the model parameters (usually concentration and time) or a threshold response level (concentration or time) (Ruijten, 2015).

As an alternative to the probability probit model, personal damage can be alternatively expressed by damage endpoints, and particularly:

- LC₅₀ (Lethal concentration 50%)
- LC₁ (Lethal concentration 1%)
- IDLH (Immediately Dangerous to Life and Health)
- LOC (level of concern)

The LC₅₀ and LC₁ are the levels of concentration of a toxic in air, which correspond to 50% and 1% probability of death of the exposed population. Although the exposure duration is not explicitly mentioned in these indices, a reference value of 30 min is often considered.

For a different exposure time t , the following expression may be used (TNO, 1992):

$$LC_{50}(t_{exp}) = LC_{50}(30\text{min}) \left(\frac{0.5}{t_{exp}} \right)^{\frac{1}{n}} \quad (229)$$

Where t_{exp} is expressed in hours and n is an empirical coefficient that can be approximately taken as equal to 3.

IDLH is the index proposed by the National Institute of Occupational Safety and Health, USA, and represents the maximum concentration of a toxic substance that can be inhaled by an individual for 30min before non-reversible effects are produced. Generally, IDLH can be related to LC_{50} from the following expression:

$$IDLH = 0.1 LC_{50}(30\text{min}) \quad (230)$$

LOC is the index defined by the US Environmental Protection Agency as the concentration of the toxic substance above which there may be a serious immediate health effect to anyone exposed for 30 min, and is related to IDHL as follows:

$$LOC = 0.1 IDHL \quad (231)$$

Other endpoints that can be used in ADAM are Protective Action Criteria for Chemicals (PACs) defined in the [U.S. Department of Energy database](#)⁵, typically used as emergency exposure limits. These combines the three public exposure guideline systems (AEGs, ERPGs, and TEELs) with hierarchy-based criteria.

Substances' Probit functions

Differently from the case of fire and explosion which are independent from the specific flammable, the probit coefficients a , b , and n depends on the toxic substance under consideration. Since test data on humans are not available, almost all information for the derivation of probit functions originates from test animals. In some circumstances, human information is available from accidental data, but as the actual levels of exposure are poorly characterized, the associated data on the substance lethality are very much unreliable.

Probit coefficients are available in the ADAM database for a large number of toxic substances. These values were taken from authoritative sources such as the TNO "Green Book" (TNO, 1992), the Lees' Loss Prevention Guidebook (Lees, 2005), the AIChE Guidelines for CPQRA (AIChE, 2010), and the [RIVM probit function website](#)⁶. A similar comprehensive list of probit functions can also be found in Appendix 3 of the Irish HSE Policy document on Land Use Planning (HSE, 2009).

A point to note is the presence of several alternative probit functions for the same substances -typically for those with greater diffusion- that require a certain care in the appropriate choice to be made. In ADAM it was implemented the criterion of selecting the RIVM values by default, when available. This is justified by the rigorous process followed by RIVM and the use of up to speed information on toxicity data.

⁵ <https://sp.eota.energy.gov/pac/>

⁶ http://www.rivm.nl/en/Topics/P/Probit_functions/Probit_function_status_overview

References

AGA (1974), "American Gas Association, LNG Safety Program: Consequences of LNG Spills on Land", IS-3-1, American Gas Association, Arlington, VA, July 1974.

AiChE (2010) Guidelines for Process Safety Documentation, CCPS (Center for Chemical Process Safety), John Wiley & Sons

Appleton P.R. (1984), "A study of axi-symmetric two-phase flashing jets", report R303, SRD, Culcheth, Warrington, Cheshire, UK.

Babrauskas V., (1983), "Estimating large pool fire burning rates", *Fire Techn.* 19 pp. 251-261

Baker Q.A., Doolittle C.M., Fitzgerald G.A., and Tang M.J., (1998), "Recent developments in the Baker–Strehlow VCE analysis methodology", *Process Safety Progress*, 17, pp. 297-301

Baker Q.A., Tang M.J., Scheier E.A., and Silva G.J., (1996), "Vapor cloud explosion analysis", *Process Safety Progress*. 15 pp. 106-109

Bakkum E.A., Duijm N.J. (2005), "Vapour cloud dispersion", TNO-Yellow-Book-CPR-14E, Chapter 4, Editors: C.J.H. van den Bosch, R.A.P.M. Weterings, third revision 2005

Bankoff G., Frerks G., Hilhorst D. (2004) "Mapping Vulnerability: Disasters, Development and People". ISBN-13: 978-1853839634, ISBN-10: 039305912X.

Berke, P., Masterson, J. and Salvesen, D. (2016). "Beyond the Basics: Best Practices for Local Mitigation Planning" (<http://mitigationguide.org/task-5/steps-to-conduct-a-risk-assessment-2/2-identify-community-assets/>)

Bowen J.G., Fletcher E.R., and Richmond D.R. (1968), "Estimate of Man's Tolerance to the Direct Effects of Air Blast", Lovelace Foundation for Medical Education and Research, Albuquerque, New Mexico, Report DASA-2113.

Brambilla S., Manca D. (2009), "Accident involving liquids: a step ahead in modelling pool spreading, evaporation and burning", *Journal of Hazardous materials*, 161 pp. 1265-1280.

Brighton P.W.M. (1985), "Evaporation from a plane liquid surface into a turbulent boundary layer", *J. Fluid Mech.* 159 pp. 3232-345

Britter R.E. (1994), "Dispersion of two phase flashing releases–FLADIS field experiment; the modelling of pseudo-source for complex releases", Report FM89/2 by CERC for ECC DGXII

Britter R.E., Weil J., Leung J., Hanna S. (2011), "Toxic industrial chemical (TIC) source emissions modeling for pressurized liquefied gases", *Atmospheric Environment*, Volume 45, Issue 1, pp. 1-25.

Britter, R.E. (1995), "Dispersion of two-phase flashing releases - FLADIS field experiments; a further note on modelling flashing release", Report FM89/3 by CERC for EEC Commission DGXII

Brkić D. (2011), "Review of explicit approximations to the Colebrook relation for flow friction", *Journal of Petroleum Science and Engineering*, Volume 77, Issue 1, pp. 34-48

Brutsaert W. (1982), "Evaporation into the atmosphere: theory, history, and applications", 2nd edition. Dordrecht: Reidel, 299 ISBN 90-277-1247-6

Burgess D.S., Strasser A., Grumer L., (1961), "Diffusive burning of liquid fuels in open trays", *Fire Res Abstr. Rev.*, 3, p.177

Casal J., (2008), "Evaluation of the effects and the consequences of major accidents in industrial plants", *Industry Safety Series Vol 8*, Elsevier.

CCPS (2010), "Vapour cloud explosion pressure vessel burst, BLEVE and flash fire hazards", Second Edition, Wiley ISBN 978-0-470—25147-8

Chamberlain G.A., (1987), "Developments in design methods for predicting thermal radiation from flares", *Chem. Eng. Res. Des.*, 65 pp. 229-309

Cook J., Bahrami Z., Whitehouse R.J., (1990), "A comprehensive program for calculation of flame radiation levels", *J. Loss Prev. Process Ind.*, 3 pp. 150-155

Crowl D.A., (2003), "Understanding explosions", CCPS Concept Book, American Institute of Chemical Engineers, NY ISBN 0-8169-0779-X

D'Alessandro P.E. Robert (2004) "Emergency venting requirements for tempered systems considering partial vapor-liquid separation with disengagement parameters greater than unity part I: Model development", *Process Safety Progress*, Volume 23, Issue 1, pp. 1-15.

Darby R. (2001), "Chemical Engineering Fluid Mechanics", Second Edition CRC Press

De Vaull G. E., King J. A. (1992), "Similarity scaling of droplet evaporation and liquid rain-out following the release of a superheated flashing liquid to the environment", 85th Annual Meeting, Air and Waste Management Assoc., Kansas City, MO, June 21-26.

Eisenberg, N.A., Lynch, C.J., and Breeding, R.J., (1975) "Vulnerability model: a simulation system for assessing damage resulting from marine spills (VMI)". US Coast Guard, Office of Research and Development, Report n°. CGD-137-75, NTISAD-015-245.

Elkottb M.M. (1982), "Fuel atomisation for spray modelling", *Progress in Energy and Combustion Science*, 8(1), pp. 61-91

Engelhard W.F.J.M. (2005), "Heat flux from fires", TNO-Yellow-Book-CPR-14E, Chapter 6, Editors: C.J.H. van den Bosch, R.A.P.M. Weterings, third revision 2005

Ermak D.L., (1990), "User's manual for SLAB: an atmospheric dispersion model for denser-than-air releases", Lawrence Livermore National Laboratory, Livermore, California, UCRL-MA-105607

Fengying L., Jun B., Huang L., Qu C., Yang J., Quanmin B. (2010) "Mapping human vulnerability to chemical accidents in the vicinity of chemical industry parks". *Journal of Hazardous Materials* 179, pp. 500–506.

Fisher H. G., Forrest H. S., Grossel S. S., Huff J. E., Muller A. R., Noronha J. A., Shaw D. A., Tilley B. J., (1992) "Emergency Relief System Design Using DIERS Technology: The Design Institute for Emergency Relief Systems (DIERS) Project Manual", Copyright © 1992 *American Institute of Chemical Engineers*, ISBN: 9780816905683

Green D. and Perry R. (2007), "Perry's Chemical Engineers' Handbook", October 2007, 8th Edition, McGraw-Hill ISBN, 0-07-142294-3, Section 4-9 Residual Enthalpy and Entropy from PVT correlations

Hanna H.R. and Britter R.E. (2002), "Wind flow and vapour cloud dispersion at industrial and urban sites", *AIChE Center for Chemical Process Safety*, p. 208

Hasegawa K., Sato K., (1977) "Study on the fireball following steam explosion of n – pentane", *Loss Prev. Safety Prom. Proc. Ind.*, 2, p. 297

Heskestad, G. (1984), "Engineering relations for fire plumes", *Fire Safety Journal* 7 pp. 25-32

Holtrman H.J., "Kinetics and evaporation of water drops in air", IMAG report 2003 – 12, Wageningen UR July 2003

Hooper W.B. (1981), "The two-K method predicts", *Chemical Engineering*, pp. 96-100

HSE (1986), "The effect of explosions in the process industry" *Loss Prevention Bulletin*, Health Safety Executive publications, vol. 68, pp. 37-47

HSE (2009), "Policy & Approach of the Health & Safety Authority to COMAH Risk-based Land-use Planning" 07 September 2009, Health and Safety Authority <http://www.hsa.ie/eng/Your Industry/Chemicals/Legislation Enforcement/COMAH/L and Use Planning/Land Use Planning.pdf>

Hurst NW, Nussey C and Pape RP. (1989) "Development and Application of a Risk Assessment Tool (RISKAT) in the Health and Safety Executive", *Chem, Eng, Res, Des.*, 67 pp. 362-372.

ICChemE (1989), Thermal Radiation Monograph, "Calculation of the Intensity of Thermal Radiation from Large Fires" Institution of Chemical Engineers *Industries* 11, pp. 307-321.

Johnson A.D., Brightwell H.M., Carsley A.J. (1994), "A model for predicting the thermal radiation hazards from large-scale horizontally released natural jet fires", *ICChemE Symposium Series* No 134, pp. 123-142

Johnson D.W. (1999 bis), "RELEASE an aerosol model with potential, International Conference and Workshop on Modeling Consequences of Accidental Releases of Hazardous Materials", San Francisco.

- Johnson D.W., Woodward J.L. (1999), "A Model with Data to Predict Aerosol Rainout in Accidental Releases", *Center of Chemical Process Safety (CCPS)*, New York
Journal of the Power Division, Vol. 88, Issue 2, pp. 157-182
- Kalghatgi G. T. (1983), "The Visible Shape and Size of a Turbulent Hydrocarbon Jet Diffusion Flame in a Cross-Wind." *Comb. Flame* 52 pp. 91-106
- Kalghatgi G. T. (1984), "Lift-off Heights and Visible Lengths of vertical turbulent diffusion flames in still air", *Comb. Sci. Tech* 41 pp. 17-29
- Kapias T. and Griffiths R. F. (2001), "REACTPOOL: A new model for accidental releases of water reactive chemicals", HSE Contract Research Report 331/2001
- Kay P.J., Witlox H. W.M., Bowen P. J., (2010), "Sub-cooled and flashing liquid jets and droplet dispersion II. Scaled experiments and derivation of droplet size correlations", *Journal of Loss Prevention in the Process Industries*, 23, pp. 849-856
- Kostowski W.J., Skorek J., (2012) "Real gas flow simulation in damaged distribution pipelines", *Energy*, 45 pp. 481-488
- Kukkonen J. (1990), "Modelling source terms for the atmospheric dispersion of hazardous substances", *Commentationes Physico-Matematicae* 115/1990, Dissertation No 34, The Finnish Society of Sciences and Letters
- Kunz O. and Wagner W. (2012), "The GERG-2008 Wide-Range Equation of State for Natural Gases and Other Mixtures: An Expansion of GERG-2004", *J. Chem. Eng. Data* 57 (11), pp. 3032-3091
- Lautkaski R. (2008), "Experimental correlations for the estimation of the rainout of flashing liquid releases - Revisited," *J. Loss Prev. Proc. Ind.*, vol. 21, pp. 506-511.
- Lees F (1994), "The assessment of major hazards: a model for fatality injury from burns" *Transicheme*, Part B, 72 (August)
- Lees F. (2005), "Lees' Loss Prevention in the Process Industries: Hazard Identification, Assessment and Control", Vol 2, Chapter 17, Third Edition, ISBN: 978-0-7506-7555-0
- Lenzing T., Friedel L., Cremers J., Alhusein M., (1998), "Prediction of the maximum full lift safety valve two-phase flow capacity", *Journal of Loss Prevention in the Process Industries* 11 (5), pp. 307-321
- Leung J. C. and Fisher H. G., (1982), "Two-Phase Flow Venting from Reactor Vessels." *Journal of Loss Prevention in the Process Industries* 2(2), pp. 78-86.
- Lihou D.A., Maund J.K. (1982), "Thermal radiation hazards from fireballs. The Assessment of major hazards" *Institution of Chemical Engineers*, Rugby, U.K p. 191

MacKay D., Mastugu R.S., "Evaporation rates off liquid hydrocarbons spill on land and water", *Can. J. Chem. Eng.* 31 (1973) pp. 434-439

Mann L.R.B. (1981) "Thermal hazards from propane (LPG) fireballs", *Combust. Sci. Technol.* 25 p. 141

Melhem G.A. and Saini R. (1992), "A Model for the Dispersion of Two-Phase Flashing Multicomponent Jets", *Process Plant Safety Symposium*, Houston Texas (Editors: William F. Early, II, P.E., Victor H. Edwards, Ph.D., P.E., Elizabeth A. Waltz), AIChE.

Mercx W.P.M., van den Berg A.C. (2005), "Vapour Cloud Explosions", TNO-Yellow-Book-CPR-14E, Chapter 5, Editors: C.J.H. van den Bosch, R.A.P.M. Weterings, third revision

Mudan K., and Croce P. (1988), Fire Hazard Calculations for Large Open Hydrocarbon Fires, SFPE Handbook of Fire Protection Engineering, 1st ed., National Fire Protection Association, Quincy, Ma., Section 2, pp. 2-45 to 2-87.

Mudan K.S., (1987) "Geometric view factors for thermal radiation hazard assessment", *Fire Safety Journal*, 12 pp. 89-96

Nellis G., Klein S. (2008), Heat Transfer, Cambridge University Press, New York

Numerical Recipes in C: the art of scientific computing, 2nd Edition (1992) Cambridge University Press, New York, NY, USA ©1992 ISBN: 0-521-43108-5

Opschoor G. (1979), "Methods for the calculation of the Physical Effects of the escape of dangerous material (Report)", TNO, Voorburg, The Netherlands PA, pp. 844–859.

Opschoor G., van Loo R.O.M., Pasman H.J., (1992) "Methods for Calculation of Damage Resulting from Physical Effects of the Accidental Release of Dangerous Materials", International Conference on Hazard Identification and Risk Analysis, Human Factors, and Human Reliability in Process Safety, Orlando January 15-17, 1992.

Papaevangelou G., Evangelides G., Tzimopoulos C., (2010) "A new explicit equation for the friction coefficient in the Darcy–Weisbach equation", Proceedings of the 10th Conference on Protection and Restoration of the Environment: PRE10, July 6–9, Greece Corfu, 166, pp. 1–7

Paulson C.A. (1970), "The mathematical representation of wind speed and temperature profiles in the unstable atmospheric surface layer", *Journal of Applied Meteorology*, 9, pp. 857-861

Peng J.N.S., and Robinson D. B. (1976), "A New Two-Constant Equation of State". *Industrial and Engineering Chemistry: Fundamentals* 15 59–64. doi:10.1021/i160057a011

Pierorazio A. J., Thomas J. K., Baker J. K., and Ketchum D. E., (2005). "An update to the Baker Strehlow-Tang vapor cloud explosion prediction methodology flame speed table" *Process Safety Progress* 24 (1) pp. 59-65

Pritchard M.J. and Binding T.M., (1992), "FIRE2 a new approach for predicting thermal radiation levels from hydrocarbon pool fires", *ICHEME Symp. Series* 140 pp. 491-503

Raphael M. (1962), "Prediction of Temperature in Rivers and Reservoirs",

Redlich O., Kwong J.N.S. (1949), "On the Thermodynamics of Solutions". *Chem. Rev.* 44 (1), 233–244. doi:10.1021/cr60137a013

Rew P.J. and Hulbert W.G. (1996), "Development of a Pool fire thermal radiation model", HSE Contract Research Report 96/1996

Rew P.J., Spencer H., Maddison T., (1988) "The sensitivity of risk assessment of flash fire vents to modelling assumptions", *ICHEME Symposium Series* n. 144, pp. 265-278

RIVM (1999), "Guidelines for Quantitative Risk Assessment", Purple Book, CPR 18E, The Hague

Roberts A.F. (1982), "Thermal radiation hazards from releases of LPG from pressurized storage", *Fire Safety Journal*, 4 (3) pp. 197-212

Ruijten M.M.W.M., Arts J.H.E., Boogaard P.J., Bos P.M.J. Muijser H., Wijbenga A. (2015). "Method for derivation of probit functions for acute inhalation toxicity". RIVM Report 2015-0102.

Sánchez Pérez JF, González Ferradás E., Díaz Alonso F, Palacios García D., Mínguez Cano MV, Bautista Cotorruelo JA (2010) New Probit equations for the calculation of thermal effects on humans, *Process Safety and Environmental Protection* 8 (2010) 109–113

SFPE Handbook of Fire Protection Engineering, National Fire Protection Association, edition 4th , Chapter 3 by Craig L. Beyler, (2008)

Shokri M., and Beyler C.L., (1989), "Radiation from Large Pool Fires", *Journal of Fire Protection Engineering* 1(4), pp.141–150. Symposium (International) on Combustion. The Combustion Institute, Pittsburgh

Tang M.J., Baker Q.A. (1999) "A new set of blast curves from vapour cloud explosions", *Process Safety Progress* 18, pp. 235-240

Tang M.J., Baker Q.A. (2000) "Comparison of blast curves for vapour cloud explosions", *J. Loss Prev. Proc. Indus.*, 13 pp. 433-438

Thibodeaux (1979), "Chemo dynamics: Environmental Movement of Chemicals in air, Water and Soil", pp. 458-461, 1979 John Wiley & Sons

Thomas P.H., (1963) "The size of flames from natural fires", *Proceedings of the 9th Symposium on Combustion*, New York, NY, Academic Press, pp. 844–859

TNO (1992) "Methods for the determination of possible damage of people and objects resulting from the release of hazardous materials. Green Book, CRR 16, ISBN 90-5307-052-4.

Tsao C.K. & Perry W.W. (1979) "Modifications to the vulnerability model: a simulation model for assessing damage resulting from marine spills" ADA-075-231 US COAST GUARD.

Tuve G.L, Bolz R.E. (1976), "Handbook of tables for applied engineering science", 2nd edition, CRC Press, Cleveland

van den Berg A.C. (1985) "The Multi-Energy method. A framework for vapour cloud explosion blast prediction" *J. Hazard Mater* 12, pp. 1-10

van den Berg A.C., Mos A.L. (2005) "Research to improve guidance on separation distance for multi-energy method (RIGOS)", *HSE Research Report* 369, ISBN 0 7176 6146 6

van den Bosch C.J.H. (2005), "Pool Evaporation", TNO-Yellow-Book-CPR-14E, Chapter 3, Editors: C.J.H. van den Bosch, R.A.P.M. Weterings, third revision 2005

van den Bosch C.J.H., Duijm N.J. (2005), "Outflow and Spray release", TNO-Yellow-Book-CPR-14E, Chapter 2, Editors: C.J.H. van den Bosch, R.A.P.M. Weterings, third revision 2005

Viecenz H.J., (1980) "Blasenaufstieg und Phasenseparation in Behältern bei Dampfeinleitung und Druckentlastung", Dissertation Univ. Hannover

Webber D.M. (1987) "Heat conduction under a spreading pool", SRD R421

Webber D.M. (1990) "A model for pool spreading and vaporisation and its implementation in the computer code G*A*S*P", UKAEA Report SRD R507

Webber D.M. (1991), "Source Terms", *J. Loss Prev. Process Ind.*, Vol 4 pp. 5-15

Webber D.M. (2012), "On models of spreading pools", *J. Loss Prev. Process Ind.*, Vol 25 pp. 923-926

Webber D.M. and Jones S.J. (1987), "A model of spreading vaporising pools" in *Proc. International conference on Vapour Cloud Modelling*, Boston Massachusetts, USA, ed. J Woodward, pub. AIChE.

Webber D.M. and Jones S.J. (1989), "A users' guide to GASP on microcomputers", UKAEA Report SRD/HSE R521

Welker J.R. and Sliepcevich C.M. (1996), "Bending of wind-blow flames from liquid pools", *Fire Technology* 2, pp. 127-135

Wheatley C.J. (1987), "Discharge of liquid ammonia to moist atmospheres—survey of experimental data and model for estimating initial conditions for dispersion calculations", report R410, SRD, Culcheth, Warrington, Cheshire, UK

Williamson R.E., Threadgill E.D. (1974) "A simulation for the dynamics of evaporating spray droplets in agricultural spraying", *Transactions of the ASAE* 17, pp. 254-261

Witlox H. W.M., Harper M., (2013), "Two-phase jet releases, droplet dispersion and rainout I. Overview and model validation", *Journal of Loss Prevention in the Process Industries*, 26, pp. 453-461

Witlox H. W.M., Harper M., Bowen P. J., Cleary V. (2007), "Flashing liquid jets and two-phase droplet dispersion II. Comparison and Validation of droplet size and rainout formulations", *Journal of Hazardous Materials*, 142, pp. 797-809

Witlox H. W.M., Harper M., Oke A., Bowen P. J., Kay P. J. (2010), "Sub-cooled and flashing liquid jets and droplet dispersion I. Overview and model implementation/validation", *Journal of Loss Prevention in the Process Industries*, 23, pp. 831-842

Witlox W.M., Bowel P.J. (2002), "Flashing liquid jets and two-phase dispersion: a review", HSE CONTRACT RESEARCH REPORT 403/2002

Woodward J.L. (2014), "Source Modelling – Aerosol formation and rainout, Reference Module in Chemistry", *Molecular Sciences and Chemical Engineering*, pp. 1-27

Zeman O., (1982), "The dynamics and modelling of heavier-than-air cold gas releases", *Atmos. Environ.*, 16 pp. 741-751

GETTING IN TOUCH WITH THE EU

In person

All over the European Union there are hundreds of Europe Direct information centres. You can find the address of the centre nearest you at: <http://europa.eu/contact>

On the phone or by email

Europe Direct is a service that answers your questions about the European Union. You can contact this service:

- by freephone: 00 800 6 7 8 9 10 11 (certain operators may charge for these calls),
- at the following standard number: +32 22999696, or
- by electronic mail via: <http://europa.eu/contact>

FINDING INFORMATION ABOUT THE EU

Online

Information about the European Union in all the official languages of the EU is available on the Europa website at:

<http://europa.eu>

EU publications

You can download or order free and priced EU publications from EU Bookshop at: <http://bookshop.europa.eu>. Multiple copies of free publications may be obtained by contacting Europe Direct or your local information centre (see <http://europa.eu/contact>).

JRC Mission

As the science and knowledge service of the European Commission, the Joint Research Centre's mission is to support EU policies with independent evidence throughout the whole policy cycle.



EU Science Hub
ec.europa.eu/jrc



@EU_ScienceHub



EU Science Hub - Joint Research Centre



Joint Research Centre



EU Science Hub